Waste and Biomass Valorization (2025) 16:2029–2073
https://doi.org/10.1007/s12649-025-02965-2

REVIEW ARTICLE

A Comprehensive Review on Biomass Waste-Derived Biochar for Sustainable Adsorptive Remediation of Hazardous Radio-Contaminants

Stephen Sunday Emmanuel[1] · Ademidun Adeola Adesibikan[1] · Odunayo T. Ore[2] · Ajibola A. Bayode[3] · Hamza Badamasi[4] · Saheed O. Sanni[5,6] · Obianuju Patience Ilo[7]

Received: 30 September 2024 / Accepted: 3 February 2025 / Published online: 13 February 2025

Abstract

Radio-contaminant and biomass waste remain a threat to the ecosystem, especially, the water bodies, the lifeline of the ecosystem. This paper reviewed radio-contaminant adsorption from aqueous environments using biomass waste-derived biochar (BWDBC). This review aims to analyze the extensive body of literature on the topic, pinpoint important pragmatic findings on research domains, figure out problematic issues and knowledge gaps that could provide a basis for future research endeavors, and project future research hotspots. The maximum reported adsorption capacity for radio-contaminant was 1527.02 mg/g for uranium using wheat straw BWDBC. Chelation/complexation, pore diffusion, ion exchange, precipitation, van der Waals forces, π-π interactions, and electrostatic interactions through oxygenated, and oxime functional groups are the main mechanisms of radio-contaminant adsorption. The majority of radio-contaminant adsorption was best described by the pseudo-second-order kinetic, Langmuir isotherm, and Thomas model (for column adsorption). Most exhausted BWDBC can be eluted/regenerated mostly with acid/base and reused up to 3–6 times with an adsorption performance of > 75% in most cases while upholding their original structural integrity. In authentic radio-wastewater and competitive adsorption scenarios, the existence of other ions typically reduced the sorption of radio-contaminants. Glancing forward, research on innovative hybrid techniques, neural network modeling, density functional theory simulations, and techno-economic analysis should be considered. This study advances not just the remediation of water pollution but also responsible consumption, sustainable waste management systems, and circular economy.

Statement of Novelty

This review offers the first comprehensive analysis of biomass waste-derived biochar for the adsorptive remediation of hazardous radio-contaminants from aqueous environments. While numerous studies have explored the use of biochar for various contaminants, none have thoroughly synthesized the current body of knowledge specifically focused on radio-contaminants. This work critically assesses key findings from experimental studies, identifies knowledge gaps, and offers novel insights into the mechanisms of adsorption, including complexation, pore diffusion, and π-π interactions. By detailing the maximum reported adsorption capacities, regeneration potential, and challenges in authentic radio-wastewater scenarios, this review provides empirical knowledge gaps and problematic issues as well as future research hotspots that can provoke insightful

✉ Stephen Sunday Emmanuel
stephenemmanuel6011@gmail.com

[1] Department of Industrial Chemistry, Faculty of Physical Sciences, University of Ilorin, P. M. B. 1515, Ilorin, Nigeria

[2] Department of Chemistry, Kogi State University, P.M.B. 222, Kabba, Nigeria

[3] Department of Chemical Sciences, Redeemer's University, P.M.B. 230, Ede, Osun State, Nigeria

[4] Department of Chemistry, Federal University Dutse, Dutse, Jigawa State, Nigeria

[5] College of Chemical Engineering, Sichuan University of Science & Engineering, Zigong 643000, China

[6] Department of Biotechnology and Chemistry, Vaal University of Technology, Private Bag X021, Vanderbijlpark 1900, South Africa

[7] School of Geography, Archaeology and Environmental Studies, University of the Witwatersrand, Johannesburg, South Africa

thought of researchers in the future in the area of hybrid techniques and neural network modeling. The study significantly contributes to advancing sustainable waste biomass valorization and water remediation strategies while aligning with global objectives in waste management and the circular economy.

Graphical Abstract

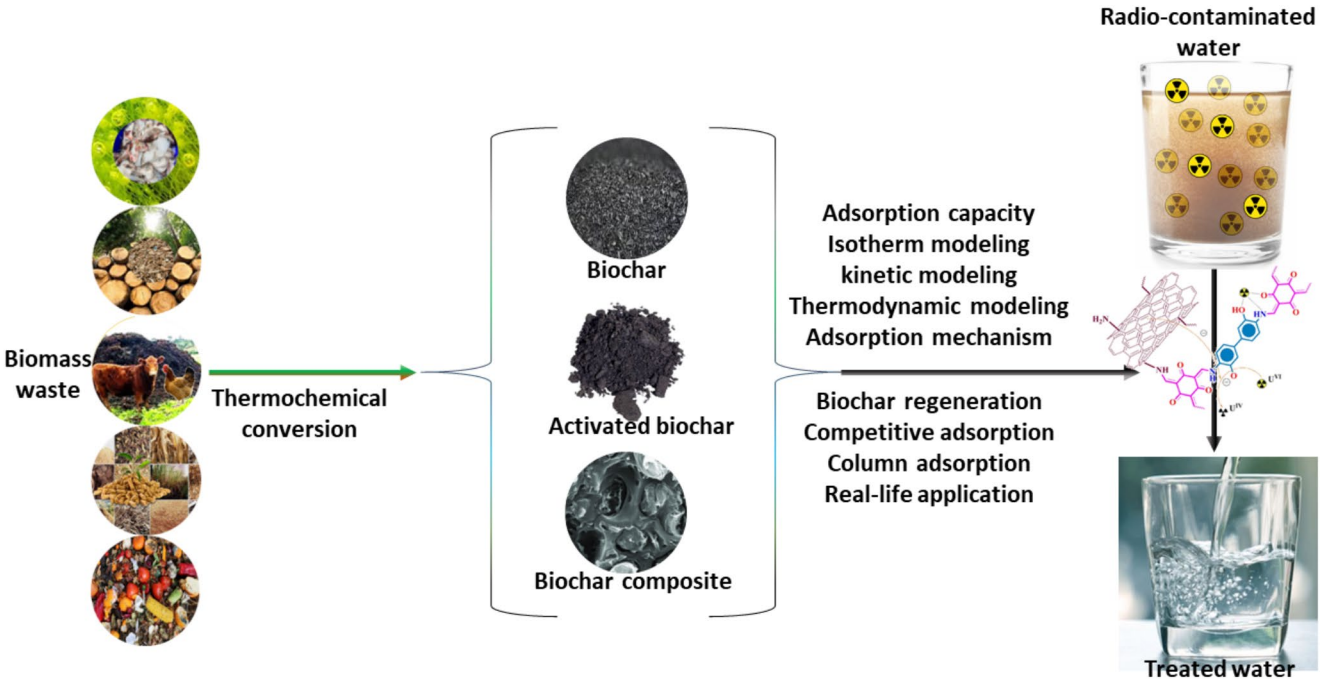

Keywords Adsorption · Biochar · Circular economy · Radionuclide pollutant · Sustainable development goal (SDG)

Introduction

Radioactive pollutants and biomass waste continue to pose an imminent danger to the environment, especially to the water bodies, the lifeline of all ecosystems. In particular, because of the continuous development of nuclear technology, increasing trends in the expansion of the application scope of nuclear engineering [1, 2], wars, ship accidents, plane crashes, unregulated release of spent nuclear fuel, metal smelting, electroplating, nuclear medicine, mining, and agricultural radiology, radioactive contamination has emerged as one of the most serious environmental issues [2, 3]. Also, it has been reported that up to 617,294 pounds of biomass waste are generated worldwide and the worst hazard to human existence, particularly for future generations, is the daily disposal of a sizable amount of this biomass waste into the earth and the marine system [4]. More specifically, according to statistics, biomass waste, including food waste from food processing companies and agricultural waste from farms constitutes about 49% of municipal solid waste because of the farming business and food production that has grown rapidly in reaction to increasing industrialization and global population expansion [5, 6]. In fact, it is predicted that over the next 50 years, we may lose over 5–8% of our arable land and probably face new illnesses, genetic mutation, food poisoning, respiratory issues, and an ecological calamity associated with water insecurity if we keep disposing of this biomass waste at the present tempo [4, 7]. Therefore, managing biomass waste is one of the 21st century's most important responsibilities and the transition towards a circular economy through the conversion of waste to valuable materials like biochar (BC) using various thermochemical techniques has emerged as one of the best feasible options to maximize biomass waste potential [8–11]. The biochar produced from the thermochemical conversion of biomass waste has a better surface area, does not require activation like activated carbon, and is rich in functional groups that make it a better adsorbent in adsorption operation [10, 12–14]. The adsorption technique is one of the oldest, most inexpensive, and effective methods among available radio-contaminant remediation techniques [2, 3]. Moreover, the adsorption method is simple, industrializable, does not generate many secondary pollutants, removes radio-contaminants in aqueous media at very low

concentrations and the adsorbent e.g. biochar can be recovered, regenerated, and reused [2, 15, 16].

Notably, based on our wide literature survey, there are review works on the application of biomass waste-derived biochar for the removal of pollutants like dye, heavy metals, etc., and the removal of radio-contaminants using materials like metallic nanoparticles, covalent organic frameworks, etc. Interestingly, to the best of our knowledge, there is no single review on the application of biomass waste-derived biochar for the adsorptive sequestration of radio-contaminants. Thus, this present study takes its novelty in being the first review paper comprehensively directed toward the adsorption of radio-contaminants using biomass waste-derived biochar.

The prime goal of this review study is to afford an in-depth discussion of the state-of-the-art pragmatic advances on the adsorptive removal of radio-contaminants from aqueous environments using biomass waste-derived biochar. Specifically, the adsorption capacity of different BWDBCs for various hazardous radio-contaminants was evaluated. In addition, this study delivers insightful information on different model interpretations by critically dissecting adsorption isotherms, kinetics, and thermodynamics regarding radio-contaminant sequestration by BWDBC. This work also logically examined the stability and reusability of spent BWDBCs as this is among the main factors influencing the widespread adoption of BWDBC by investors, and environmental and industrial engineers. An elaborate elucidation of the radio-contaminant adsorption mechanism was also provided. Works on authentic radio-wastewater clean-up and competitive adsorption scenarios were also reviewed.

The above-mentioned review objectives were accomplished by evaluating and summarising the extensive body of literature pertaining to the topic, pinpointing important pragmatic findings on particular research domains, figuring out problematic issues and knowledge gaps that could provide a basis for future research endeavors, and projecting future research hotspots.

Properties of Biomass Waste-Derived Biochars

Regardless of the thermochemical technique employed for the valorization of biomass waste into biochar, characterizing the as-produced biochar and examining its architectural properties offers valuable clarity into its functionality, stability, durability, degradability, recyclability, suitability, sustainability, and general applicability as an adsorbing material, particularly in adsorptive cleanup strategies [17, 18]. Notably, various factors have been shown to be responsible for the properties of biochar, including the kind of feedstock, operational temperature, and duration [17, 19]. Figure 1 briefly presents some frequently used methods for characterizing and extracting data on the properties of biochar based on the information they may offer [18]. The next paragraphs focus on summarily elaborating on some of these important biochar properties, including morphology,

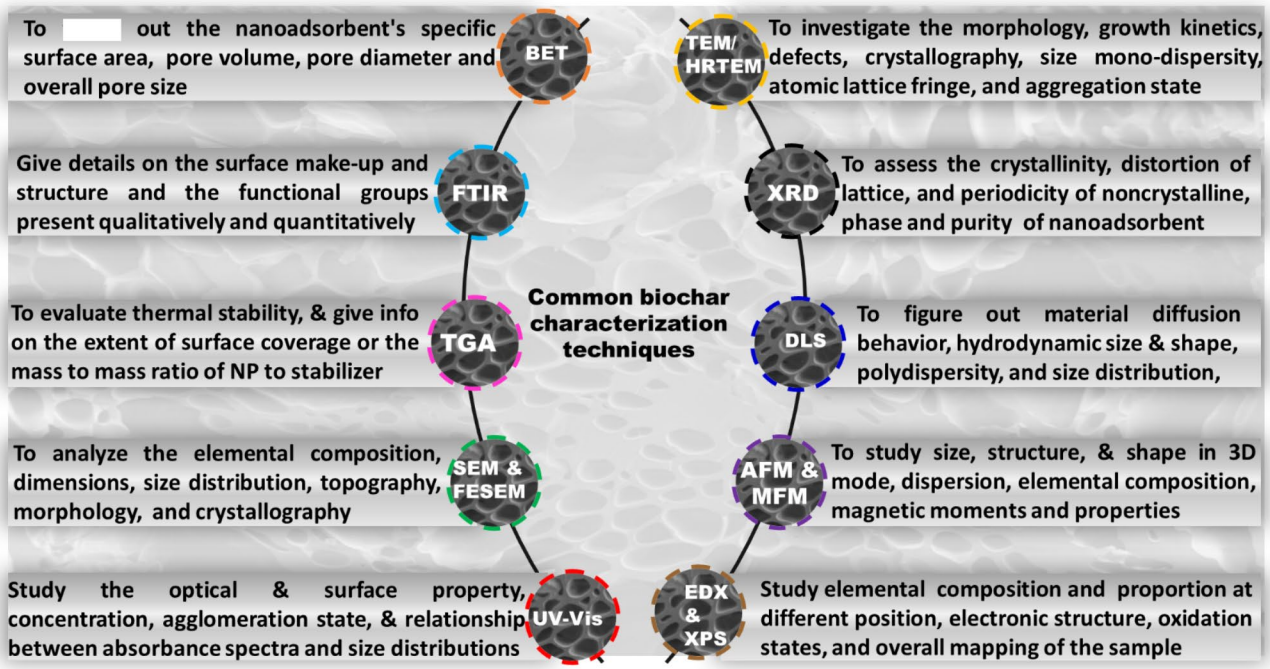

Fig. 1 Common biochar characterization techniques [18]

pore size, specific surface area, functional group, and pore volumes.

Surface Charge and Functional Group

Notably, for efficient radio-contaminant removal, the surface charge of the biochar determines how it interacts and binds with the adsorbate throughout the adsorption process. However, the architectural functional group determines the kind and strength of biochar surface charge. Furthermore, using data on the biochar's surface charge provides a great hint regarding the adsorption mechanism [18]. For instance, biochars that are rich in functional groups usually have a higher point of zero charge (pH_{pzc}) compared to those that are not rich in oxygenated functional groups [20]. A high pHpzc can result in good electrostatic interactions between the radio-contaminant and the biochar surface, thus, facilitating excellent adsorption operation [20, 21]. Moreover, biochars with pHpzc < pH are negatively charged (largely due to protonation of functional groups) and thus can adsorb cationic radio-contaminants [22–24] while biochars with pHpzc > pH are positively charged (largely due to deprotonation of functional groups) and thus can adsorb anionic radio-contaminants [23, 25, 26]. Additionally, research has also shown that inner-sphere and outer-sphere surface complexation governs the uptake of radio-contaminant when pHpzc > pH and pHpzc < pH respectively [27]. The functional groups are usually determined by FTIR [28], whilst the concentration of oxygenated surface functional groups on the biochar is measured by Boehm titration [23, 26]. Interestingly, functional groups, such as C = O [29, 30], OH [28, 31], COOH [32, 33], NH_2 [34, 35], etc., typically work as complexing/coordinating agents during the adsorption operation and offer vital guidance on the elucidation of the mechanism of biochar-radio-contaminant interaction. In addition, when cleaning up radio-contaminant water, the oxygen-bearing/polar functional groups normally act as vacant adsorption sites to facilitate adsorption operation [23]. The details about radio-contaminant uptake mechanisms by various biomass waste-derived biochars are discussed in the next session.

Shape/Morphology

The shape of biochars has a significant impact on how they interact with the adsorbate (radio-contaminant). The optimal response of the adsorption-desorption system during pollutant cleanup operations is determined by the shape of the material [17, 18]. Remarkable, advancement has been achieved in developing more potent biomass waste-derived biochar for radio-contaminant remediation by better understanding how the shapes of material. Morphologically, it has been speculated that triangular shapes are formed at lower temperatures while spherical/irregular shapes are usually formed at high temperatures [18]. Moreover, owing to the volatilization and decomposition of biomass waste structural components such as alkaloids, saponins, tannins, and flavonoids during the thermochemical process, irregular morphology is usually observed [36]. Also, according to Bai's research group [37], complex biomass composition can as well result in biochar with irregular shape. Furthermore, because the precursor/starting biomass waste material has distinct inherent geometries, several studies have empirically demonstrated that the biomass precursor can influence the form of the generated biochar [38].

Surface Area Pore Volume, and Size/Diameter

Generally, biochar surface area and size determine how well the adsorption system works during the pollutant cleanup process [18, 39]. The surface area is the primary indication of an accessible adsorption site and adsorption capacity, and it is typically characterized by the BET method [28, 34]. In conjunction, the average particle size, volume (PV), and pore diameter/size (PD/S), an index of the typical total volume and width of the material pores [34], significantly influence the adsorbate binding behavior and adsorptive performance of biochar. Data of the SSA, PV, and PS of many biochars that have been reported in scientific publications for the sorption of radio-contaminants is shown in Table 1. Notably, following the IUPAC pore diameter classification [40, 41], the majority of biochars that have been used for the removal of radio-contaminants fall within the mesoporous caliber of material with PD of 2–50 nm [34, 37, 42, 43] while very few are microporous with PD of < 2 nm [44–47]. Based on one or two studies, it can also be deduced that biomass waste-derived biochar composite usually has improved surface area, PV, and PS in comparison to the bare version [43, 47–49]. Similarly, activated biochar has better properties compared to un-activated biochar [20]. In addition, studies have also revealed that an upsurge in biomass waste thermochemical conversion process leads to an upsurge in surface area and pore volume [37]. The better the surface area, and porosity, the better the radio-contaminant adsorption output. In summary, the surface of the biochar becomes more reactive with adsorbates with size biochar size reduction, leading to an exponential increase in SSA in relation to volume and a dose-dependent increase in adsorption efficiency [18].

Table 1 Summary of important properties of biomass waste-derived biochar used for the adsorption of radio-contaminants

Biomass waste biochar	Morphology	SSA (m^2g^{-1})	PV (cm^3g^{-1})	PD (nm)	References
Lotus seedpods	Thin nanosheet	65.21	0.20	12.34	[34]
Artemia egg shell@Cu_2O/Cu^0	Amorphous	13	0.045	7.8	[50]
Salvadora persica branches	Irregular	9.05	-	-	[36]
Peach wood garden waste + urban sludge	-	2.22–150	0.02–0.15	10–40	[37]
Reed straw	Rough	50.147	0.167	6.487	[30]
Spent coffee ground@ bismuth	Spherical	124.5	0.063	5.7	[48]
Spent coffee	Rough and wrinkled	2.8	0.007	3.1	[20]
Bamboo powder	Tubular	-	-	-	[51]
KOH-activated peanut shell	Irregular	172.23	0.31	-	[39]
Orange peel@magnesium silicate	Nanosheets	73.9	-	20–40	[43]
Acidosasa edulis shoot shell	Irregular	6.368	0.008516	5.35	[23]
Watermelon rind@ Fe_3O_4	-	86.35	0.03	-	[49]
Rice husk@Fe_2O_3	Fine granular and fibrous	109.65	0.21	7.55	[22]
Soybean pods@Prussian blue	Cubic	496.21	0.13	3.17	[38]
Lotus seedpods@NH_2	Thin nanosheet	20.65	0.06	11.41	[34]
Citrullus lanatus L. seeds@$MnFe_2O_4$	Fine granular and fibrous	-	-	-	[52]
Bamboo powder@ MoS_2-PO_4	Flower-like	-	-	-	[51]
Corn straws@$ZnFe_2O_4$	Octahedral	523	0.32	3.29	[53]
Luffa rattan	Irregular	-	-	-	[54]
Woody + leaf waste	-	10	0.010	-	[24]
Rice straw (Oxidized)	Fine granular and fibrous	-	-	-	[33]
Banana peel@Fe_3O_4	Irregular and spherical	-	-	-	[55]
NaOH-activated spent coffee	Smooth	664.6	0.225	3.8	[20]
Rice straw	Amorphous and fiber-like	167	0.164	2.8	[56]
Spent coffee grounds@$FeCl_3$	Irregular	431.7	0.186	1.7[a]	[47]
Matamba fruit shell	Irregular honeycomb and concave	-	-	-	[57]
KOH-activated fish scales	Irregular	1074.73	0.829625	1.5450[a]	[46]
Coconut shell@ $Ti_3C_2T_x$ and@polydopamine@ polyethyleneimine	Sheet	51.6	0.041	2.62	[58]
Bamboo residues@polyethyleneimine@NaOH	Irregular	-	-	-	[35]
H_2O_2-modified residual coffee waste	-	4.8	0.005	4.2	[59]
Camphor wood sawdust@GO	Sheet-like	97	0.124	0.724[a]	[45]
Oil palm frond	-	366.6	0.176	3.3	[60]
Camphor tree leaves	Flake	65.91	15.14	-	[25]
NaOH@H_2O_2-modified residual coffee waste	-	5.9	0.006	4.1	[59]
Magnetic crayfish shells	Regular honeycomb	38.12	0.18	14.41	[61]
Microcystis@Fe_3O_4	Spherical	-	-	-	[27]
horse manure@Bi_2O_3	Spherical	-	-	-	[62]
Residual coffee waste	-	6.6	0.008	7.4	[59]
Bamboo residues@polyethyleneimine@HNO_3	Irregular	-	-	-	[35]
Palm kernel shell	-	377.0	0.169	2.8	[60]
KOH-activated bamboo shoot shell	Fibrous cylindrical	2412	1.26	1.42[a]	[44]
Phosphorus-doped pomelo peel	Sponge-like	1521	2.50	7.26	[63]
Spent coffee grounds	Irregular	11.02	0.009	3.39	[21]
Spent coffee ground	Irregular	4.9	0.005	8.0	[48]
Matamba fruit shell	Honeycomb and irregular hollow-rounded-inward concaves	-	-	-	[64]

[a] = microporous, [b] = mesoporous

Summary of the Mechanism of Radio-Contaminant Uptake by BWDBC

Generally, to fully comprehend radio-contaminant uptake accurately, it is necessary to analyze the chemical and physical interaction mechanisms between the radio-nuclide ion and BWDBC. Moreover, having a thorough understanding of the adsorption mechanism is crucial in designing a workable adsorption system and improving the quality of the adsorbent. In this section, the nature of the adsorption mechanism of different radio-contaminants by various biomass waste-derived biochar is summarily discussed and comprehensively presented in Table 2 as reported based on experiments and characterization. In addition, functional groups participating in the radio-contaminant sorption operation were also summarized in this table for better understanding and clarity. As observed in Table 2, except for amino/imine/amide/amine groups [25, 34–36, 46, 48, 58], C=C [43, 49] C-C [22] and phosphate group [65] the main BWDBC functional groups participating in the adsorption of various radio-contaminants are the oxygen-containing groups, particularly the hydroxy, carbonyl, and carboxyl groups. In addition, oxygen-containing groups like Mg-O-Si and $Mg(OH)_2$ as in the case of adsorption of U^{6+} using orange peel@magnesium silicate BC [43], SiOH as in the case of adsorption of Sr^{2+} [32, 56] and Ba^{2+} using rice straw biochar, Fe–O, P-O and P=O for the adsorption of U^{6+} using magnetized watermelon rind [49], bamboo powder@ MoS_2-PO_4 [51] and $KMnO_4$-modified pig manure [66] biochar respectively is also participating functional group in the adsorption of the aforementioned radio-contaminants. Specifically, spectroscopic analysis like XPS, XRD, and FTIR has been employed in identifying the specific functional groups and surfaces involved in interactions through the evaluation of shift in various peaks assignment, which also makes it possible to determine the chemical bonds that underlie chemical or physical interactions during radio-contaminant adsorption [2].

Furthermore, the involvement of oxygen-containing functional groups has also been confirmed using density function theory (DFT). For example, in the adsorption of Sr^{2+} using residual coffee waste-based biochar, the binding free energies between Sr^{2+} and carboxylic, carbonyl, and alcohol functional groups on the surfaces of biochar were simulated by DFT using the $C_{54}H_{18}$ graphene frameworks as shown in Fig. 2 [59]. Similarly, as shown in Fig. 3, DFT simulation was also employed to analyze the involvement of the OH group in the adsorption of Cs^+ using biochar from coconut shell@ $Ti_3C_2T_x$ and@polydopamine@ polyethyleneimine [58]. In conclusion, Table 2 shows that chelation/complexation (especially inner-sphere complexation), pore diffusion, ion exchange, π electrons coordination, precipitation, van der Waals forces, covalent bonding, π-π interactions, and electrostatic interactions/attractions via various functional groups mentioned above are the main mechanism governing the adsorption of radio-contaminants by biomass waste-derived biochar.

Adsorption Performance Evaluation of Biomass Waste-Derived Biochar for Radionuclide Pollutant

The performance of the biomass waste-derived biochar in adsorbing radio-contaminants from the aqueous environment is covered in this section. The maximum adsorption capacity (q_{max}) is used to report performance. Because removal efficiency is so reliant on the initial radio-contaminant concentration and the BWDBC dose, this won't provide an accurate picture of the performance of the BWDBC and thus was not employed. Conversely, the adsorption capacity denotes the innate ability of the particular BWDBC for radio-contaminants. The temperature and pH of the adsorption affect the BWDBC's performance. Table 3 presents these parameters in addition to the q_{max} values which can be found by experiments or isotherms like Langmuir [82].

For example, to eliminate Cs^+ and Sr^{2+} radio-contaminants from water, three gasified BCs made from combinations of wood, chicken manure, and food waste biomass, as well as KOH-activated BC (40% food waste + 60% wood) were utilized. The KOH-activated BC derived from food waste and wood biomass showed the highest q_{max} of 43.0 and 62.7 mg/g for Sr^{2+} and Cs^+ respectively among the biomass waste-derived BCs employed. This superior adsorption output by the KOH-activated BC was opined to be due to the enrichment impact of the functional groups as a result of alkaline activation as demonstrated in the FTIR analysis before and after adsorption as shown in Fig. 4a-d [28]. The q_{max} obtained for the removal of Cs^+ by the KOH-activated BC is also superior to the one (20.5 mg/g) reported for garden waste biomass-derived biochar containing woody and leaf waste [24]. However, the q_{max} recorded for Sr^{2+} by the KOH-activated BC is inferior to the 133.11 mg/g and 120.0 mg/g reported for the adsorption of Sr^{2+} by KOH-activated peanut shell [39] and rice straw [32]. In another study, Bamboo shoot shell BC and its composite containing ZnO NPs (BC@ZnO) were explored for the removal of TcO_4- using ReO_4- surrogate. According to the Langmuir isotherm, Bamboo shoot shell BC@ZnO's q_{max} for TcO_4- adsorbed was 25.916 mg/g, almost two times greater than Bamboo shoot shell BCs with adsorption capacity of 13.417 mg/g. The higher sorption capacity of Bamboo shoot shell BC@ZnO over Bamboo shoot shell BC is most likely due to the presence of ZnO nanoparticles, which enhances

Table 2 Overview of adsorption mechanism of radio-contaminants by biomass waste-derived biochar

Biomass waste biochar	Radionuclide pollutant adsorbed	Mechanism	Functional group	References
lotus seedpods	U^{6+}	Complexation	amino, carboxyl, and hydroxyl	[34]
Mesquite wood waste	Cs^{+}	cation-π interaction, aromatic π-system interaction, covalent bonding, outer-sphere complexation, and ESI	OH, NH_2, and COOH	[28]
rice straw	U^{6+}	surface complexation, chemisorption, inner-sphere complexation	-	[33]
Salvadora persica branches	Th^{4+}	IEX interaction, chemisorption, and chelation	amino groups and oxygen of hydroxyl and carbonyl groups	[36]
reed straw	U^{6+}	Chemisorption and complexation	O-H and C=O	[30]
Mesquite wood waste+chicken manure	Cs^{+}	cation-π interaction, aromatic π-system interaction, covalent bonding, outer-sphere complexation, and ESI	OH, NH_2, and COOH	[28]
spent coffee ground@ bismuth	I^{-}	ESA	+vely charged amide groups	[48]
spent coffee	Sr^{2+}	Physisorption, ESA, van der Waals forces, and π electrons coordination	O-containing groups	[20]
bamboo powder@MoS_2	U^{6+}	covalent bond interaction and chemisorption	C-O	[51]
KOH-activated peanut shell	Sr^{2+}	Chemisorption	OH and C–H	[39]
macauba endocarp	U^{6+}	Chemisorption	hydroxyls and carboxylic acids	[67]
camphor leaves@Bi_2O_3	I_2	coordination complex and chemisorption	OH	[68]
orange peel@magnesium silicate	U^{6+}	inner-sphere surface complexion	C=C, C-OH, C=O, Mg-O-Si and $Mg(OH)_2$	[43]
rice straw	Sr^{2+}	ESA, IEX, outer-sphere surface complexation, physisorption, and chemisorption	COOH and SiOH	[32]
Mesquite wood waste+food waste	Cs^{+}	cation-π interaction, aromatic π-system interaction, covalent bonding, outer-sphere complexation, and ESI	OH, NH_2, and COOH	[28]
Acidosasa edulis shoot shell	Tc^{7+}	outer-sphere complexation and electronic attraction	hydroxyl and carboxyl groups	[23]
Salvadora persica branches	U^{6+}	IEX interaction, chemisorption, and chelation	amino groups and oxygen of hydroxyl and carbonyl groups	[36]
KOH-activated Mesquite wood waste+food waste	Cs^{+}	cation-π interaction, aromatic π-system interaction, covalent bonding, outer-sphere complexation, and ESI	OH, NH_2, and COOH	[28]
HNO_3-modified Cow manure	U^{6+}	surface complexation and ESI	Carboxyl groups	[69]
corn stalk	IO_3^{-}	Chemisorption, IEX, ESA, and oxidation-reduction	hydroxyl, carboxyl, and ester groups	[31]
spent coffee	Co^{2+}	Physisorption, ESA, van der Waals forces, and π electrons coordination	O-containing groups	[20]
Fe_3O_4@pine needles	U^{6+}	inner-sphere complexation and cation-π interaction	carboxylic and hydroxyl groups	[70]
Mesquite wood waste	Sr^{2+}	Chelation, outer-sphere complexation, and ESI	OH,–NH_2, and–COOH	[28]
Magnetized watermelon rind	U^{6+}	IEX, inner surface complexation, ESI, complex surface coordination, and precipitation	OH, C=C, C–H, C–O, and Fe–O	[49]
rice husk@Fe_2O_3	U^{6+}	inner-sphere surface complexation and chemisorption	C-C, OH, C=C, C-O, C=O, O-C=O and ferrites oxygen	[22]
soybean pods@Prussian blue	Cs^{+}	Chemisorption, weak van der Waals effect, and complexation	oxygen-containing groups	[38]

Table 2 (continued)

Biomass waste biochar	Radionuclide pollutant adsorbed	Mechanism	Functional group	References
Mesquite wood waste + chicken manure	Sr^{2+}	Chelation, outer-sphere complexation, and ESI	OH, NH_2, and COOH	[28]
corn stalk	IO_3^-	Chemisorption, IEX, ESA, and oxidation-reduction	hydroxyl, carboxyl, and ester groups	[31]
Citrullus lanatus L. seeds@$MnFe_2O_4$	U^{6+}	Complexation and chemisorption	carbonyls, hydroxyls, and some carboxylic groups	[52]
Bamboo shoot shell@ZnO	Tc^{7+}	Complexation and chemisorption		[71]
bamboo powder@ MoS_2-PO_4	U^{6+}	covalent bond interaction and chemisorption	P-O and C-O	[51]
Mesquite wood waste + food waste	Sr^{2+}	Chelation, outer-sphere complexation, and ESI	OH, NH_2, and COOH	[28]
Corn straws@$ZnFe_2O_4$	Th^{4+}	Complexation	carboxyl group and a hydroxyl group	[53]
Luffa rattan	U^{6+}	ESI, complexation, and physical adsorption	carboxyl groups and hydroxyl groups	[54]
Woody + leaf waste	Cs^+	Complexation and π-π interactions	Oxygen-containing groups	[24]
rice straw (Oxidized)	U^{6+}	surface complexation, chemisorption, inner-sphere complexation	OH, COOH and C–O	[33]
Fe_3O_4@banana peel	Sr^{2+}	IEX		[55]
NaOH-activated spent coffee	Ba^{2+}	Chemisorption, ESA, π electrons coordination, surface complexation, and IEX	O-containing groups	[20]
rice straw	Sr^{2+}	weak IEX, chemisorption, complexation, and pore-filling	COOH, OH, and SiOH	[56]
spent coffee grounds@$FeCl_3$	Sr^{2+}	Chemisorption, inner layer complexation, Van der Wall's force, and outer-sphere complexation		[47]
Wheat straw	U^{6+}	IEX, chemisorption, complexation, ESI, pore filling, H-bond, and π-πinteraction	carbonyl, carboxyl, and hydroxyl groups	[72]
KOH-activated Mesquite wood waste + food waste	Sr^{2+}	Chelation, outer-sphere complexation, and ESI	OH, NH_2, and COOH	[28]
palm tree fibers	Th^{4+}	inner-sphere complexation	Carboxylic	[73]
NaOH-activated spent coffee	Co^{2+}	Chemisorption, ESA, π electrons coordination, surface complexation, and IEX	O-containing groups	[20]
pine needles	U^{6+}	ESI		[74]
Opuntia ficusindica cactus fibres	Th^{4+}	inner-sphere complexation	Carboxylic	[75]
spent coffee	Ba^{2+}	Physisorption, ESA, van der Waals forces, and π electrons coordination	O-containing groups	[20]
KOH-activated fish scales	U^{6+}	Chemisorption and inner-sphere surface complexation	Carboxyl and amino groups	[46]
Wheat straw	Th^{4+}	IEX, chemisorption, complexation, ESI, pore filling, H-bond, and π-πinteraction	carbonyl, carboxyl, and hydroxyl groups	[72]
H_2O_2-modified pig manure	U^{6+}	surface complexation, chemisorption, micropore filling, ESA, and IEX		[66]
corn cob	U^{6+}	surface complexation, ESA, and precipitation	OH, and COOH	[76]
coconut shell@ $Ti_3C_2T_x$ and@polydopamine@ polyethyleneimine	Cs^+	Chemisorption and coordination	hydroxyl and amino groups	[58]
Bamboo residues@polyethyleneimine@NaOH	U^{6+}	inner-sphere surface complexation, amide bonding, acetal linkage, imine bonding and H-bonding	Imine, amide, and amine groups	[35]
H_2O_2-modified residual coffee waste	Sr^{2+}	ESI, outer-sphere adsorption, and IEX	Carbonyls	[59]

Table 2 (continued)

Biomass waste biochar	Radionuclide pollutant adsorbed	Mechanism	Functional group	References
cotton straw	U^{6+}	Chemisorption and complexation	phosphate group and oxygen-containing groups	[65]
Olive pomace	Th^{4+}	Chemisorption and ESI		[77]
NaOH-activated spent coffee	Sr^{2+}	Chemisorption, ESA, π electrons coordination, surface complexation, and IEX	O-containing groups	[20]
$KMnO_4$-modified pig manure	U^{6+}	surface complexation, chemisorption, micropore filling, ESA, and IEX	NH_2, P=O and OH	[66]
rice straw	Ba^{2+}	weak IEX, chemisorption, complexation, and pore-filling	COOH, OH, and SiOH	[56]
HNO_3-modified wheat straw	U^{6+}	surface complexation and ESI	Carboxyl groups	[69]
cow manure@ TiO_2@SiO_2	Th^{4+}	complexation	hydroxyl groups	[78]
camphor wood sawdust@GO	Sr^{2+}	Chemisorption	hydroxyl, carboxyl, and carbonyl groups	[45]
camphor tree leaves	U^{6+}	ESA, inner-sphere surface complexation, and chemisorption	hydroxyl, carboxyl, and amine groups	[25]
NaOH@H_2O_2-modified residual coffee waste	Sr^{2+}	ESI, chemisorption, outer-sphere adsorption, and IEX	carboxylic acids	[59]
watermelon rind	U^{6+}	inner surface complexation, ESI, complex surface coordination, and precipitation	OH, C=C, C–H, and C–O	[49]
magnetic crayfish shells	Sr^{2+}	Chemisorption and IEX		[61]
Microcystis@Fe_3O_4	U^{6+}	inner-sphere and outer-sphere surface complexation	oxygen-containing groups	[27]
bamboo shoot shell	Tc^{7+}	Chemisorption, ESI, and redox interaction	hydroxyl and carboxyl group	[29]
horse manure@Bi_2O_3	U^{6+}	surface complexation, IEX, ESA, chemisorption precipitation, and reduction	oxygen-containing groups	[62]
Residual coffee waste	Sr^{2+}	ESI, outer-sphere adsorption, and IEX	carbonyls	[59]
Bamboo residues@polyethyleneimine@HNO_3	U^{6+}	inner-sphere surface complexation, amide bonding, acetal linkage, imine bonding and H-bonding	Imine, amide, and amine groups	[35]
teak peel	Sr^{2+}	IEX, chemisorption, weak van der Waals, ESA, and surface complexation	oxygen-containing group	[79]
KOH-activated bamboo shoot shell	Tc^{7+}	Chemisorption	oxygen-containing group	[44]
NaOH-modified peanut husk	Sr^{2+}	surface complexation	oxygen-containing group	[80]
spent coffee grounds	Sr^{2+}	chemisorption	oxygen-containing group	[21]
orange peel@MnO_2	U^{6+}	inner-sphere surface complexation and chemisorption		[42]
spent coffee ground	I^-	ESA	+vely charged amide groups	[48]
bamboo shoot shell	Tc^{7+}	ESI		[26]
coconut shell@ $Ti_3C_2T_x$ and@polydopamine@ polyethyleneimine	U^{6+}	Chemisorption and coordination	hydroxyl and amino groups	[58]
HNO_3 oxidized *Luffa cylindrica* sponges	Th^{4+}	inner-sphere surface complexation and IEX	Carboxylic and hydroxyl group	[81]
Matamba fruit shell	I^-	weak van der Waals forces, π-π electron donor-acceptor, ESI, and π-stacking interaction		[64]
cow manure@ TiO_2@SiO_2	U^{6+}	complexation	hydroxyl groups	[78]

Where Tc^{7+} is surrogated by Re^{7+} or Cr^{7+}, ESI=electrostatic interaction, ESA=electrostatic attraction, IEX=ion exchange

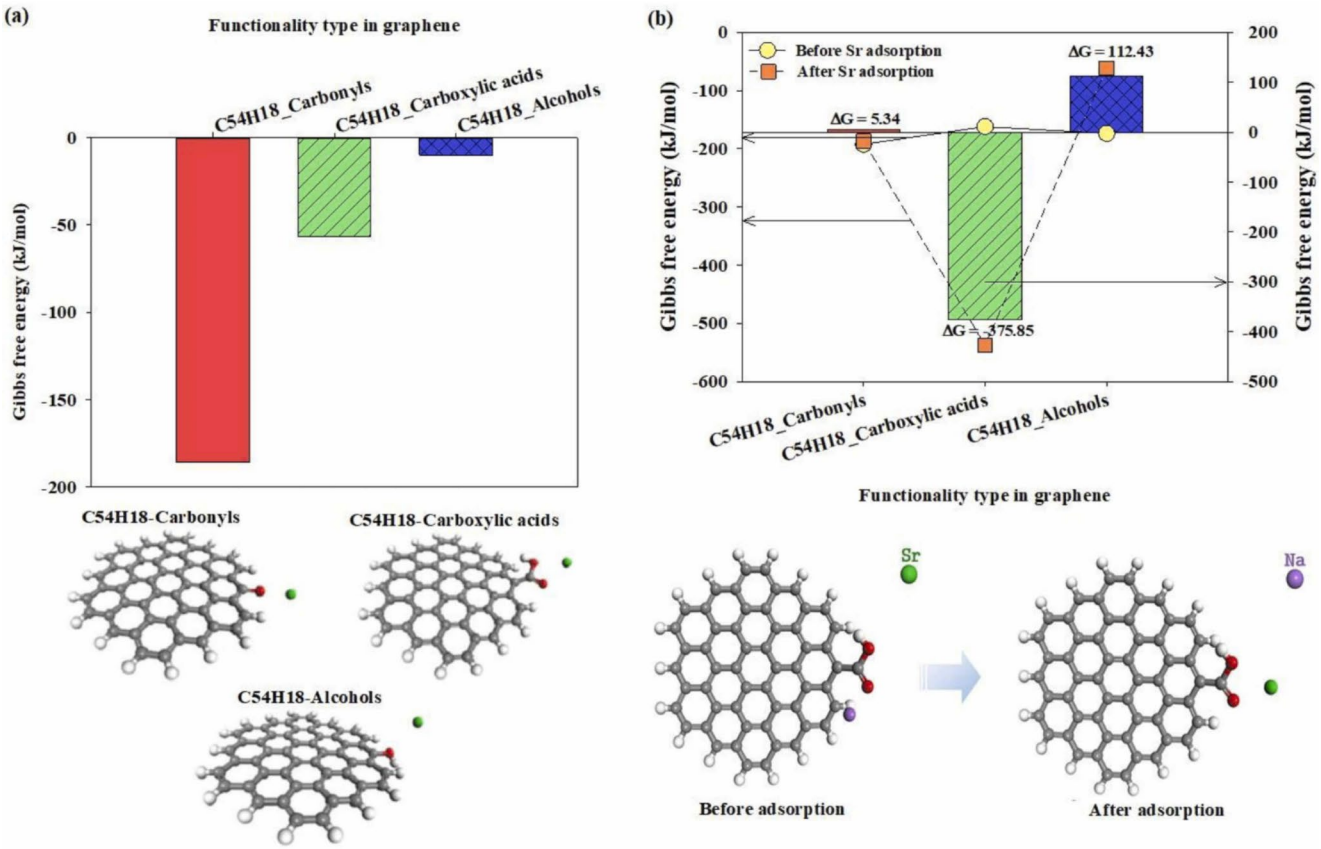

Fig. 2 The (**a**) binding free energy of Sr^{2+} to the $C_{54}H_{18}$ graphene frameworks decked with carboxylic, carbonyl, and alcohol and the (**b**) thermodynamic possibility of the Na-to-Sr replacement in the $C_{54}H_{18}$ graphene frameworks decked with and carboxylic, carbonyl, and alcohol functional group [59]

the sorption sites of Bamboo shoot shell BC@ZnO [71]. A remarkable adsorption performance of 590.8 mg/g was also recorded by calcium phosphate-modified cotton straw BC for the removal of U^{6+}. Notably, following adsorption, the XRD peak intensity rose (Fig. 4e), suggesting that modified cotton straw BC was successful in adsorbing U^{6+}. In addition, the BC FTIR spectra are shown in Fig. 4f, where a distinct, high-intensity peak at 921 cm^{-1} is visible upon U^{6+} adsorption. This peak represents the stretching vibration of O═U═O and shows that BC has been successful in adsorbing uranium [65].

In another experiment [33], oxidized biochar—which is produced by modifying biochar generated from rice straw—was effectively used as an efficient adsorbent for the removal of U^{6+} from contaminated water. Because of its large surface area, oxidized rice straw BC exhibited the highest U^{6+} adsorption capability when tested. Specifically, at pH 5.5, the highest adsorption quantity was reported by the Langmuir model to be 242.65 mg/g for oxidized rice straw BC in contrast to 162.54 mg/g for the non-oxidized rice straw BC. It was opined that the superior adsorption capacity of oxidized rice straw BC is due to an enhanced oxygen content following modification (oxidation) with nitric acid as shown in the EDS mapping in Fig. 5. Furthermore, it was accentuated that following U^{6+} adsorption, the FTIR spectra of oxidized rice straw BC revealed a new peak at about 911 cm^{-1}, which is associated with the stretching vibrations of the $[U=O=U]^{2+}$ linear structure. This peak's presence confirmed that uranyl ions were adsorbed by the oxidized biomass waste-derived biochar [33]. Also, Albayari's research team [36] synthesized a low-cost BC sorbent using waste *Salvadora persica* branches and employed the biomass waste-derived BC for the sequestration of U^{6+} and Th^{4+} radio-contaminants from water. This finding revealed that the highest elimination efficiencies for both U^{6+} and Th^{4+} are almost 99%, with the corresponding q_{max} of 85.71 mg/g and 84.97 mg/g [36]. This adsorption capacity is in close range with the one (81 mg/g) obtained for the adsorption of Th^{4+} by activated BC derived from *Opuntia ficusindica* cactus fibers [75].

Also, Li and co-workers [22] explored the adsorption of U^{6+} by rice husk@Fe_2O_3 BC. At pH 4, the maximum adsorption capacity was found to be 53.01 mg/g. Furthermore, the XPS study showed that U^{6+} sorbed by rice husk@

Fe_2O_3 BC was reduced to U^{4+} by Fe_3O_4. In addition, the SEM picture of rice husk@Fe_2O_3 BC before and following U^{6+} adsorption was displayed in Fig. 6a and **b**. A remarkably large number of NPs were disposed of on the surface of the porous BC. The EDS spectrum (Fig. 6b) shows that the primary constituents of the composites were U (26%), C (40%), O (20%), and Fe (14%). This indicates that the U^{6+} radio-pollutant was adsorbed onto the rice husk@Fe_2O_3 BC surface. Moreover, the five reflections observed in the original rice husk@Fe_2O_3 BC were enfeebled following U^{6+} uptake according to the XRD analysis as shown in Fig. 6c. Also, in contrast to raw rice husk@Fe_2O_3 BC, the OH band at 3432 cm^{-1} progressively grew broader and weaker, and following U^{6+} uptake, the C=O group band vanished as shown in the FTIR analysis displayed in Fig. 6d and this is in agreement with the XPS analysis which revealed that the manifestation of U 4f peak at 385.18 eV for U^{6+}-sorbed rice husk@Fe_2O_3 BC confirmed U^{6+} uptake by the biomass waste-derived BC composite [22].

Sun and co-workers [51] also investigated the adsorption of U^{6+} by bamboo powder@MoS_2-PO_4 BC and the maximum adsorption capacity was found to be 161.29 mg/g. In addition, from the SEM analysis image displayed in Fig. 7a-b, it was seen that after U^{6+} adsorption, bamboo powder@MoS_2-PO_4 BC retained its original flower-like cluster structure, suggesting that the BC composite exhibited strong structural stability. Moreover, the atomic ratio of oxygen and phosphorous dramatically dropped between the EDS data obtained before and after U^{6+} uptake as shown in Fig. 7c and **d** respectively, which may be related to P-O on the bamboo powder@MoS_2-PO_4 BC surface interacting with $[O=U=O]^{2+}$ [51].

In another report [72], wheat straw biochar was explored for the removal of U^{6+} and Th^{4+}. The biochar was found to demonstrate a remarkable adsorption capacity of 1527.02 and 1158.16 mg/L respectively at pH 5 and 20 °C. In addition, to clearly depict the structure of the biochar, SEM (Fig. 8A-C) and TEM (Fig. 8D-F) pictures of the material were acquired both before and after the uptake of U^{6+} and Th^{4+}. Specifically, the exterior and interior surfaces of the raw biochar without radionuclide adsorption had smooth pore walls. The BC surface and intra-pores become rough and bumpy when U^{6+} and Th^{4+} adsorption achieve equilibrium. The corrosion of the BC and the coating of radioactive ions might be the reason for this roughness. In addition, as shown in Fig. 8G and **H**, following U^{6+} and Th^{4+} uptake, the EDS spectra showed new peaks for U^{6+} and Th^{4+}, respectively, that were not present on the raw wheat straw BC [72]. Similarly, an excellent U^{6+} adsorption capacity of 369.9 mg/g, 661.7 mg/g, and 979.3 mg/g was also recorded for H_2O-modified pig manure BC, H_2O_2-modified pig manure BC, and $KMnO_4$-modified pig manure BC at pH 4 and a temperature of 25 °C [66].

The adsorption capacity of various BWDBCs for radio-contaminants is summarised in Table 3. Over the years, a large variety of BWDBCs have been used for radio-contaminant clean-up. Considering the threshold of q_{max} >1000 mg/g, wheat straw BWDBC stands out with 1527.02 mg/g q_{max} for U^{6+} and 1158.16 mg/g q_{max} for Th^{4+} at pH 5 and 20°C temperature [72] while $KMnO_4$-modified pig manure BC, camphor leaves@Bi_2O_3 BC, and cow manure@ TiO_2@SiO_2 BC came close from behind with q_{max} of 979.3 mg/g for U^{6+} [66], 885.8 mg/g for I^- [68], and 710.4 mg/g for Th^{4+} [78]. These BWDBCs have been noted to take up more radio-contaminant than their weight. In addition, the performance of the BWDBCs in terms of radio-contaminant sorption is dictated by its nature. Nano-BWDBCs often have tiny pore diameters and require more time for radio-contaminants to diffuse intra-particle prior to adsorption. However, its wide surface area, which promotes adsorption, is its main benefit. Moreover, the surfaces of BWDBCs produced by thermochemical methods are often heterogeneous [82]. These surfaces have a high potential for radio-contaminant sorption because they are energetically heterogeneous. They also have a range of functional groups that may interact chemically with radio-contaminants. More so, regarding the nature of the BWDBCs, Table 3 shows no discernible pattern because there are so many variables that might influence the adsorption process. Nevertheless, it was noticed that activated and or nanoparticle functionalized BWDBCs performed excellently than bare BWDBCs. Furthermore, the majority of radio-contaminant adsorption studies were carried out at an acid or near-neutral pH range at temperatures ranging from 15°C to 45°C and this is a testament to the fact that BWDBCs can be employed for the sequestration of radio-contaminants in harsh environments.

Equilibrium Isotherm and Kinetics Modeling

Equilibrium isotherms and kinetics modeling are crucial to adsorption technology and research [94]. They also offer helpful details for characterizing porous solids like BWDBC, gaining a deeper understanding of the adsorption mechanism, and controlling and designing cost-effective industrial-scale adsorption systems [23, 55, 95, 96]. The empirical findings of the isotherm and kinetic best fit for radio-contaminant adsorption in various literature are briefly reviewed in this segment and summarized in Table 4. Specifically, the surface orientation, active spot layout, and the kind of forces between the targeted adsorbate pollutant determine the adsorbent-adsorbate interaction and relationship throughout the adsorption operation. More specifically,

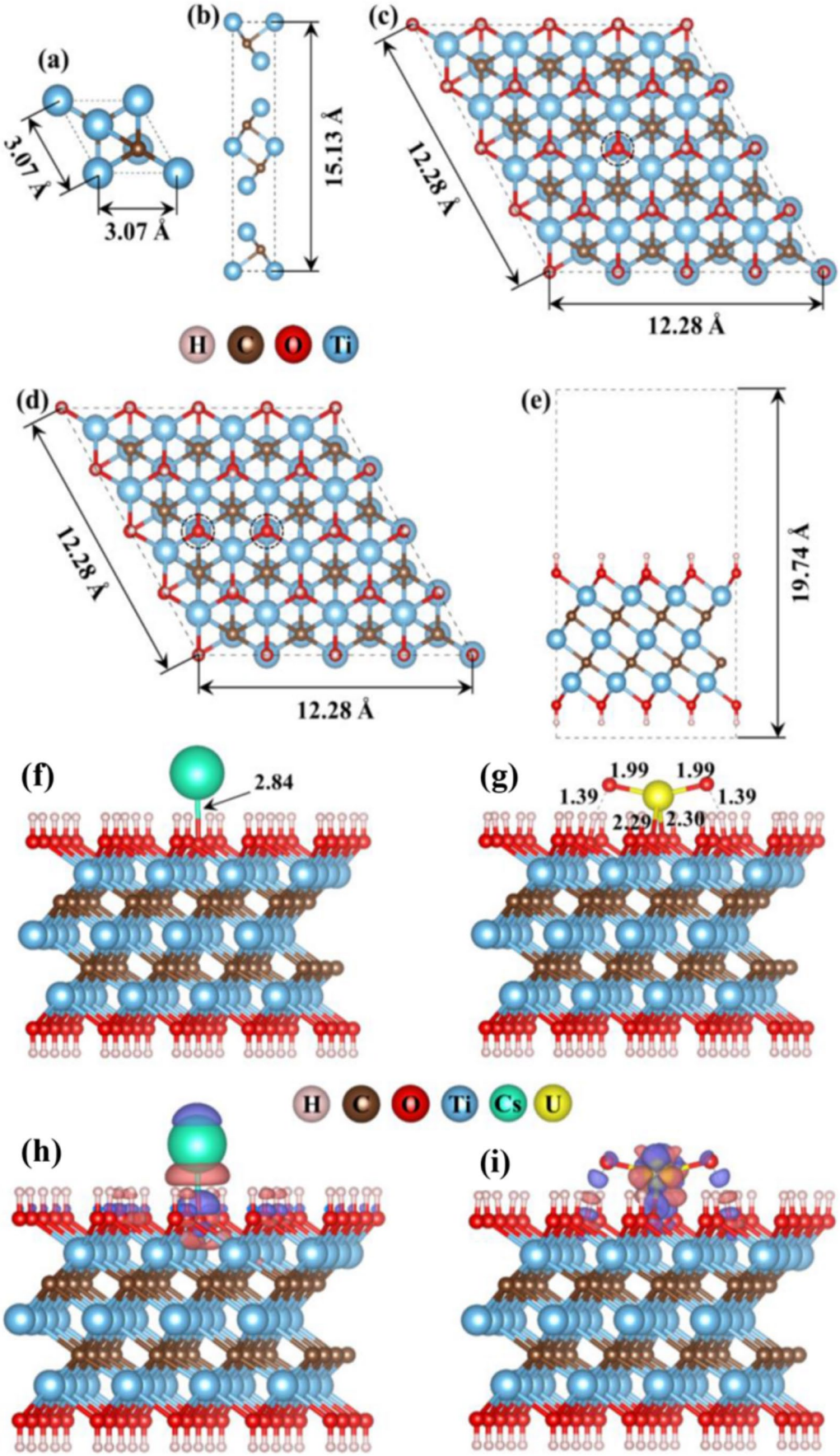
(a)
3.07 Å
3.07 Å
(b)
15.13 Å
(c)
12.28 Å
12.28 Å
H C O Ti
(d)
12.28 Å
12.28 Å
(e)
19.74 Å
(f)
2.84
(g)
1.99 1.99
1.39 1.39
2.29 2.30
H C O Ti Cs U
(h)
(i)

Fig. 3 The (**a**) top view and (**b**) lateral view of the unit cell for bare Ti_3C_2 MXene. The top views (**c, d**) together with a lateral view (**e**) of deprotonated $Ti_3C_2(OH)_2$ models and the deprotonated OH groups are highlighted by black circles. The optimized complex configuration of (**f**) $Ti_3C_2(OH)_2$-Cs and (**g**) $Ti_3C_2(OH)_2$-UO_2. Bond lengths were in Å. The differential charge density of (**h**) $Ti_3C_2(OH)_2$-Cs complex and (**i**) $Ti_3C_2(OH)_2$-UO_2 complex at charge density isosurface of 0.001 and 0.01 e/Bohr^3, respectively. The purple regions designated charge accumulation, and the pink areas epitomized charge depletion [58]

when the adsorption process achieves an equilibrium state, the adsorption isotherm shows how the targeted adsorbate distributes across the liquid and solid phases [95]. On the other hand, the adsorption kinetics is customarily described as a curve defining the time reliance of bulk solution radio-contaminant concentration during adsorption operation at a specific experimental process condition [2, 30, 95]. Notably, different models have been hypothesized for modeling the experimental isotherm and kinetic data from various radio-contaminant adsorption operations using BWDBC, and the optimum fit is usually established by how near their corresponding R^2 (coefficients of determination) is to one (1) [34]. As observed in the pool of literature presented in Table 4, it can be observed that with only a few exceptions, such as the Redlich–Peterson isotherm model [28, 33, 42, 44, 80], Temkin isotherm model [29, 55], and Sips [28, 33, 42], the Langmuir (LIM) classical model was revealed to be the best match in the vast majority of the radio-contaminant adsorption studies under consideration follow by Freundlich isotherm model (FIM). This finding suggests that the radio-contaminant adsorptions by various biomass waste-derived biochars are widely favored by reversible [91] monolayer adsorption because of their energetically homogeneous surface [28, 34, 91] followed by irreversible [91] multilayer adsorption on a heterogenous surface (just a few) [28, 34, 48, 91]. In addition, the LIM fitting also implied that the radio-contaminant uptake by BWDBC is governed largely by chemisorption (robust chemical interaction between radio-contaminant and the BWDBC functional groups) [20, 28, 36, 46], the adsorption output of each biochar active spot is identical with all the adsorption spots possessing alike adsorption energy, and radio-contaminant adsorbates do not interact with one another and neither do adjacent site affect each other throughout the adsorption operation [28, 34]. Conversely, FIM fitting implied that the radio-contaminant uptake by BWDBC is governed largely by physisorption and the biochar active spot has dissimilar affinities and uptake energies where the surface is continuously filled until the lower-energy spots are full, starting with the high-energy spots [2, 28, 34].

Furthermore, Table 4 shows that the kinetics of radio-contaminant adsorption by BWDBC are mostly pseudo-second-order (PSO) in the majority of the studies. Consequently, either the Elovich [64, 71, 83] or pseudo-first-order [20, 28, 46, 55, 59, 61] models were identified as the best-match models in very few other articles. As the chief best-match kinetic model, the pseudo-second-order posits that the rate of adsorption of radio-contaminant is directly proportional to the numerical strength of the available sites on the BWDBC [28] and the amount of radionuclide ions present in the solution. More so, the fitting of PSO suggests a chemisorption mechanism by many studies including [20, 28, 30, 34, 36, 48, 59], etc. as against PFO suggesting physisorption [20, 28, 59] and this corroborates the dominance of LIM. This chemisorb phenomenon might involve primarily chemical reactions between functional groups on BWDBC and the radio-contaminants as reported in the case of adsorption of Cs^+ and Sr^{2+} using KOH-activated Mesquite wood waste + food waste BC for example [28].

In addition, according to diffusion model summarized in Table 4, adsorption of radio-contaminants onto BWDBC from the aqueous phase involves tercet stages namely, film diffusion (the transport of the adsorbate from the bulk phase to the exterior surface of the BWDBC), intra-particle diffusion (the transport into the BWDBC by either pore diffusion and/or surface diffusion) and the adsorption on the surface of the BWDBC. The sulky of these stages, that is, the rate-limiting step, controls and determines the overall rate of the radio-contaminant adsorption operation. Many studies [33, 34, 42, 44, 48, 59] have shown that the intra-particle diffusion step is the only rate-limiting step, while a few others [36, 58, 66] have argued that it is not the only rate-limiting step. In conclusion, it can be inferred that adsorption isotherm and kinetics have a strong dependence on the chemical and/or physical characteristics of the biomass waste-derived biochar and the targeted radio-contaminants which also govern the adsorption mechanism [23].

Adsorption Thermodynamic

Without gainsaying, the significance of adsorption thermodynamics cannot be overstated, because it provides clarity on sorption spontaneity/favourability, the (exo)endothermic phenomena of the operation, system disorderliness/randomness, adsorption physicochemical characteristics and how temperature affects adsorption efficiency [2]. Moreover, the degree of electrostatic interaction mechanism between the biochar and radio-contaminant adsorbate at a certain temperature may be determined thermodynamically. Thus, one crucial element in the radio-contaminant adsorption system is the solution's temperature as it typically has an impact on the stability of the radionuclide-BWDBC complex and the ionization of the BC moieties, which in turn influences how the radio-contaminant and biomass waste-derived biochar interact [33, 80].

By and large, the nature of radio-contaminant uptake by biomass waste-derived biochar from temperature impact variations is expounded based on adsorption ΔG^o (free energy), ΔS^o (entropy), and ΔH^o (Gibbs enthalpy) [2]. The values of these thermodynamic parametric variables determined at different temperatures from various literature on the adsorption of radio-contaminants by BWDBC are listed in Table 5. The ΔG^o determines the physical adsorption that is driven by the mode of the energy interaction process, such as H-bonding, van der Waals, and the π–π interaction [12] between the BWDBC and radio-contaminants. A ΔG^o value less than zero indicates that the radio-contaminant adsorption process is spontaneous [21, 45, 72, 80] while a ΔG^o value above zero indicates that the adsorption is non-spontaneous [12]. Surprisingly, as observed in Table 5 the adsorption process of all radio-contaminants reported for various BWDBCs is spontaneous (negative ΔG^o) except for the adsorption of IO_3^- by corn stalk BC [31] Th^{4+} by Salvadora persica branches (at 313 K) [36] and Sr^{2+} by rice straw [32] where the ΔG^o values are positive. Nevertheless, it was accentuated that high temperature is favorable for the adsorption of the radio-contaminants [31, 32] and this is consistent with the high-temperature adsorption favourability report for other studies. Also, from the thermodynamic data presented in Table 5, a general pattern of increase in ΔG^o negativity (ΔG^o tends to minus scale) was observed in most cases as the temperature increases (283–333 K), demonstrating improved spontaneous radio-contaminant adsorption operation by BWDBC at high temperatures with a few exceptions as summarized in Table 5. This high-temperature favorability might be due to the fact that at elevated temperatures, the biochar pores get puffy, then triggering the activation of more surface sites [12]. In addition, it has been established that when the ΔG^o value is between −20 and 0 kJ/mol [2], the radio-contaminant adsorption mechanism is physisorption while if the ΔG^o value is between −400 and −80 kJ/mol, the mechanism will be chemisorption [2]. However, Choi's research group [55] differs in this regard as physisorption was insinuated despite the ΔG^o value being between −400 and −80 kJ/mol as seen in Table 5. Although, in a few cases [47, 51, 52, 72]where ΔG^o is < -20 kJ/mol but > -80 kJ/mol, a chemisorption mechanism was reported. As for the ΔH^o, the -ve (<0 kJ/mol) and +ve (>0 kJ/mol) values observed in Table 5 demonstrate that the uptake of radio-contaminants by BWDBC is either exothermic (emission of heat to the surroundings) or endothermic (gaining of heat from the surrounding) in nature, in substantiation with the temperature impact. More specifically, when the measured value of $\Delta H°$ goes lower than 21.0 kJ/mol or lies between 21.0 and 418.4 kJ/mol, it indicates that physisorption and chemisorption predominate in the radio-contaminant adsorption process, respectively [2]. Although, researchers [20, 80] opined that $\Delta H° < 40$ kJ/mol signifies the physisorption mechanism, while $\Delta H° > 40$ kJ/mol signifies the chemisorption mechanism. For example, in a particular study [20], it was observed that as the $\Delta H°$ crossed to above 40 kJ/mol (Table 5**)** for the adsorption of Co^{2+}, $Sr^{2+,}$ and Ba^{2+} using NaOH-activated spent coffee BC the adsorption mechanism changed from physisorption that was noted for $\Delta H° < 40$ kJ/mol using un-activated BC to chemisorption. The authors accentuated that such change is a result of NaOH activation which brings about the enhancement of O-containing functional groups [20]. This is consistent with the report of Kausar's team [80]. In their observation of the adsorption of Sr^{2+} using NaOH-modified peanut husk, the sorption mechanism was physisorption as the value of $\Delta H°$ was <40 kJ mol^{-1} [80]. Notably, a metric for assessing the degree of irregularity [12] between the molecules of the BWDBC and the radio-contaminant is ΔS^o. Specifically, the +ve value of ΔS^o for the uptake of radio-contaminant on various active sites of the BWDBC demonstrates an upsurge in adsorption randomness [35, 44, 59], and the attraction of the biochar for the radio-contaminant ions was high. The positive shift in entropy values in various previous research indicates that there is an upsurge in randomness at the solid-liquid interface during the adsorption operation as presented in Table 5. Moreover, at positive levels of ΔS^o, the mobility of radio-contaminant ions on the biochar surface site surges with temperature, leading to an upsurge in the kinetic energy of the radio-contaminant ions. Conversely, the negative value of ΔS^o indicates a decrease in randomness/disorderliness between the radio-contaminant ions and biomass waste-derived BC [35, 36, 39, 44, 48, 80]. Additionally, the reversibility of the adsorption process is implied by a -ve value of $\Delta S°$ and vice-versa [2]. In our opinion, the claim that $\Delta H° < 21.0$ or 40 kJ/mol is physisorption automatically includes all exothermic radio-contaminant adsorption operations, whereas, there are a few studies [36, 39, 44, 58] where the radio-contaminant adsorption is exothermic but the mechanism involve chemisorption. Thus, future researchers should pay attention to this ambiguity.

Regenerability and Recyclability Studies

The regenerability and recyclability performance of adsorbents like BWDBC play a practical role and have implications based on their technical viability, economic factors, and exploitation of resources when making an inclusive evaluation of the materials and method [33, 38, 65, 97]. More so, the regeneration and recyclability of the BC are the main two-in-one features for judging its commercialization probability [23, 98]. Thus, in this section, available works

Table 3 Overview of adsorption performance evaluation of biomass waste-derived biochar for radio-contaminants

Biomass waste biochar	Radionuclide pollutant adsorbed	q_{max} (mg/g)	pH	Temp (°C)	Method of q_{max} determination	References
lotus seedpods	U^{6+}	329.53	5	25	Langmuir	[34]
Mesquite wood waste	Cs^{+}	32.02		25	Langmuir	[28]
Artemia egg shell@Cu_2O/Cu^0	I^{-}	86.8	7	20		[50]
rice straw	U^{6+}	162.54	5.5	25	Langmuir	[33]
Salvadora persica branches	Th^{4+}	84.97	4	25	Langmuir	[36]
rice straw	Sr^{2+}	175.95	7	35	Langmuir	[83]
peach wood garden waste + urban sludge	I^{-}	223				[37]
reed straw	U^{6+}	46.35	5	25	Langmuir	[30]
Mesquite wood waste + chicken manure	Cs^{+}	36.21		25	Langmuir	[28]
spent coffee ground@ bismuth	I^{-}	253.71×10^{-3}	7	25	Experiment	[48]
spent coffee	Sr^{2+}	4.99	7	35	Langmuir	[20]
bamboo powder	U^{6+}	100.14	5.5	25	Langmuir	[51]
NaOH modified duckweed	Th^{4+}	104.1	~2.7	22	Langmuir	[84]
wheat straw + Sodium lignosulfonate	I^{-}	467.38		20		[85]
Cow manure	U^{6+}	64	4.5	25	Langmuir	[69]
KOH-activated peanut shell	Sr^{2+}	133.11	4.92		Langmuir	[39]
macauba endocarp	U^{6+}	417	3	25	Experiment	[67]
Bamboo shoot shell	Tc^{7+}	13.417	1	25	Langmuir	[71]
orange peel	U^{6+}	165.4	5.5	25.15	Langmuir	[42]
camphor leaves@Bi_2O_3	I_2	885.8			Langmuir	[68]
orange peel@magnesium silicate	U^{6+}	352.6	4	25	Langmuir	[43]
rice straw	Sr^{2+}	120.0	6		Experiment	[32]
Mesquite wood waste + food waste	Cs^{+}	41.04		25	Langmuir	[28]
Acidosasa edulis shoot shell	Tc^{7+}	14.60	1	35	Experiment	[23]
Salvadora persica branches	U^{6+}	85.71	4	25	Langmuir	[36]
KOH-activated Mesquite wood waste + food waste	Cs^{+}	62.73		25	Langmuir	[28]
HNO_3-modified Cow manure	U^{6+}	73.3	4.5	25	Langmuir	[69]
corn stalk	IO_3^{-}	10.31	6	45		[31]
spent coffee	Co^{2+}	3.99	7	35	Langmuir	[20]
Fe_3O_4@pine needles	U^{6+}	623.7	6	25		[70]
Mesquite wood waste	Sr^{2+}	19.44		25	Langmuir	[28]
macaúba endocarp	U^{6+}	400			Experiment	[86]
Watermelon rind@ Fe_3O_4	U^{6+}	323.56	4	20	Langmuir	[49]
Phalaris seed peel@ SiO_2@Fe	^{133}Ba	31			Langmuir	[87]
rice husk@Fe_2O_3	U^{6+}	53.01	4	45		[22]
soybean pods@Prussian blue	Cs^{+}	207.20	7	55	Experiment	[38]
lotus seedpods@NH_2	U^{6+}	367.99	5	25	Langmuir	[34]
walnut shell	I^{-}	508			Experiment	[88]
horse manure	U^{6+}	186.0	4	25	Langmuir	[62]
Mesquite wood waste + chicken manure	Sr^{2+}	22.89		25	Langmuir	[28]
corn stalk	IO_3^{-}	16.87	6	45		[31]
Citrullus lanatus L. seeds@$MnFe_2O_4$	U^{6+}	27.61	4	25	Langmuir	[52]
Bamboo shoot shell@ZnO	Tc^{7+}	25.916	1	25	Langmuir	[71]
bamboo powder@ MoS_2-PO_4	U^{6+}	161.29	6	25	Langmuir	[51]
Mesquite wood waste + food waste	Sr^{2+}	26.76		25	Langmuir	[28]
wheat straw	U^{6+}	8.6	4.5	25	Langmuir	[69]
Corn straws@$ZnFe_2O_4$	Th^{4+}	42.315	4	15	Langmuir	[53]
Luffa rattan	U^{6+}	382	6	25		[54]
Woody + leaf waste	Cs^{+}	20.5	6	25	Langmuir	[24]
rice straw (Oxidized)	U^{6+}	242.65	5.5	25	Langmuir	[33]
Banana peel@Fe_3O_4	Sr^{2+}	23.827	9		Langmuir	[55]
fiddle-leaf fig seed	I^{-}	343.97		30	Langmuir	[89]

Table 3 (continued)

Biomass waste biochar	Radionuclide pollutant adsorbed	q_{max} (mg/g)	pH	Temp (°C)	Method of q_{max} determination	References
NaOH-activated spent coffee	Ba^{2+}	11.12	7	35	Langmuir	[20]
Citrullus lanatus L. Seeds	U^{6+}	21.24	4	25	Langmuir	[52]
rice straw	Sr^{2+}	59.8	8	50	Experiment	[56]
walnut shells@Fe_3O_4	U^{6+}	4.71	4.31	35		[90]
spent coffee grounds@$FeCl_3$	Sr^{2+}	40.02	5	25	Langmuir	[47]
Wheat straw	U^{6+}	1527.02	5	20	Langmuir	[72]
Matamba fruit shell	I^-	2.122*				[57]
KOH-activated Mesquite wood waste + food waste	Sr^{2+}	42.95		25	Langmuir	[28]
orange peel	U^{6+}	144.7	4	25	Langmuir	[43]
soybean pods	Cs^+	58.10	7	55	Experiment	[38]
Banana peel	Sr^{2+}	26.730	9		Langmuir	[55]
H_2O-modified pig manure	U^{6+}	369.9	4	25	Langmuir	[66]
palm tree fibers	Th^{4+}	42	3		Langmuir	[73]
phosphoric-activated fiddle-leaf fig seed	I^-	420.47		30	Langmuir	[89]
NaOH-activated spent coffee	Co^{2+}	5.44	7	35	Langmuir	[20]
pine needles	U^{6+}	62.7	6	25	Langmuir	[74]
spent coffee grounds	Sr^{2+}	41.20	5	25	Langmuir	[47]
Microcystis	U^{6+}	54.46	6	45	Langmuir	[27]
Opuntia ficusindica cactus fibres	Th^{4+}	81	3			[75]
spent coffee	Ba^{2+}	6.94	7	35	Langmuir	[20]
KOH-activated fish scales	U^{6+}	291.98	5	20		[46]
Brewer's spent grain	Sr^{2+}	3.036	7	45	Langmuir	[91]
Wheat straw	Th^{4+}	1158.16	5	20	Langmuir	[72]
Luffa sponge	I^-	162.9				[92]
H_2O_2-modified pig manure	U^{6+}	661.7	4	25	Langmuir	[66]
crayfish shells	Sr^{2+}	22.670	8	25	Langmuir	[61]
corn cob	U^{6+}	163	6	25	Langmuir	[76]
coconut shell@ $Ti_3C_2T_x$ and@polydopamine@ polyethyleneimine	Cs^+	40.3			Langmuir	[58]
Bamboo residues@polyethyleneimine@NaOH	U^{6+}	212.70	5	25	Langmuir	[35]
H_2O_2-modified residual coffee waste	Sr^{2+}	5.57	5	25	Experiment	[59]
cotton straw	U^{6+}	590.8			Langmuir	[65]
Olive pomace	Th^{4+}	153.85	4	45	Langmuir	[77]
NaOH-activated spent coffee	Sr^{2+}	6.62	7	35	Langmuir	[20]
$KMnO_4$-modified pig manure	U^{6+}	979.3	4	25	Langmuir	[66]
rice straw	Ba^{2+}	73.9	8	50	Experiment	[56]
HNO_3-modified wheat straw	U^{6+}	355.6	4.5	25	Langmuir	[69]
cow manure@ TiO_2@SiO_2	Th^{4+}	710.4	4.5	25	Langmuir	[78]
camphor wood sawdust@GO	Sr^{2+}	4.055	6	35	Langmuir	[45]
Oil palm frond	I^-	274.8				[60]
Brewer's spent grain	Co^{2+}	5.516	7	45	Langmuir	[91]
camphor tree leaves	U^{6+}	98.29				[25]
NaOH@H_2O_2-modified residual coffee waste	Sr^{2+}	10.91	5	25	Experiment	[59]
watermelon rind	U^{6+}	135.86	4	20	Langmuir	[49]
HNO_3 oxidized pine needles	Th^{4+}	181	3			[93]
magnetic crayfish shells	Sr^{2+}	21.902	8	25	Langmuir	[61]
Microcystis@Fe_3O_4	U^{6+}	49.19	6	45	Langmuir	[27]
bamboo shoot shell	Tc^{7+}	63.11		30	Experiment	[29]
horse manure@Bi_2O_3	U^{6+}	516.5	4	25	Langmuir	[62]
Residual coffee waste	Sr^{2+}	5.07	5	25	Experiment	[59]
Bamboo residues@polyethyleneimine@HNO_3	U^{6+}	185.5	5	25	Langmuir	[35]
palm kernel shell	I^-	101.9				[60]
teak peel	Sr^{2+}	26.63	8	25	Langmuir	[79]

Table 3 (continued)

Biomass waste biochar	Radionuclide pollutant adsorbed	q_{max} (mg/g)	pH	Temp (ºC)	Method of q_{max} determination	References
KOH-activated bamboo shoot shell	Tc^{7+}	73.11	2	25	Langmuir	[44]
NaOH-modified peanut husk	Sr^{2+}					[80]
phosphorus-doped pomelo peel	U^{6+}	603		40		[63]
spent coffee grounds	Sr^{2+}	51.81	5	25	Langmuir	[21]
orange peel@MnO_2	U^{6+}	246.3	5.5	25.15	Langmuir	[42]
spent coffee ground	I^-	23.32×10^{-3}	7	25	Experiment	[48]
bamboo shoot shell	Tc^{7+}	46.46	1	25	Langmuir	[26]
coconut shell@ $Ti_3C_2T_x$ and@polydopamine@ polyethyleneimine	U^{6+}	239.7			Langmuir	[58]
HNO_3 oxidized *Luffa cylindrica* sponges	Th^{4+}	70	3	23		[81]
Matamba fruit shell	I^-	43.65**	7.5	20	Experiment	[64]
cow manure@ TiO_2@SiO_2	U^{6+}	675.1	4.5	25	Langmuir	[78]

Where Tc^{7+} is surrogated by Re^{7+} or Cr^{7+}, ** = mmol/g, *= mmol/L

on regenerability and recyclability studies are empirically discussed.

For instance, in order to examine the reusability of oxidized rice straw BC in real-world scenarios, studies about the BC regeneration potential were carried out. In this investigation, 1.0 mol/dm^3 HCl was used as an eluent to wash spent BC three times before vacuum drying. The treated spent BC was then employed for the adsorption of U^{6+}. Five rounds of the aforementioned procedures were used to assess the oxidized rice straw's reusability potential. The outcome demonstrates that following these cycles, the adsorption performance dropped somewhat from 95 to 91%. Oxidized rice straw BC demonstrated a comparatively high efficiency of greater than 90% towards U^{6+} adsorption even after five regeneration cycles, with a little decline. The unfinished U^{6+} desorption on the surface of the BC and the solid in solution loss were the causes of the minor reduction in uptake capacity. Because of this, the results suggest that oxidized rice straw BC has a great deal of potential to function as an environmentally benign adsorbent for the sequestration of U^{6+} from aqueous environment [33]. Similarly, utilizing a 0.1 M KOH eluting agent, the adsorbed Re^{7+} was extracted from spent Acidosasa edulis shoot shell BC. Over 94% of the Re^{7+} that were sorbed were desorbed from the BC. It is evident that a large amount of Re^{7+} was recovered in this investigation, most likely due to the ease with which OH- ions could replace rhenium anions at the sorption sites on Acidosasa edulis shoot shell BC. The adsorption capacity of Acidosasa edulis shoot shell *BC* was found to decrease from 4.42 to 3.78 mg/g somewhat after three cycles when using as seen in Table 6. This might be explained by the quantity of BC lost throughout the adsorption-desorption process, as well as surface degradation from constant contact with the eluent [23]. An analogous reasonable elucidation for the reduction in adsorption capacity of Fe_3O_4@pine needles for U^{6+} was also given by Philippou's research team [70]. In this study, 0.1 mol/L Na_2CO_3 was employed as eluent to circumvent partial Fe_3O_4 dissolution, and after four rounds, the U^{6+} uptake percentage and desorption decreased from 99.5 to 87.2% and 99.6 to 62.6%, accordingly [70]. In another comparable adsorption-desorption research for the removal of U^{6+} using watermelon rind@Fe_3O_4 BC, 0.1 mol/L Na_2CO_3 was employed as the desorbing agent to prevent partial Fe_3O_4 dissolution. The findings show that following the 3rd round of adsorption-desorption, the BC's uptake capability for U^{6+} decreases. The percentages of adsorption and elution are reduced from 99 to 44% and from 99 to 40%, respectively, following the 3rd round. One plausible clarification for the decrease in the adsorption % during the desorption tests might be the modest quantities of U^{6+} lost after each round [49].

In another experiment [39], desorption research was conducted using 0.01 g of KOH-activated peanut shell BC and 50 ml of a 0.5 mg/L strontium solution in a conical flask. The mixture was swirled at 200 RPM for 70 min at room temperature in order to determine the reusability of the PSABC. The samples were subsequently filtered, and distilled water was used to rinse the supernatant. Five successive cycles of adsorption-desorption tests were used to examine the reusability of the adsorbent. Eluents in the following five concentrations were tested: 0.1 mol/L of HNO_3, NaOH, H_2SO_4, HCl, and CH_3COOH. Following the adsorption experiment, 50 mL of desorbing eluents were added to the filtered KOH-activated peanut shell BC to conduct a desorption investigation. The suspensions were filtered after being vigorously stirred for 12 h at 25 °C. Following desorption, the same BC was employed for adsorption. The patterns of Sr^{2+} desorption by five eluents are depicted in Fig. 9a, which displays the subsequent trend. HNO_3 is superior to EDTA, HCl, CH_3COOH, and NaOH. According to the findings, HNO_3

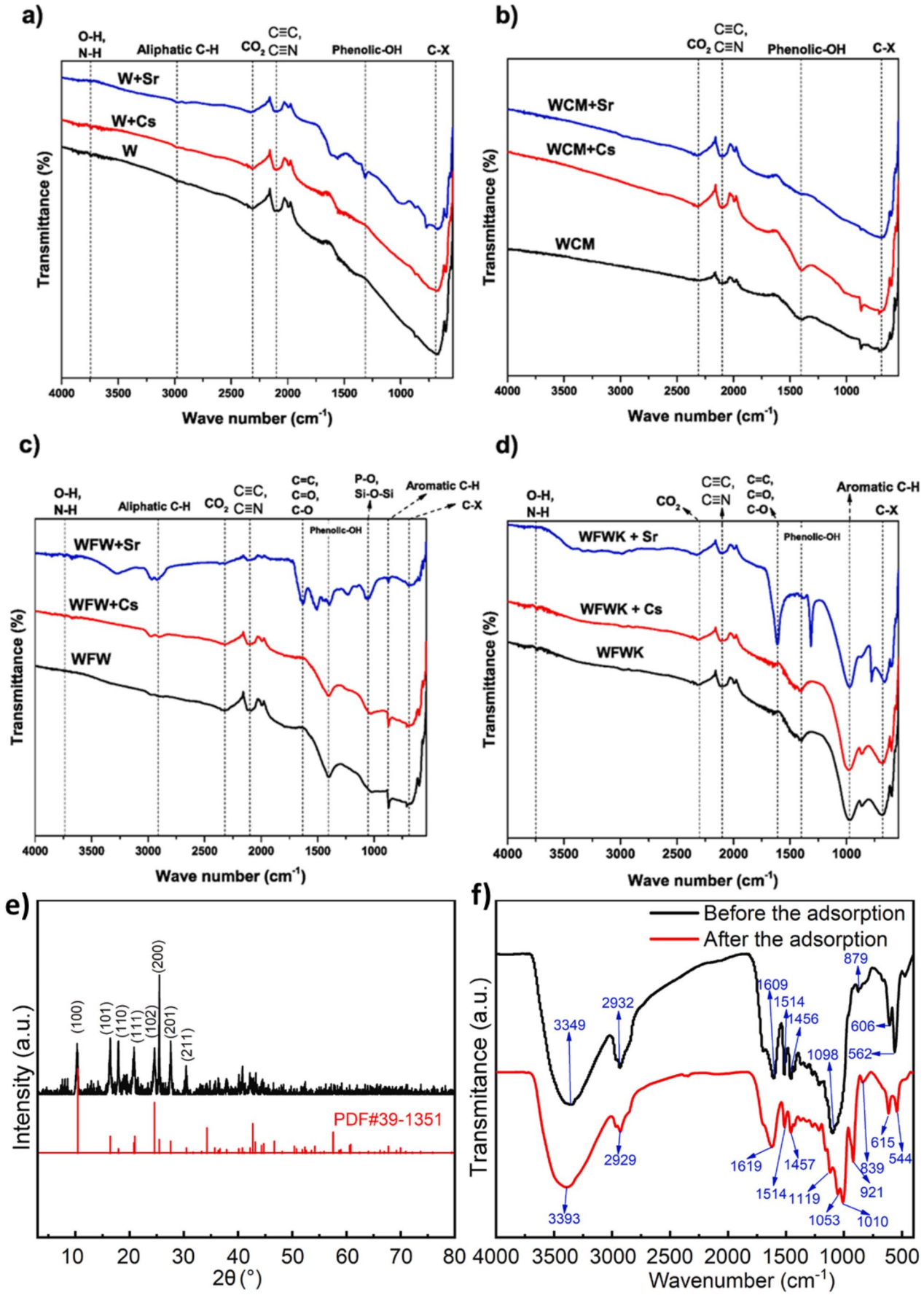
a)
O-H, N-H
Aliphatic C-H
C≡C, CO2 C≡N
Phenolic-OH
C-X
W+Sr
W+Cs
W
Transmittance (%)
Wave number (cm-1)
b)
C≡C, CO2 C≡N
Phenolic-OH
C-X
WCM+Sr
WCM+Cs
WCM
Transmittance (%)
Wave number (cm-1)
c)
O-H, N-H
Aliphatic C-H
CO2 C≡C, C≡N
C=C, C=O, C-O
P-O, Si-O-Si
Aromatic C-H
C-X
Phenolic-OH
WFW+Sr
WFW+Cs
WFW
Transmittance (%)
Wave number (cm-1)
d)
O-H, N-H
CO2
C≡C, C≡N
C=C, C=O, C-O
Aromatic C-H
C-X
Phenolic-OH
WFWK + Sr
WFWK + Cs
WFWK
Transmittance (%)
Wave number (cm-1)
e)
(100)
(101)
(110)
(111)
(102)
(200)
(201)
(211)
PDF#39-1351
Intensity (a.u.)
2θ (°)
f)
Before the adsorption
After the adsorption
3349
2932
1609
1514
1456
879
606
562
1098
3393
2929
1619
1457
1514
1119
1053
1010
921
839
615
544
Transmitance (a.u.)
Wavenumber (cm-1)

Fig. 4 (**a-d**) FT-IR analysis of wood waste, wood waste + chicken manure, wood + food waste, and KOH-activated wood waste + food waste BC before and after the adsorption of Sr^{2+} and Cs^{+} [28]. (**e-f**) XRD and FTIR spectra of calcium phosphate-modified cotton straw BC after U^{6+} adsorption [65]

performed well when it came to maximal Sr^{2+} desorption. As a result, HNO_3 was chosen for additional BC desorption research in order to investigate its reusability. The regeneration performance of BC with HNO_3 as the eluent is displayed for five cycles in Fig. 9b. Figure shows that there was a 5–8% performance decline in BC for five cycles, but no discernible drop in Sr^{2+} adsorption performance [39]. In parallel, in the case of the adsorption-desorption study of teak peel BC for the removal of Sr^{2+}, 0.1 mol/L HNO_3 eluent gave a better desorption efficiency compared to HCl and other eluents as shown in Fig. 9e. Specifically, with a desorption performance of over 99%, 0.1 mol/L HNO_3 may efficiently desorb the adsorbed Sr^{2+}, and the desorption equilibrium can be reached in less than 10 min. In addition, the teak peel BC reusability is examined using 0.1 mol/L HNO_3. As can be presented in Fig. 9f, teak peel BC exhibits its outstanding reusability and only marginally loses its adsorption capacity after five adsorption-desorption rounds, suggesting that it has a lot of promise for use in real-world applications [79]. A somewhat good recyclability result was also obtained for the adsorption-desorption of Cs^{+} and U^{6+} using coconut shell@ $Ti_3C_2T_x$ and@polydopamine@ polyethyleneimine BC as presented in Fig. 9c and **d** [58] and adsorption of U^{6+} using NaOH modified bamboo residues@polyethyleneimine BC as presented in Table 6. The authors accentuated that the respective modified BC, as seen in Fig. 10, retains their original architectural structure upon regeneration (with 0.01 mol/L HCl), with polyethyleneimine remaining attached to the surface of the bamboo residues BC. These findings show that NaOH and HNO_3-modified bamboo residues@polyethyleneimine BC are both viable and affordable materials with good stability and reusability [35].

In another study [42], the following tests were conducted to evaluate orange peel@MnO_2 BC's reusability performance for U^{6+}. First, the previously used orange peel@ MnO_2 BC was regenerated by drying in a vacuum oven and washing three times with 1.0 mol/L HCl. Second, many tests were conducted on the retrieved orange peel@MnO_2 BC's adsorption capability. There were five adsorption-desorption cycles completed. The outcome is displayed in Fig. 11a. As can be shown, even after five cycles, the U^{6+} uptake quantity only slightly decreases, decreasing from 142.66 mg/g to 136.38 mg/g which is just a 4.4% reduction. The outcome demonstrates BC's outstanding durability performance [42]. In like manner, desorption tests were carried out with 0.01 and 0.1 M Na_2CO_3 solutions as the eluting agent, and the cycle was repeated six times, in order to assess the reusability and stability of cotton straw BC. Desorption efficiencies with 0.1 M Na_2CO_3 were 98%, 98%, 98%, 97%, 97%, and 96%, and with 1 M Na_2CO_3 were 98%, 98%, 98%, 93%, 90%, and 87%, as indicated in Fig. 11b. The findings showed that both eluenting agents could reach desorption efficiencies of over 96%, demonstrating good regeneration capabilities. Furthermore, following six washing rounds with 1 M Na_2CO_3, the adsorption rate decreased by just 11%, demonstrating the BC's great reusability resilience. These results imply that because of its superior regeneration and reusability qualities, cotton straw BC is a potential option for real-world uses in the extraction of U^{6+} from wastewater [65]. A comparable excellent recyclability result was also reported for the removal of Tc^{7+} as presented in Fig. 11c by bamboo shoot shell BC using 0.1 mol/L KOH as eluent [26].

Wang and co-workers [53] also conducted an adsorption-regeneration study for the removal of Th^{4+} using corn straws@$ZnFe_2O_4$ BC. In this work, the recovery of Th^{4+} from wastewater was achieved by measuring the ratio of adsorbed Th^{4+} to desorbed corn straws@$ZnFe_2O_4$. This allowed for an assessment of the reusability of corn straws@ $ZnFe_2O_4$. Following six adsorption rounds, Fig. 11d illustrates the washing of citric acid processing of regenerated adsorbents. To assess the removal efficiencies in each round, the regeneration experiment was conducted in six successive adsorption-desorption rounds. In the first four rounds, the BC's resolution rate exceeded 90%. In the 5th and 6th rounds, the resolutions were 86.28% and 88.21%, respectively, and may progressively decrease from there on. The phenomena might be linked to the structural breakdown of corn straw@$ZnFe_2O_4$ BC, the loss of corn straw@$ZnFe_2O_4$ BC in the reactor, or the blockage of binding spots by metal complexes. After six analytical rounds, the corn straw@ $ZnFe_2O_4$ BC adsorption efficiency was still very nearly 90. However, after six adsorption-desorption rounds, a comparatively high adsorption capacity of 35.14 mg/g may also be sustained. It is clear that after six rounds, the removal efficiency of Th^{4+} by corn straw@$ZnFe_2O_4$ BC did not considerably decline, and the reason for the little drop in the adsorption rate was most likely the dissolution of trace quantities of Zn^{2+} and Fe^{3+} in BC by citric acid during the analytical procedure. Furthermore, because of its superparamagnetism, it may be readily extracted from liquids containing magnetic fields following adsorption or desorption. Consequently, corn straw@$ZnFe_2O_4$ BC demonstrated strong regeneration capabilities and reusability, supporting the long-term use of sewage treatment and enabling the radionuclide Th^{4+} in wastewater to be recovered [53]. An analogous admirable recyclability performance was also reported for the removal of U^{6+} and Th^{4+} as presented in Fig. 11e-f by cow manure@ TiO_2@SiO_2 BC using

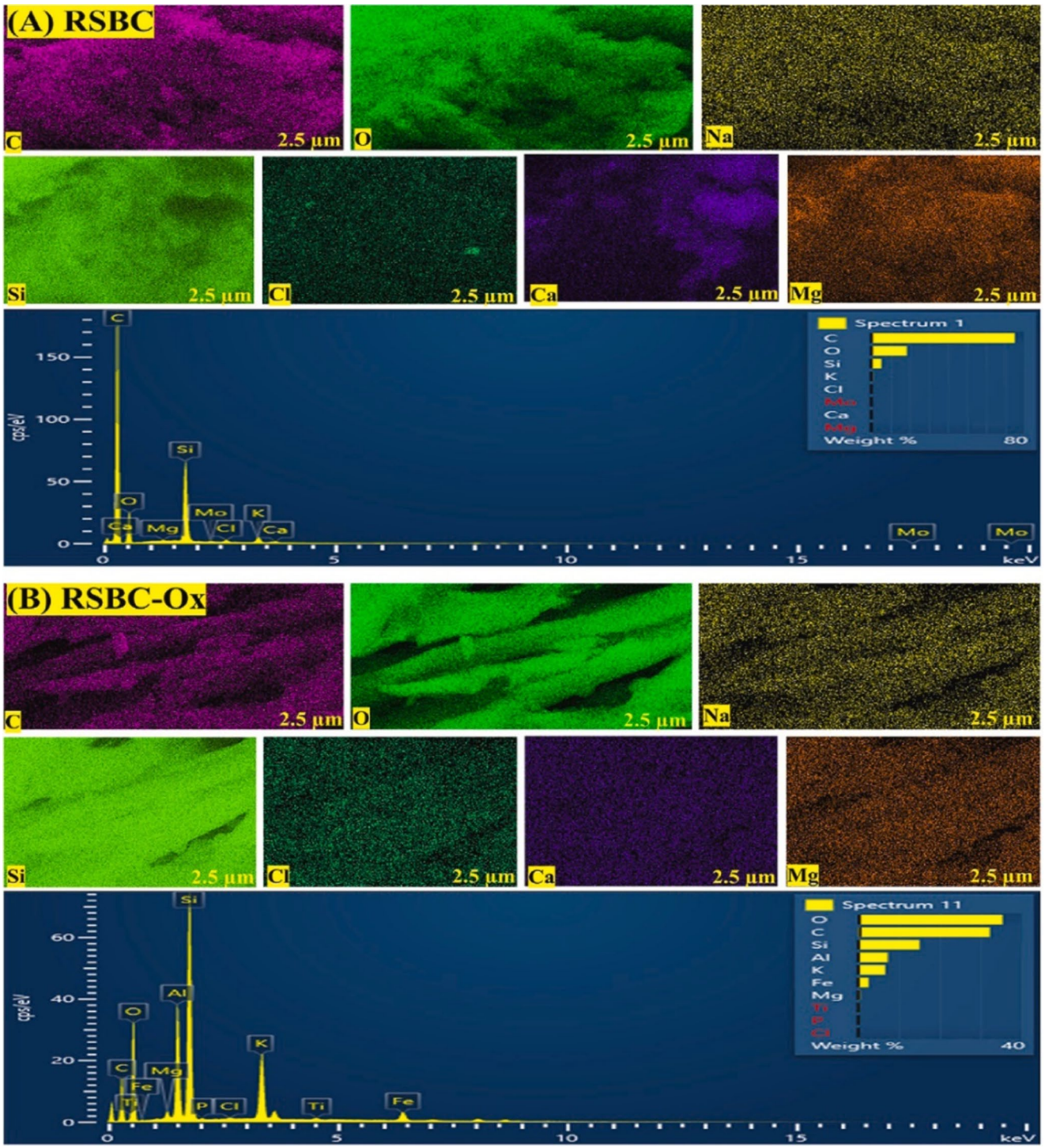

Fig. 5 Elemental mappings and EDS of (**a**) un-oxidized rice straw BC and (**b**) oxidized rice straw BC [33]

0.05 mol/L HCl as an eluting agent. In addition, the authors made it clear that the mesoporous structure of the BC composite had no noticeable change, which suggested that the microstructure of the BC composite was not spoiled during the radio-contaminant adsorption operation as shown in Fig. 12. Many bulk particles popped up on the surface of the BC composite after U^{6+} and Th^{4+} were adsorbed, and part of the mesoporous structure vanished. This phenomenon may have been caused by the complexes that formed during the separation process aggregating on the surface and filling in the mesoporous structure of BC composite. Interestingly, the bulk particles vanished and the mesoporous structure of

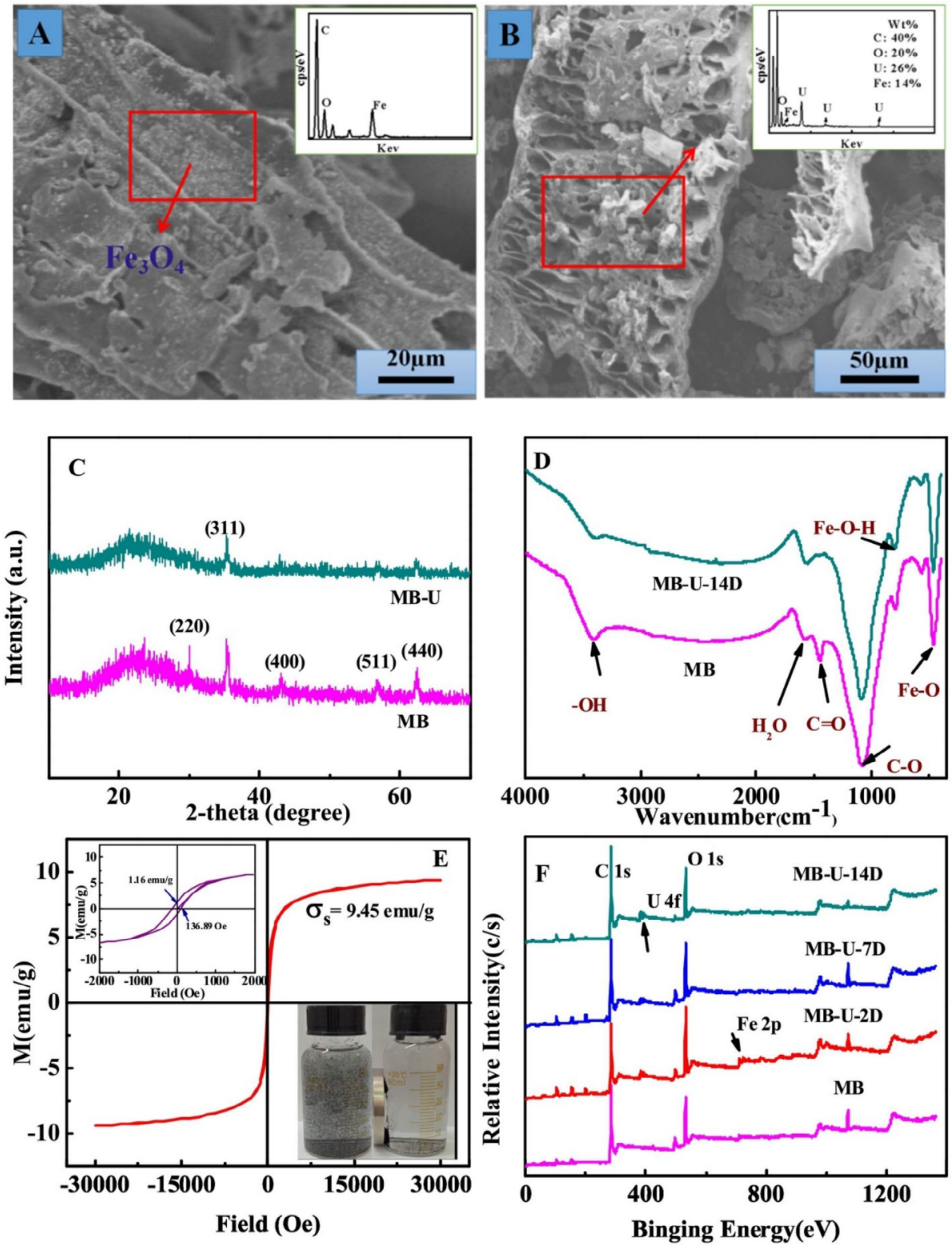

Fig. 6 Characterization of rice husk@Fe_2O_3 BC prior to and following U^{6+} uptake. (**a**–**b**) SEM pictures prior to and following U^{6+} uptake, respectively; (**c**) XRD analysis; (**d**) FTIR analysis; (**e**) magnetic hysteresis loops; (**f**) XPS analysis. (MB = rice husk@Fe_2O_3 BC; MB-U = U^{6+} adsorption onto rice husk@Fe_2O_3 BC) [22]

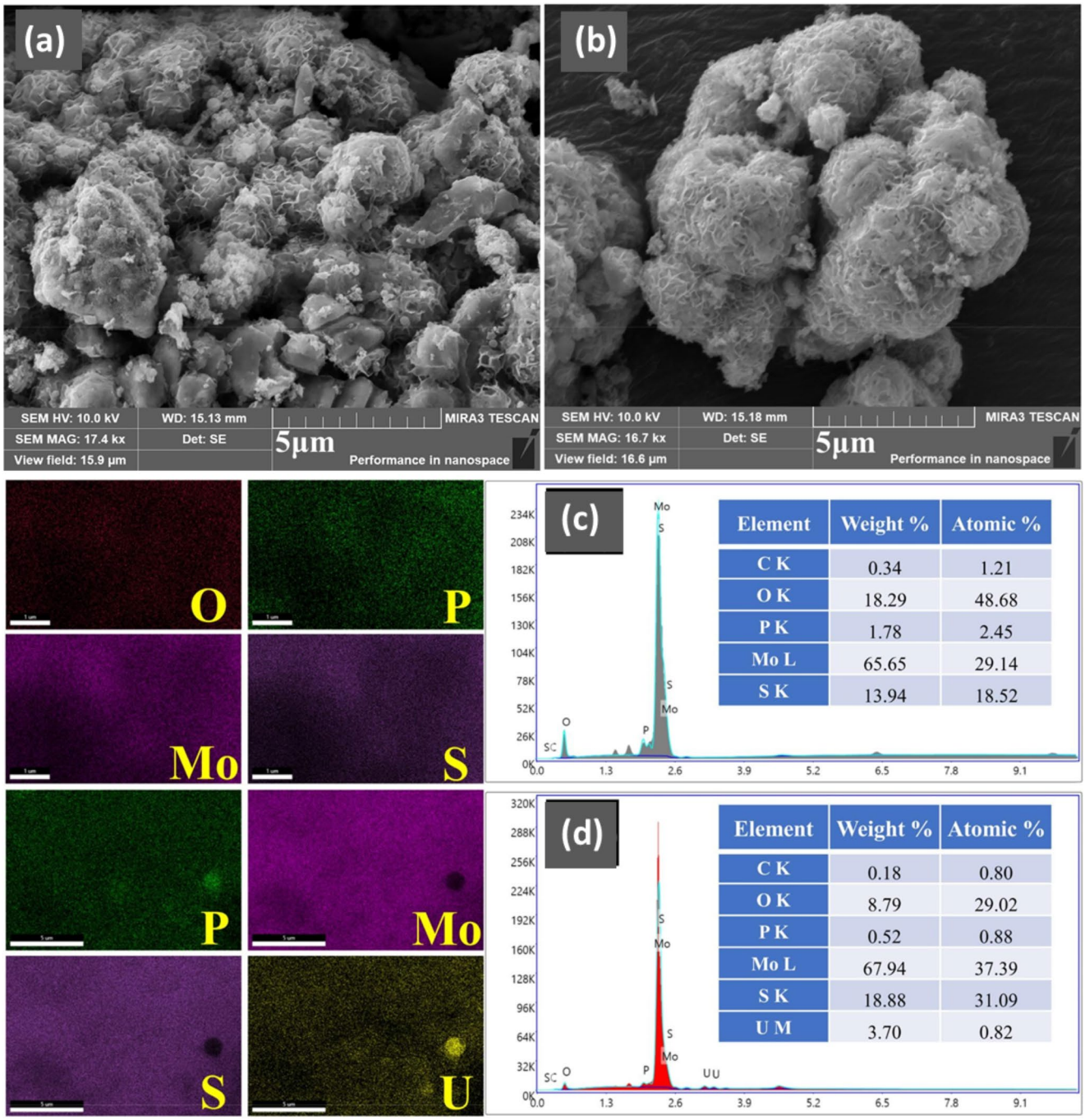

Fig. 7 SEM pictures of (**a**) bamboo powder@MoS_2-PO_4 BC and (**b**) bamboo powder@MoS_2-PO_4 -U. EDS mapping of (c) bamboo powder@MoS_2-PO_4 BC and (d) bamboo powder@MoS_2-PO_4 -U [51]

the BC composite was restored following desorption, further supporting the theory that complexation served as the primary mechanism for BC composite separation from U^{6+} and Th^{4+} [78].

Remarkably, as summarized in Table 6, a range of eluents has been employed to elute sorbed radio-contaminant from the expended BWDBC and or to regenerate the recovered BWDBC, including HCl, citric acid, Na_2CO_3, and KOH. Mechanistically, according to Ahmed and co-workers, when HCl or HNO_3 is employed, the regeneration mechanism is the reversible ion exchange between BC and radio-contaminant [33]. In addition, the chief adsorption mechanism of radio-contaminant onto the BWDBC is suggested to be chemisorption by successful elution/regeneration by strong acids or bases, whereas physisorption is suggested to be the

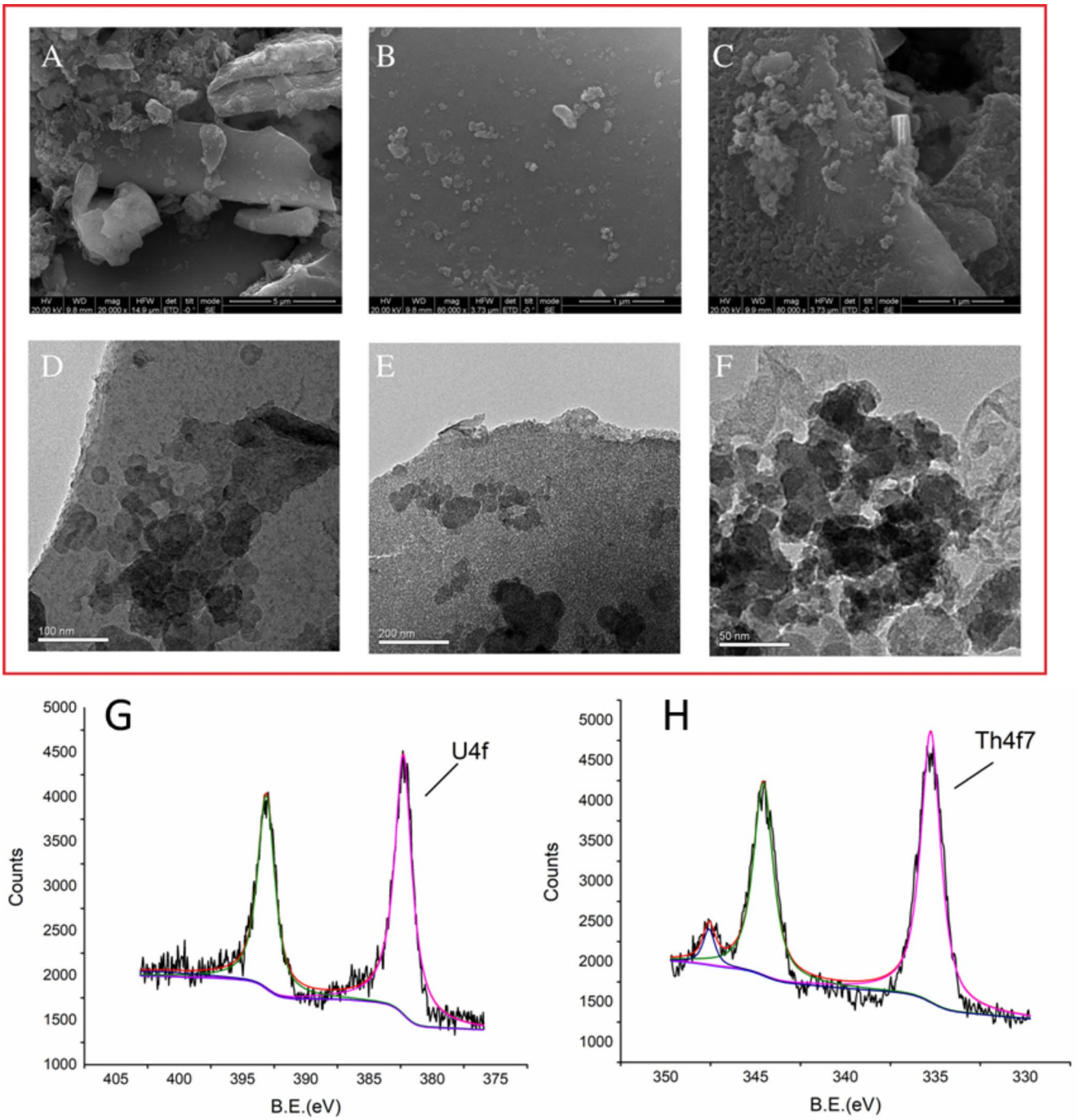

Fig. 8 SEM pictures of (**A**) raw wheat straw BC, (**B**) wheat straw BC after U^{6+} adsorption, and (**C**) wheat straw BC after Th^{4+} adsorption. TEM of (**D**) raw wheat straw BC, (**E**) wheat straw BC after U^{6+} adsorption, and (**F**) wheat straw BC after Th^{4+} adsorption. (**G**) XPS spectra of wheat straw BC after U^{6+} adsorption reaction, (**H**) XPS spectra of wheat straw BC after Th^{4+} adsorption reaction [72]

Table 4 Overview of best-fit isotherm (BFI) and kinetic (BFK) models of biomass waste-derived biochar for the adsorption of radio-contaminants

Biomass waste biochar	Radionuclide pollutant adsorbed	BFI	R^2	BFK	R^2	Diffusion model	Ref.
lotus seedpods	U^{6+}	LIM	0.9789	PSO	0.9558	IPD is the rate-limiting step	[34]
Mesquite wood waste	Cs^{+}	RPIM	0.95	PSO	0.66		[28]
Artemia egg shell@Cu_2O/Cu^0	I^{-}	FIM	0.944	PSO	0.987	external and internal diffusion	[50]
rice straw	U^{6+}	Sips and RPIM	0.98 and 0.96	PSO	0.99	external surface diffusion, IPD (is the rate-limiting)	[33]
Salvadora persica branches	Th^{4+}	LIM	0.9961	PSO	1	external mass transfer, PD, and IPD (not only the rate-limiting step)	[36]
rice straw	Sr^{2+}	FIM	0.989	EVM	0.989		[83]
reed straw	U^{6+}	LIM	0.9906	PSO	0.9586		[30]
Mesquite wood waste + chicken manure	Cs^{+}	RPIM	0.89	PFO	0.81		[28]
spent coffee ground@ bismuth	I^{-}	FIM	0.984	PSO	0.964	liquid FD, IPD (the rate-limiting step)	[48]
spent coffee	Sr^{2+}	LIM	0.949	PFO	0.999	liquid FD and IPD	[20]
bamboo powder@MoS_2	U^{6+}	LIM	0.974	PSO	0.970	External surface adsorption and IPD	[51]
NaOH modified duckweed	Th^{4+}	LIM	0.989	PSO	0.993	liquid FD and IPD	[84]
wheat straw + Sodium lignosulfonate	I^{-}			PSO	0.99		[85]
Cow manure	U^{6+}	LIM	0.979	PSO	0.999		[69]
KOH-activated peanut shell	Sr^{2+}	FIM	0.99	PSO	0.995		[39]
Bamboo shoot shell	Tc^{7+}	LIM	0.9919	EVM	0.9734		[71]
orange peel	U^{6+}	Sips	0.989	PSO	0.99	external surface diffusion and IPD (the rate-limiting step)	[42]
camphor leaves@Bi_2O_3	I_2	LIM	0.993	PSO	0.981	Pore filling	[68]
orange peel@magnesium silicate	U^{6+}	LIM	0.991	PSO	0.998		[43]
rice straw	Sr^{2+}			PSO	0.99	IPD, PD (not the only rate-controlling step), and FD	[32]
Mesquite wood waste + food waste	Cs^{+}	RPIM	0.93	PSO	0.85		[28]
Acidosasa edulis shoot shell	Tc^{7+}	FIM	0.9812	PSO	0.9978	FD, PD and IPD	[23]
Salvadora persica branches	U^{6+}	LIM	0.9968	PSO	1	external mass transfer, PD, and IPD (not only the rate-limiting step)	[36]
KOH-activated Mesquite wood waste + food waste	Cs^{+}	RPIM	0.97	PSO	0.97		[28]
HNO_3-modified Cow manure	U^{6+}	LIM	0.958	PSO	0.999		[69]
corn stalk	IO_3^{-}	LIM	0.9997	PSO	0.9960	external diffusion and IPD	[31]
spent coffee	Co^{2+}	LIM	0.945	PFO	0.999	liquid FD and IPD	[20]
Fe_3O_4@pine needles	U^{6+}	LIM	0.992	PSO	0.99		[70]
Mesquite wood waste	Sr^{2+}	FIM	0.86	PSO	0.84		[28]
macaúba endocarp	U^{6+}			PSO	0.999	IPD	[86]
Magnetized watermelon rind	U^{6+}	LIM	0.99	PSO	0.999		[49]
rice husk@Fe_2O_3	U^{6+}	LIM	0.9897	PSO	>0.99	PD, FD and IPD	[22]
soybean pods@Prussian blue	Cs^{+}	LIM	0.971	PSO	0.988		[38]
lotus seedpods@NH_2	U^{6+}	LIM	0.9898	PSO	0.9676	IPD is the rate-limiting step	[34]
horse manure	U^{6+}	LIM	0.998	PSO	0.999		[62]
Mesquite wood waste + chicken manure	Sr^{2+}	RPIM	0.94	PFO	0.87		[28]
corn stalk	IO_3^{-}	LIM	0.9998	PSO	0.9968	external diffusion and IPD	[31]
Citrullus lanatus L. seeds@$MnFe_2O_4$	U^{6+}	LIM	0.96	PSO	0.96		[52]
Duckweed	Th^{4+}	LIM	0.929	PSO	0.991	liquid FD and IPD	[84]
Bamboo shoot shell@ZnO	Tc^{7+}	LIM	0.9925	EVM	0.9961		[71]
bamboo powder@ MoS_2-PO_4	U^{6+}	LIM	0.996	PSO	0.999	External surface adsorption and IPD	[51]
Mesquite wood waste + food waste	Sr^{2+}	RPIM	0.99	PSO	0.88		[28]
wheat straw	U^{6+}	LIM	0.975				[69]
Corn straws@$ZnFe_2O_4$	Th^{4+}	LIM	0.992	PSO	0.992		[53]
Luffa rattan	U^{6+}	LIM	0.991	PSO	1.00		[54]
Woody + leaf waste	Cs^{+}	FIM	0.998			FD and IPD	[24]

Table 4 (continued)

Biomass waste biochar	Radionuclide pollutant adsorbed	BFI	R^2	BFK	R^2	Diffusion model	Ref.
rice straw (Oxidized)	U^{6+}	Sips and RPIM	0.99	PSO	0.98	external mass transfer, pore filling, and IPD	[33]
Fe_3O_4@banana peel	Sr^{2+}	TIM	0.968	PFO	0.9966	external surface diffusion, IPD	[55]
fiddle-leaf fig seed	I^-	LIM	1.00	PSO	0.9999	FD and IPD	[89]
NaOH-activated spent coffee	Ba^{2+}	LIM	0.974	PSO	0.941	liquid FD and IPD	[20]
Citrullus lanatus L. Seeds	U^{6+}	LIM	0.91	PSO	0.85		[52]
rice straw	Sr^{2+}	LIM	0.99	PSO	0.976	boundary layer, PD, FD, and IPD	[56]
spent coffee grounds@$FeCl_3$	Sr^{2+}	LIM	0.95	PSO	1.00		[47]
Wheat straw	U^{6+}	LIM and FIM	>0.98	PSO	0.9599		[72]
KOH-activated Mesquite wood waste + food waste	Sr^{2+}	Sips	0.99	PSO	0.81		[28]
Banana peel	Sr^{2+}	TIM	0.993				[55]
H_2O-modified pig manure	U^{6+}	LIM	0.994	PSO	0.970	IPD (not the only rate-limiting step)	[66]
palm tree fibers	Th^{4+}	LIM	0.96	PSO	0.999		[73]
phosphoric-activated fiddle-leaf fig seed	I^-	LIM	0.9995	PSO	0.9992	FD and IPD	[89]
NaOH-activated spent coffee	Co^{2+}	LIM	0.932	PSO	0.935	liquid FD and IPD	[20]
pine needles	U^{6+}	LIM	0.99	PSO	0.993		[74]
spent coffee grounds	Sr^{2+}	LIM	0.949	PSO	1.00		[47]
Microcystis	U^{6+}	FIM	0.962	PSO		FD and IPD	[27]
spent coffee	Ba^{2+}	LIM	0.988	PFO	0.998	liquid FD and IPD	[20]
KOH-activated fish scales	U^{6+}	LIM	>0.99	PFO	0.980		[46]
Brewer's spent grain	Sr^{2+}	LIM	0.948	PSO	0.987		[91]
Wheat straw	Th^{4+}	LIM and FIM	>0.98	PSO	0.9535		[72]
H_2O_2-modified pig manure	U^{6+}	LIM	0.997	PSO	0.987	IPD (not the only rate-limiting step)	[66]
crayfish shells	Sr^{2+}	FIM	0.964				[61]
coconut shell@ $Ti_3C_2T_x$ and@polydopamine@ polyethyleneimine	Cs^+	LIM	0.985	PSO	0.978	IPD (not the only rate-limiting step) and membrane diffusion	[58]
Bamboo residues@polyethyleneimine@NaOH	U^{6+}	LIM	0.998	PSO	0.999	mass transfer and IPD	[35]
H_2O_2-modified residual coffee waste	Sr^{2+}	LIM	0.971	PFO	0.997	Liquid FD and IPD (rate-controlling step)	[59]
cotton straw	U^{6+}	LIM	0.965	PSO	0.980		[65]
Olive pomace	Th^{4+}	LIM	0.995	PSO	0.999	FD and IPD	[77]
NaOH-activated spent coffee	Sr^{2+}	LIM	0.958	PSO	0.966	liquid FD and IPD	[20]
$KMnO_4$-modified pig manure	U^{6+}	LIM	0.996	PSO	0.979	IPD (not the only rate-limiting step)	[66]
rice straw	Ba^{2+}	LIM	0.96	PSO	0.989		[56]
HNO_3-modified wheat straw	U^{6+}	LIM	0.985				[69]
camphor wood sawdust@GO	Sr^{2+}	FIM	0.967	PSO	0.9958		[45]
Brewer's spent grain	Co^{2+}	LIM	0.979	PSO	0.971		[91]
camphor tree leaves	U^{6+}	LIM	0.9993	PSO	0.9978	IPD	[25]
NaOH@H_2O_2-modified residual coffee waste	Sr^{2+}	LIM	0.957	PSO	0.987	Liquid FD and IPD (rate-controlling step)	[59]
watermelon rind	U^{6+}	LIM	0.99	PSO	0.989		[49]
magnetic crayfish shells	Sr^{2+}	FIM	0.969	PFO	0.972	PD, external diffusion, and IPD	[61]
Microcystis@Fe_3O_4	U^{6+}	FIM	0.988	PSO		FD and IPD	[27]
bamboo shoot shell	Tc^{7+}	TIM	0.999	PSO	0.984	FD, and IPD	[29]
horse manure@Bi_2O_3	U^{6+}	LIM	0.994	PSO	0.999		[62]
Residual coffee waste	Sr^{2+}	LIM	0.976	PFO	0.995	Liquid FD and IPD (rate-controlling step)	[59]

Table 4 (continued)

Biomass waste biochar	Radionuclide pollutant adsorbed	BFI	R^2	BFK	R^2	Diffusion model	Ref.
Bamboo residues@polyethyleneimine@HNO_3	U^{6+}	LIM	0.983	PSO	0.998	mass transfer and IPD	[35]
teak peel	Sr^{2+}	FIM	0.98	PSO	0.98	IPD, outer surface diffusion, and PD	[79]
KOH-activated bamboo shoot shell	Tc^{7+}	RPIM	0.9935	PSO	0.9519	liquid FD (primary rate-controlling step)	[44]
NaOH-modified peanut husk	Sr^{2+}	RPIM	0.999	PSO	1.00		[80]
spent coffee grounds	Sr^{2+}	LIM	0.995	PSO	0.999		[21]
orange peel@MnO_2	U^{6+}	Sips and RPIM	0.997	PSO	0.99	external surface diffusion and IPD (the rate-limiting step)	[42]
spent coffee ground	I^-	FIM	0.919	PSO	0.644		[48]
bamboo shoot shell	Tc^{7+}	FIM	0.9942				[26]
coconut shell@ $Ti_3C_2T_x$ and@polydopamine@ polyethyleneimine	U^{6+}	LIM	0.982	PSO	0.98	IPD (not the only rate-limiting step) and membrane diffusion	[58]
HNO_3 oxidized *Luffa cylindrica* sponges	Th^{4+}	LIM	0.98	PSO	0.998	IPD	[81]
Matamba fruit shell	I^-			EVM	0.9898	mesopore filling and IPD	[64]

Where Tc^{7+} is surrogated by Re^{7+} or Cr^{7+}, PD = pore diffusion, FD = film diffusion, IPD = intra-particle diffusion, PFO = pseudo-first-order, PSO = pseudo-second-order, EVM = Elovich, TIM = Temkin isotherm model, RPIM = Redlich–Peterson isotherm model, LIM = Langmuir isotherm model, FIM = Freundlich isotherm model

primary adsorption mechanism by successful elution/regeneration by organic solvents or water [99, 100].

Real-Life Application Potential and Effect of Background Ions

Exploring the performance of biomass waste-derived biochar in real radio-contaminated water and in the presence of different background ions is very germane in establishing their real-world applicability. Moreover, ionizable substances coexisting with the target adsorbate(s) in aqueous environments have prohibitory impacts that change the surface charges, hydrophobicity, ESI, and activity coefficient of the adsorbate. Furthermore, because competitive adsorption makes it possible to precisely remove the target adsorbate and to extract, isolate, and concentrate several chemicals in liquid media, it is becoming more and more significant [95]. The ratio of adsorption capacity in the presence of background ion (q_{max}) to that in the absence of background ion (q_o) can be used to illustrate the impact of ionic interaction on the radio-contaminant adsorption operation by BWDBC such that for q_{max}: $q_o > 1$ radio-contaminant adsorption is enhanced in presence of other competing ions. q_{max}: $q_o = 1$ radio-contaminant adsorption is not affected in the presence of other competing ions. q_{max}: $q_o < 1$ radio-contaminant adsorption is negatively affected in the presence of other competing ions [80].

Notably, some research has looked into this study direction as per real-life application and this is discussed in the succeeding paragraphs while the effect of background ions is summarized in Table 7. For example, the elimination of ^{241}Am from seawater, groundwater, and wastewater from the nearby wastewater treatment plant was examined following the addition of ^{241}Am to the corresponding solutions and their interaction with two distinct doses of 0.01 and 0.1 g of *Luffa cylindrica* BC and oxidized *Luffa cylindrica* BC. The ^{241}Am levels absolutely diminished in the presence of BC fibers, especially when the oxidized equivalents were present, as shown by the spectra in Fig. 13. The latter was ascribed to the development of inner-sphere complexes as a result of the carboxylic moieties' significant attraction for Am^{3+} on the oxidized *Luffa cylindrica* BC surface. Figure 13 illustrates how higher clean-up efficiencies were achieved by adding more BC [101].

In another real-sample study conducted in the summer at the School of Environmental and Safety Engineering, Changzhou University, Changzhou, China, on the adsorption capacity of soybean pods BC and soybean pods BC@ Prussian blue for Cs^+ in tap water. From the findings, the adsorption capacities of soybean pods BC and soybean pods BC@Prussian blue were 39.767, and 178.555 mg/g, respectively, when the concentration of Cs^+ hit 80 mg/L. These values are somewhat lower than those for deionized water (Soybean pods BC: 56.100 mg/g, and soybean pods BC@Prussian blue: 203.888 mg/g). In real water treatment samples, soybean pods BC@Prussian blue still have a high adsorption capacity for Cs^+ in contrast to other adsorbents. Another explanation for the decline in adsorption capacity was the possibility of soybean pods BC@Prussian blue combining with the contaminants present in tap water. In addition, the authors accentuated that the presence of alkali

Table 5 Overview of thermodynamics of adsorption of biomass waste-derived biochar for radio-contaminants

Biomass waste biochar	Radionuclide pollutant adsorbed	Temp (K)	ΔG^0 (kJ/mol)= $\Delta H - T\Delta S = -RTlnK_c$	ΔH^0 (kJ/mol)	ΔS^0 (J/mol.K)	Comment	Ref.
rice straw	U^{6+}	288	-17.13	32.94	172.78	Endothermic, and spontaneous processes associated with a disorder increase at the solid-liquid interface	[33]
		293	-18.21				
		298	-19.36				
		303	-20.15				
		313	-21.37				
Salvadora persica branches	Th^{4+}	298	−11.45	−240.17	−0.77	Exothermic, and spontaneous process associated with a randomness reduction at the solid-liquid interface	[36]
		308	−7.61				
		318	−3.77				
		313	0.07				
reed straw	U^{6+}	283	-12.65			Endothermic, and spontaneous processes associated with a disorder increase at the solid-liquid interface	[30]
		298	-15.11				
		313	-17.57				
		328	-20.03				
spent coffee ground@ bismuth	I^-	288	−13.89	5.88	68.56	Endothermic and spontaneous process associated with increased randomness at the solid-liquid interface	[48]
		298	−14.49				
		308	−15.31				
		318	−15.90				
spent coffee	Sr^{2+}	288	−25.8	27.9	0.1864	Spontaneous	[20]
		298	−27.5				
		308	−29.5				
bamboo powder@MoS_2	U^{6+}	288	–23.57	17.27	0.14171	Endothermic and spontaneous	[51]
		298	−24.98				
		308	−26.40				
		318	−27.82				
KOH-activated peanut shell	Sr^{2+}	303	− 5.117	− 21.068	− 0.053993	spontaneous and exothermic process associated with decreased randomness at the solid-liquid interface	[39]
		313	− 3.613				
		323	− 3.451				
		333	− 3.434				
orange peel	U^{6+}	288.15	−16.64	33.33	0.17343	Endothermic and spontaneous processes associated with a disorder increase at the solid-liquid interface	[42]
		293.15	−17.51				
		298.15	−18.38				
		303.15	−19.25				
		313.15	−20.98				
orange peel@magnesium silicate	U^{6+}	298	−40.223	16.801	0.19153	Endothermic and spontaneous processes associated with a degree of freedom increase at the solid-liquid interface	[43]
		308	−42.277				
		323	−45.029				
rice straw	Sr^{2+}	298	4.3	41.0	0.122	Endothermic associated with a degree of freedom increase at the solid-liquid interface	[32]
		308	4.0				
		328	1.0				
Acidosasa edulis shoot shell	Tc^{7+}	298	−26.18	11.85	0.12746	Endothermic and spontaneous processes associated with a degree of freedom increase at the solid-liquid interface	[23]
		303	−27.35				
		308	−28.73				
Salvadora persica branches	U^{6+}	298	−12.17	−218.17	−0.69	Exothermic, and spontaneous process associated with a randomness reduction at the solid-liquid interface	[36]
		308	−8.71				
		318	−5.26				
		313	−1.80				

Table 5 (continued)

Biomass waste biochar	Radionuclide pollutant adsorbed	Temp (K)	ΔG^0 (kJ/mol)= $\Delta H - T\Delta S = -RTlnK_c$	ΔH^0 (kJ/mol)	ΔS^0 (J/mol.K)	Comment	Ref.
corn stalk	IO_3^-	298	2.1539	18.7244	0.0556056	Endothermic and non-spontaneous process	[31]
		308	1.5979				
		318	1.0418				
spent coffee	Co^{2+}	288	−24.4	29.8	0.1878	Spontaneous	[20]
		298	−26.1				
		308	−28.2				
Magnetized watermelon rind	U^{6+}	293	-2.02	14.35		Endothermic and spontaneous process	[49]
		303	-2.79				
		313	-3.23				
		323	-3.74				
rice husk@Fe_2O_3	U^{6+}	288	-3.79	2.68	0.02243	Endothermic and spontaneous process	[22]
		303	-5.15				
		318	-7.55				
soybean pods@Prussian blue	Cs^+	298	–4.06	4.34	0.028	Endothermic and spontaneous process associated with high disorder at the solid-liquid interface	[38]
		308	–4.33				
		318	–4.61				
		328	–4.90				
corn stalk	IO_3^-	298	4.8745	111.0279	0.3562193	Endothermic, non-spontaneous process and spontaneous (at 318 K)	[31]
		308	1.3124				
		318	−2.2498				
Citrullus lanatus L. seeds@$MnFe_2O_4$	U^{6+}	298	−24.13	23.63	0.17	Endothermic and spontaneous	[52]
		303	−25.89				
		318	−27.45				
bamboo powder@ MoS_2-PO_4	U^{6+}	288	−25.92	21.95	0.16611	Endothermic and spontaneous	[51]
		298	−27.58				
		308	−29.24				
		318	−30.90				
Corn straws@$ZnFe_2O_4$	Th^{4+}	288	− 17.50	4.19	0.06743	Endothermic, and spontaneous processes associated with a disorder increase at the solid-liquid interface	[53]
		298	− 18.51				
		308	− 19.50				
Luffa rattan	U^{6+}	298.15	−6.74	14.88	0.072514	spontaneous and endothermic	[54]
		308.15	−7.46				
		318.15	−8.19				
rice straw (Oxidized)	U^{6+}	288	-14.04	58.26	247.41	Endothermic, and spontaneous processes associated with a disorder increase at the solid-liquid interface	[33]
		293	-15.17				
		298	-16.34				
		303	-18.27				
		313	-20.08				
Fe_3O_4@banana peel	Sr^{2+}	298	−294.13	−2.641	0.978×10^{-3}	Exothermic, and spontaneous process associated with a high disorder at the solid-liquid interface	[55]
		313	−308.8				
		328	−323.47				
fiddle-leaf fig seed	I^-	303	−2.43	9.36	0.03910	Endothermic, and spontaneous process	[89]
		313	−2.74				
		323	−2.99				
		328	−3.13				
NaOH-activated spent coffee	Ba^{2+}	288	−30.6	81.3	0.3874	Spontaneous	[20]
		298	−33.4				
		308	−38.4				

Table 5 (continued)

Biomass waste biochar	Radionuclide pollutant adsorbed	Temp (K)	ΔG^0 (kJ/mol)= $\Delta H - T\Delta S = -RT\ln K_c$	ΔH^0 (kJ/mol)	ΔS^0 (J/mol.K)	Comment	Ref.
spent coffee grounds@$FeCl_3$	Sr^{2+}	288 298 308	−21.838 −22.849 −23.936	8.359	0.104810	Endothermic, and spontaneous processes associated with a disorder increase at the solid-liquid interface	[47]
Wheat straw	U^{6+}	293 313 333	−31.89 −34.07 −36.24	36.28	0.10884	Endothermic, and spontaneous processes associated with a disorder increase at the solid-liquid interface	[72]
phosphoric-activated fiddle-leaf fig seed	I^-	303 313 323 328	−2.88 −3.13 −3.41 −3.56	9.16	0.03988	Endothermic, and spontaneous process	[89]
NaOH-activated spent coffee	Co^{2+}	288 298 308	−29.5 −31.9 −34.5	42.4	0.1878	Spontaneous	[20]
pine needles	U^{6+}	288 298 308 318 328	−12.7 −14.4 −16.1 −17.8 −19.5	36.1	0.1697	Endothermic, and spontaneous processes associated with a disorder increase at the solid-liquid interface	[74]
spent coffee grounds	Sr^{2+}	288 298 308	−21.915 −22.943 −24.022	8.419	0.105301	Endothermic, and spontaneous processes associated with a disorder increase at the solid-liquid interface	[47]
Microcystis	U^{6+}	298 308 318	−6.92 −8.66 −10.40	44.86	0.17378	Endothermic, and spontaneous	[27]
spent coffee	Ba^{2+}	288 298 308	−27.1 −28.7 −30.4	21.6	0.169	Spontaneous	[20]
Wheat straw	Th^{4+}	293 313 333	−39.30 −41.98 −44.66	63.42	0.13412	Endothermic, and spontaneous processes associated with a disorder increase at the solid-liquid interface	[72]
coconut shell@ $Ti_3C_2T_x$ and@polydopamine@ polyethyleneimine	Cs^+	298 313 333	-2.01 -2.94 -3.99	14.80	0.05645	Exothermic, and spontaneous processes associated with a randomness increase at the solid-liquid interface	[58]
Bamboo residues@polyethyleneimine@NaOH	U^{6+}	298 313 328	−6.60 −5.47 −4.52	−25.79	−0.06551	Exothermic, and spontaneous processes associated with a randomness decrease at the solid-liquid interface	[35]
H_2O_2-modified residual coffee waste	Sr^{2+}	288 298 308	–27.30 –29.33 –30.65	20.97	0.168	Endothermic, and spontaneous processes associated with a randomness increase at the solid-liquid interface	[59]

Table 5 (continued)

Biomass waste biochar	Radionuclide pollutant adsorbed	Temp (K)	ΔG^0 (kJ/mol)= $\Delta H - T\Delta S = -RT\ln K_c$	ΔH^0 (kJ/mol)	ΔS^0 (J/mol.K)	Comment	Ref.
cotton straw	U^{6+}	283.16	−3.40	5.45	7.23		[65]
		293.16	−3.34				
		303.16	−3.26				
		313	−3.18				
NaOH-activated spent coffee	Sr^{2+}	288	−30.2	58.2	0.2004	Spontaneous	[20]
		298	−33.2				
		308	−36.3				
camphor wood sawdust@GO	Sr^{2+}	298	−17.80	261.1	0.933	Endothermic, and spontaneous processes associated with a randomness increase at the solid-liquid interface	[45]
		303	−19.89				
		308	−27.19				
NaOH@H_2O_2-modified residual coffee waste	Sr^{2+}	288	−30.09	46.09	0.26512	Endothermic, and spontaneous processes associated with a randomness increase at the solid-liquid interface	[59]
		298	−33.29				
		308	−35.37				
Microcystis@Fe_3O_4	U^{6+}	298	−6.08	14.25	0.06823	Endothermic, and spontaneous	[27]
		308	−6.76				
		318	−7.44				
Residual coffee waste	Sr^{2+}	288	−26.86	20.69	0.16522	Endothermic, and spontaneous processes associated with a randomness increase at the solid-liquid interface	[59]
		298	−28.64				
		308	−30.16				
Bamboo residues@polyethyleneimine@HNO_3	U^{6+}	298	−5.06	−21.80	−0.05592	Exothermic, and spontaneous processes associated with a randomness decrease at the solid-liquid interface	[35]
		313	−4.37				
		328	−3.40				
KOH-activated bamboo shoot shell	Tc^{7+}	298	−2.86	−63.91	−0.20477	Exothermic, and spontaneous processes associated with a randomness decrease at the solid-liquid interface	[44]
		303	−1.83				
		308	−1.81				
NaOH-modified peanut husk	Sr^{2+}	303	−0.01221	13.48	-0.0042×10^{-3}	Endothermic, and spontaneous processes associated with a randomness decrease at the solid-liquid interface	[80]
		308	−0.01219				
		313	−0.01217				
		323	−0.01215				
		333	−0.01213				
spent coffee grounds	Sr^{2+}	288	−5.484	14.396	0.069221	Endothermic and spontaneous processes associated with a disorder increase at the solid-liquid interface	[21]
		298	−6.352				
		308	−6.860				
orange peel@MnO_2	U^{6+}	288.15	−13.49	57.67	0.24697	Endothermic and spontaneous processes associated with a disorder increase at the solid-liquid interface	[42]
		293.15	−14.73				
		298.15	−15.96				
		303.15	−17.20				
		313.15	−19.67				
spent coffee ground	I^-	288	−8.47	−13.93	−18.82	Exothermic and spontaneous processes associated with a disorder decrease at the solid-liquid interface	[48]
		298	−8.30				
		308	−8.29				
		318	−7.83				

Table 5 (continued)

Biomass waste biochar	Radionuclide pollutant adsorbed	Temp (K)	ΔG^0 (kJ/mol)= $\Delta H - T\Delta S = -RTlnK_c$	ΔH^0 (kJ/mol)	ΔS^0 (J/mol.K)	Comment	Ref.
coconut shell@ $Ti_3C_2T_x$ and@polydopamine@ polyethyleneimine	U^{6+}	298 313 333	-11.57 -12.33 -13.32	3.291	0.04988	Exothermic, and spontaneous processes associated with a randomness increase at the solid-liquid interface	[58]

Where Tc^{7+} is surrogated by Re^{7+} or Cr^{7+}

Table 6 Overview of adsorption-desorption studies

Biomass waste biochar	Radionuclide pollutant adsorbed	Eluting/Regenerating agent	% adsorbed @ 1st cycle	No. of cycle	% adsorbed @ nth cycle	References
rice straw	U^{6+}	1.0 mol/L HCl	95	5	>90	[33]
KOH-activated peanut shell	Sr^{2+}	0.1 mol/L HNO_3	~84	5	~76	[39]
Acidosasa edulis shoot shell	Tc^{7+}	0.1 mol/L KOH	>94	3	>75	[23]
Fe_3O_4@pine needles	U^{6+}	0.1 mol/L Na_2CO_3	99.6	4	62.6	[70]
Watermelon rind@ Fe_3O_4	U^{6+}	0.1 mol/L Na_2CO_3	99	3	44	[49]
soybean pods@Prussian blue	Cs^+	0.1 mol/L HCl	>90	3	>80	[38]
Corn straws@$ZnFe_2O_4$	Th^{4+}	0.5 mol/L citric acid	>95	6	86.08	[53]
Citrullus lanatus L. seeds@$MnFe_2O_4$	U^{6+}	0.5 mol/L HCl	>80	5	>60	[52]
Banana peel@Fe_3O_4	Sr^{2+}	0.1 mol/L HNO_3	>60	3	>40	[55]
pine needles	U^{6+}	0.05 mol/L HCl	99.11	4	88.37	[74]
KOH-activated fish scales	U^{6+}		94	5	83	[46]
Brewer's spent grain	Sr^{2+}	0.01 mol/L HNO_3	100	5	32.7	[91]
coconut shell@ $Ti_3C_2T_x$ and@polydopamine@ polyethyleneimine	Cs^+	1 mol/L HCl	~90	4	>75	[58]
Bamboo residues@polyethyleneimine@NaOH	U^{6+}	0.01 mol/L HCl	>85	5	>75	[35]
cotton straw	U^{6+}	0.1 mol/L Na_2CO_3	98	6	96	[65]
Olive pomace	Th^{4+}	1.0 mol/L HNO_3	100	2	100	[77]
Brewer's spent grain	Co^{2+}	0.01 mol/L HNO_3	100	5	36.2	[91]
Microcystis@Fe_3O_4	U^{6+}	0.1 mol/L Na_2CO_3	~30	5	>25	[27]
Bamboo residues@polyethyleneimine@HNO_3	U^{6+}	0.01 mol/L HCl	>80	5	>66	[35]
teak peel	Sr^{2+}	0.1 mol/L HNO_3	>99	5	>80	[79]
phosphorus-doped pomelo peel	U^{6+}	0.5 mol/L HNO_3	>97	5	>97	[63]
orange peel@MnO_2	U^{6+}	1.0 mol/L HCl	~100	5	~95.60	[42]
bamboo shoot shell	Tc^{7+}	0.1 mol/L KOH	97.1	3	~80	[26]
coconut shell@ $Ti_3C_2T_x$ and@polydopamine@ polyethyleneimine	U^{6+}	1 mol/L HCl	~90	4	>75	[58]
cow manure@ TiO_2@SiO_2	U^{6+}	0.05 mol/L HCl	>90	5	>87.6	[78]
Citrullus lanatus L. Seeds	U^{6+}	0.5 mol/L HCl	>60	5	<40	[52]
Fish scales	U^{6+}		72	5	60	[46]
cow manure@ TiO_2@SiO_2	Th^{4+}	0.05 mol/L HCl	>95	5	>92.5	[78]
cotton straw	U^{6+}	1 mol/L Na_2CO_3	98	6	87	[65]

metals and their coexisting ions (sulfate, nitrate, and chloride ions) in tap water also influences the adsorption output. In particular, the rivalry between K^+, Na^+, and Cs^+ would impact the sorbents' ability to remove Cs^+ [38].

Also, Philippou's research group [102] employed *Luffa Cylindrica* fibers BC coated Ag and non-Ag BC to clean up Po^{4+} from the seawater sample. When comparing the seawater sample treated with *Luffa Cylindrica* fibers BC@Ag to the blank sample, which did not receive BC treatment, and the sample treated with non-coated *Luffa Cylindrica* fibers BC, it is evident that the Po^{4+} concentration in the seawater sample has significantly decreased (~90%) while 30% of the Po^{4+} is eliminated in the sample that had *Luffa Cylindrica* fibers BC treatment. Additionally, the tubular form of the biochar fibers gives them a large exterior surface area, which is linked to rapid material exchange and a greater number of surface binding sites for better Po^{4+} radio-contaminant adsorption [102]. In another research [74], pine

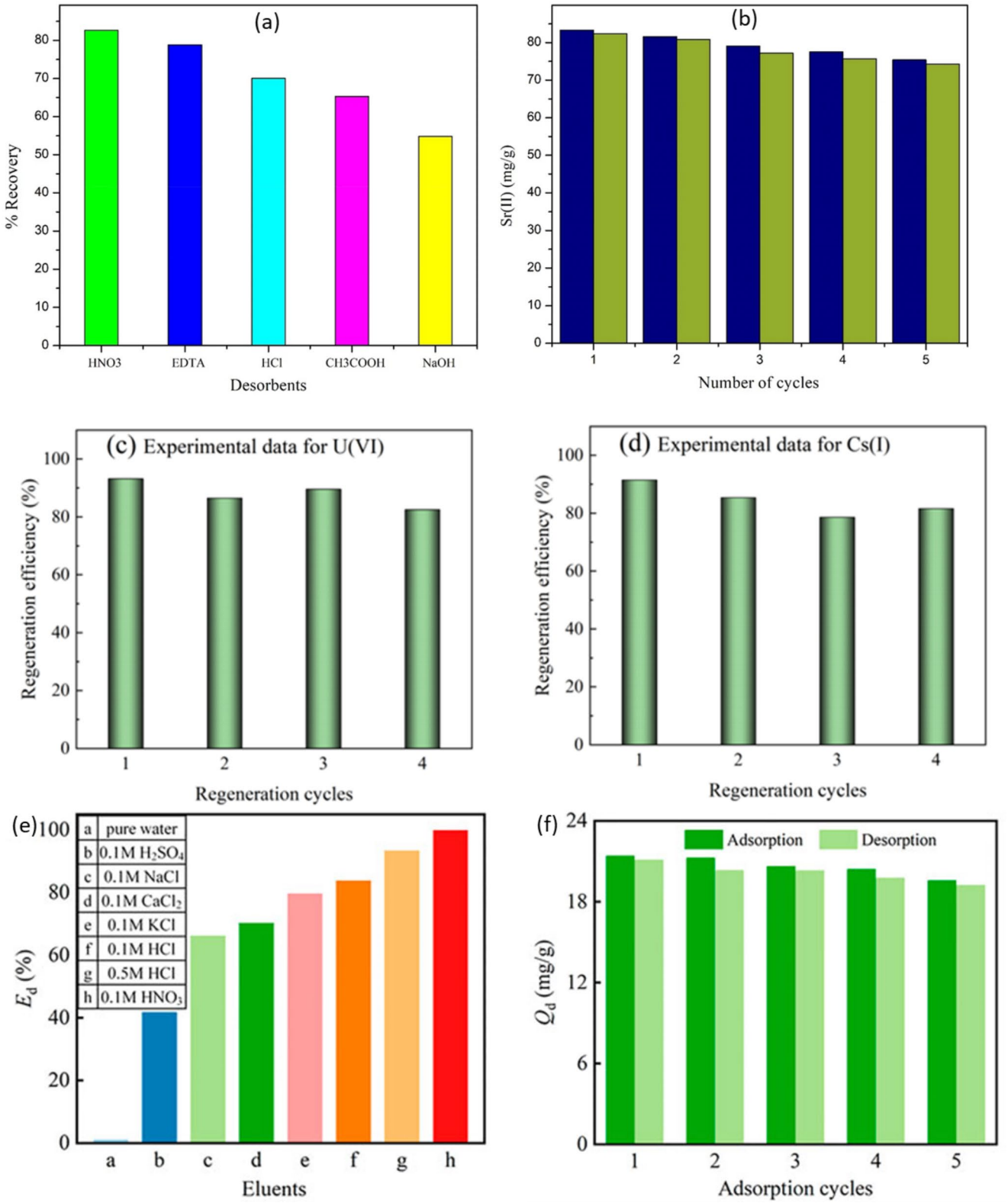

Fig. 9 **(a)** Impact of eluent on desorption of adsorbed Sr^{2+} and regeneration of KOH-activated peanut shell (**b**) Adsorption–desorption cyclic performance study for Sr^{2+} adsorption using KOH-activated peanut shell [39]. Adsorption–desorption cyclic performance study for (**c**) U^{6+} and (**d**) Cs^{+} adsorption using coconut shell@ $Ti_3C_2T_x$ and@ polydopamine@ polyethyleneimine BC [58]. (**e**) Desorption efficiency of Sr^{2+} by different eluting agents, (**f**) the recyclability performance of teak peel BC [79]

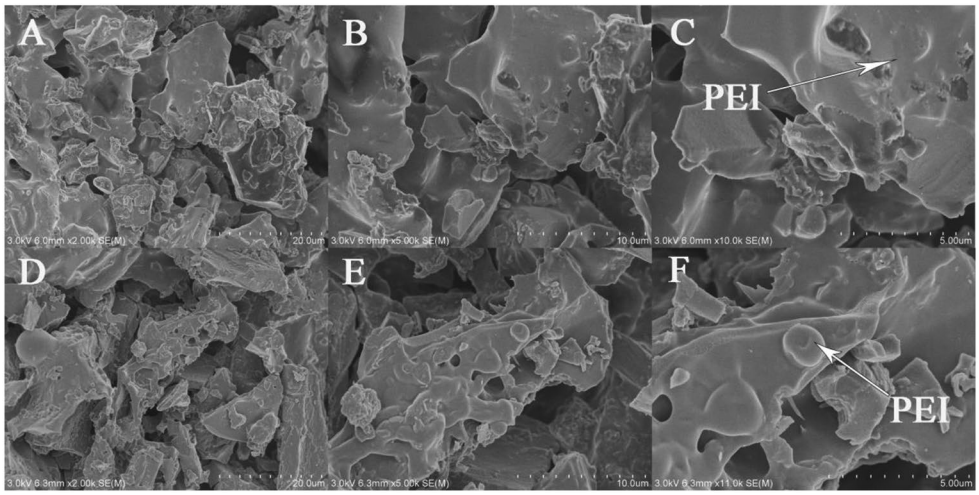

Fig. 10 The SEM image of the (**A, B, C**) NaOH-modified bamboo residues@polyethyleneimine BC and (**D, E, F**) HNO_3-modified bamboo residues@polyethyleneimine BC after regeneration [35]

needles biochar was employed to remove simulated U^{6+} nuclear industrial effluent to show off its adsorption capabilities and usefulness in extracting U^{6+} from wastewater mixed with other ions. The wastewater was generated following the uranium hydrometallurgy plant's resin adsorption tail liquid composition. 15 mg/L U^{6+}, 10 g/L SO_4^{2-}, 1 g/L NO_3^-, 0.2 g/L Mg^{2+}, 0.5 g/L Ca^{2+}, and 1.6 g/L Fe^{3+} were all present in the wastewater. It was looked at how much adsorbent was used to remove U^{6+} from wastewater. The proportion of U^{6+} that was adsorbable rose when the BC dose was raised. With 2.0 g biochar, it was feasible to remove all of the U^{6+} (~99.9%) from 1.0 L of industrial effluent that contained 15.0 mg of U^{6+} [74].

In another report [46], in order to assess the applicability of KOH-activated fish scales in a variety of waterways, artificial ground, and surface waters were utilized to mimic water tainted with uranium. The uptake capabilities of KOH-activated fish scales toward U^{6+} in deionized water were greater than those of synthetic groundwater with 228.22 mg/g and synthetic surface water with 252.31 mg/g, as indicated in Fig. 14c. Notwithstanding this, over 49% of U^{6+} was adsorbed on KOH-activated fish scales in a variety of fluids, indicating the material's wide application potential in the disposal of U^{6+} wastewater [46].

Also, Liao and co-workers [78]explored the dynamic of adsorption of Th^{4+} and U^{6+} using cow manure@ TiO_2@ SiO_2 BC. The results of five times of continuous adsorption at Ci = 5 mg/L for U^{6+} and Th^{4+} show that the dynamic elimination effectiveness of cow manure@ TiO_2@SiO_2 BC reached 99.5% and 99.8%, respectively as presented in Fig. 14a, and nearly totally captured the pollutants in the solution. These results were below the World Health Organization's limit of 30 µg/L for U^{6+} and 246 µg/L for Th^{4+}, further demonstrating the high efficiency of cow manure@ TiO_2@SiO_2 BC in U^{6+} and Th^{4+} removal. The dynamic U^{6+} and Th^{4+} elimination efficiencies of cow manure@TiO_2@ SiO_2 BC in various water systems are displayed in Fig. 14b. The findings demonstrated that the water system did not affect the dynamic adsorption efficiency of cow manure@ TiO_2@SiO_2 BC for Th^{4+} (over 97%), indicating the good selectivity of cow manure@TiO_2@SiO_2 BC for Th^{4+}. Cow manure@TiO_2@SiO_2 BC dynamic adsorption behavior for U^{6+} was dependent on the water system, which may have been caused by ions in the water system itself occupying active spots. Nevertheless, cow manure@TiO_2@SiO_2 BC U^{6+} removal efficiency was still greater than 75%, demonstrating the material's promise for treating wastewater containing U^{6+} and Th^{4+} [78]. By and large, the background ions affect the adsorption of radio-contaminants based on the proximity and the largeness of hydration/ionic radii. Specifically, competing ions with a big hydration radius (HR) can be effortlessly captured/trapped by the BWDBC, diminishing the interaction between radio-contaminant species and active spots [62]. Also, background ions with HR that are very close to the HR of the radio-contaminants of interest tend to compete strongly and have a negative impact on the entire adsorption capacity and efficiency. For example, the HR of cesium ion and sodium ion is 3.25 and 3.6 Å, respectively, and because of these comparable HR, Cs^+, and Na^+ ions contend to bind with the mesquite wood waste-base BC during Cs^+ adsorption operation [28]. As shown in Fig. 14d, the author also relates the negative impact of Ni, Na, Mn, and Cd to their ionic radii that are close to that of the adsorbed Sr^{2+} and Co^{2+} by brewer spent grain BC [91].

In another study, it was found that $NaClO_4$ shows a minor ionic effect on the adsorption of U^{6+} using oxidized rice straw BC. The authors opined that this may be because of the larger ionic size and low charge density of Na^+, which cause significant interactions between the other sodium ions and the surrounding H_2O molecules rather than the oxidized rice straw BC employed. In addition, it was accentuated that the outer-sphere reacts more readily to any alteration in

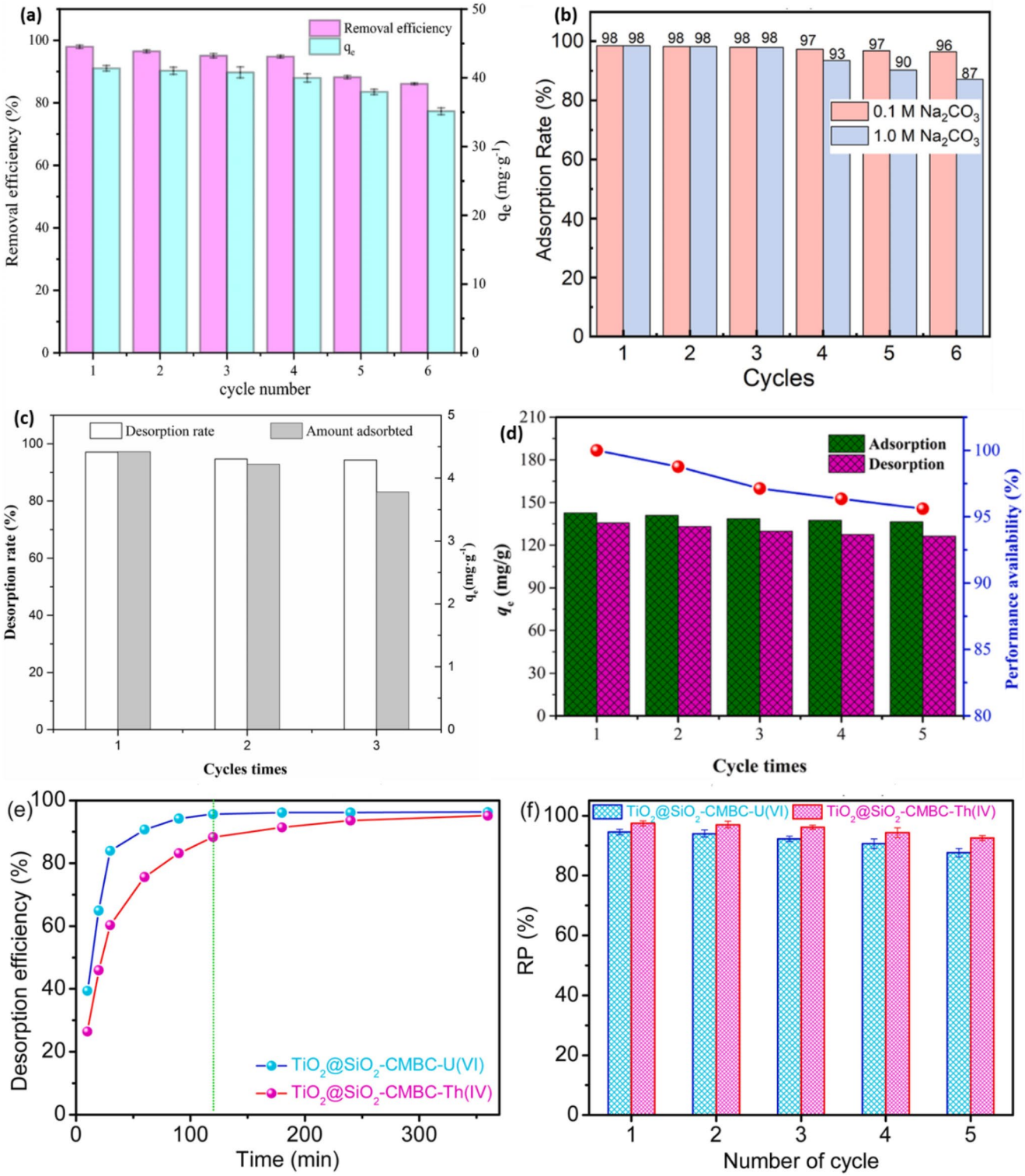

Fig. 11 Adsorption-desorption of (**a**) corn straws@$ZnFe_2O_4$ for Th^{4+} [53], (**b**) cotton straw BC for U^{6+} [65], (**c**) bamboo shoot shell for Tc^{7+} [26], (**d**) orange peel@MnO_2 for U^{6+} [42]. (**e**) Desorption efficiency at different times and (**f**) recyclability performance of cow manure@TiO_2@SiO_2 for U^{6+} and Th^{4+} [78]

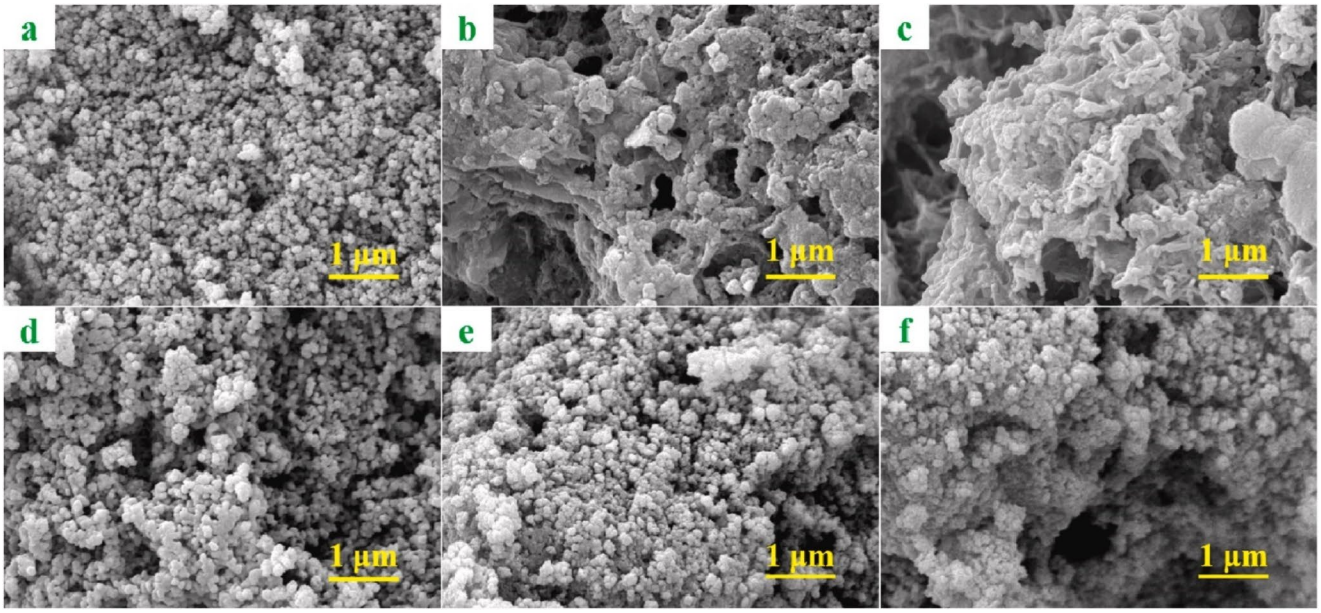

Fig. 12 SEM images (**a**) cow manure@ TiO_2@SiO_2, (**b**) cow manure@ TiO_2@SiO_2 after U^{6+} uptake, (c) cow manure@ TiO_2@SiO_2 after Th^{4+} uptake, (d) cow manure@ TiO_2@SiO_2 after stirring in deionized H_2O, (e) cow manure@ TiO_2@SiO_2-U after the elution and (f) cow manure@ TiO_2@SiO_2-Th after the elution [78]

ionic strength than inner-sphere complexes and this proves that the mechanism of adsorption of U^{6+} by the biochar is inner-sphere complexation [33]. Similarly, the obtained results for the investigation on the effect of Na^+, Ca^{2+}, $Mg^{2+,}$ and K^+ showed no discernible impact on the removal of U^{6+} adsorption, most likely because inner-sphere complexation is primarily responsible for U^{6+} adsorption on orange peel@magnesium silicate BC [43]. In another experiment, the HR ratio, charge, and electronegativity of the coexisting ions were examined concerning their impacts on the removal characteristics of horse manure@Bi_2O_3 BC and horse manure BC to U^{6+}. Except for Al^{3+}, Ca^{2+}, CO_3^{2-}, and PO_4^{3-}, the adsorption behavior of horse manure@Bi_2O_3 BC for U^{6+} was independent of the majority of coexisting ions, as seen in Fig. 15a and **b**. The adsorption effectiveness of horse manure@Bi_2O_3 BC to U^{6+} fell from 93.9 to 20.6%, particularly for Al^{3+}, but this had no discernible impact on the adsorption behavior of horse manure@Bi_2O_3 BC for K^+ and Na^+. The biochar could readily absorb the cations with a wide HR, minimizing the interaction between U^{6+} species and active sites. The adsorption efficiency of horse manure@Bi_2O_3 BC to U^{6+} dropped from 93.9 to 76.7% for Ca^{2+} as well. However, the adsorption behavior of horse manure@Bi_2O_3 BC for Zn^{2+} and Mg^{2+} remained unaffected significantly. In addition, the following factors were used to explain the negative effects of CO_3^{2-} and PO_4^{3-} on U^{6+} adsorption by horse manure@Bi_2O_3 for anions: firstly, horse manure@Bi_2O_3 surface charge distribution would be altered by the presence of CO_3^{2-} and PO_4^{3-} in the solution, resulting in distinct ESI with U^{6+} species; secondly, UO_2CO_3 and $UO_2PO_4^-$ formed in the solution, and horse manure@Bi_2O_3 found it challenging to capture these stable and soluble complexes [62]. Contrarily, as shown in Fig. 15c, **the** Ahmed research team [52] reported that the uptake capacity of *Citrullus lanatus* L. seeds@$MnFe_2O_4$ BC for $U^{6+}$was observed to remain high in the presence of K^+, Mg^{2+}, Ca^{2+}, Na^+, Cl^-, SO_4^{2-} CO_3^{2-} and NO_3^- ions, demonstrating that the co-existing ions have no meaningful effect on the adsorption operation [52] and this is in very good agreement with what was reported in Fig. 15d for the the effect of NO_3^-, Cl^-, and PO_4^{3-} on the adsorption of U^{6+} by magnetized watermelon rind BC [49].

Column Adsorption Studies

Research on the effectiveness of adsorption in a column setup is quite common since the results of a study may have practical applications. Moreover, in order to minimize downtime, industrial operations are mostly continuous. Such industrial applications are easier to achieve using column adsorption [82]. In addition, one important test of the practicality of newly discovered adsorbents is dynamic column adsorption [63].

Although there is a dearth of studies on column adsorption research on radio-contaminants clean-up by biomass waste-derived biochar. However, a few studies found in the literature are pragmatically discussed below and summarized in Table 8.

Table 7 Overview of competitive adsorption performance evaluation of biomass waste-derived biochar for radio-contaminants

Biomass waste biochar	Radionuclide pollutant adsorbed	Competing species	Maximum change with competing species	References
Mesquite wood waste	Cs^{+}	Na^{+}	reduced by 38.1%	[28]
Artemia egg shell@Cu_2O/Cu^0	I^{-}	Cl^{-}	No significant reduction	[50]
rice straw	U^{6+}	$NaClO_4$	Minor effect	[33]
rice straw	Sr^{2+}	Ca^{2+}	Show significant effect	[83]
Mesquite wood waste + chicken manure	Cs^{+}	Na^{+}	Obvious reduction	[28]
horse manure@Bi_2O_3	U^{6+}	SO_4^{2-}	Minor effect	[62]
KOH-activated peanut shell	Sr^{2+}	Ca^{2+}	Decrease by 32.03%	[39]
horse manure@Bi_2O_3	U^{6+}	CO_3^{2-}	Significant effect	[62]
horse manure@Bi_2O_3	U^{6+}	Cl^{-}	No significant effect	[62]
orange peel@magnesium silicate	U^{6+}	Ca^{2+}	no significant impact	[43]
Artemia egg shell@Cu_2O/Cu^0	I^{-}	NO_3^{-}	No significant reduction	[50]
Mesquite wood waste + food waste	Cs^{+}	Na^{+}	Obvious reduction	[28]
KOH-activated peanut shell	Sr^{2+}	Mg^{2+}	Decrease by 10.90%	[39]
KOH-activated Mesquite wood waste + food waste	Cs^{+}	Na^{+}	Reduced by 6%	[28]
rice straw	Sr^{2+}	Na^{+}	Show significant effect	[83]
orange peel@magnesium silicate	U^{6+}	Mg^{2+}	no significant impact	[43]
horse manure@Bi_2O_3	U^{6+}	ClO_4^{-}	No significant effect	[62]
KOH-activated peanut shell	Sr^{2+}	K^{+}	Almost insignificant effect	[39]
Fe_3O_4@pine needles	U^{6+}	$NaClO_4$	not affected	[70]
Mesquite wood waste	Sr^{2+}	Ca^{2+}	Decreased by 7.8%	[28]
Magnetized watermelon rind	U^{6+}	Cl^{-}	No significant effect	[49]
horse manure@Bi_2O_3	U^{6+}	NO_3^{-}	No significant effect	[62]
orange peel@magnesium silicate	U^{6+}	Na^{+}	no significant impact	[43]
soybean pods@Prussian blue	Cs^{+}	Na^{+}	reduced significantly,	[38]
Magnetized watermelon rind	U^{6+}	NO_3^{-}	No significant effect	[49]
Mesquite wood waste + chicken manure	Sr^{2+}	Ca^{2+}	Decreased by 6.1%	[28]
horse manure@Bi_2O_3	U^{6+}	Mg^{2+}	No significant effect	[62]
Citrullus lanatus L. seeds@$MnFe_2O_4$	U^{6+}	SO_4^{2-}	No significant effect	[52]
KOH-activated peanut shell	Sr^{2+}	Na^{+}	Almost insignificant effect	[39]
Bamboo shoot shell@ZnO	Tc^{7+}	I^{-}	Low impact	[71]
Mesquite wood waste + food waste	Sr^{2+}	Ca^{2+}	Decreased by 5.2%	[28]
rice straw	Sr^{2+}	K^{+}	Show little effect	[83]
soybean pods@Prussian blue	Cs^{+}	Ca^{2+}	reduced significantly,	[38]
Bamboo shoot shell@ZnO	Tc^{7+}	NO_2-	Low impact	[71]
orange peel@magnesium silicate	U^{6+}	K^{+}	no significant impact	[43]
Citrullus lanatus L. seeds@$MnFe_2O_4$	U^{6+}	CO_3^{2-}	No significant effect	[52]
Magnetized watermelon rind	U^{6+}	PO_4^{3-}	No significant effect	[49]
Artemia egg shell@Cu_2O/Cu^0	I^{-}	SO_4^{2-}	No significant reduction	[50]
Bamboo shoot shell@ZnO	Tc^{7+}	NO_3-	Low impact	[71]
rice straw (Oxidized)	U^{6+}	$NaClO_4$	Minor effect	[33]
rice straw	Sr^{2+}	Mg^{2+}	Little effect	[83]
Citrullus lanatus L. seeds@$MnFe_2O_4$	U^{6+}	Ca^{2+}	No significant effect	[52]
horse manure@Bi_2O_3	U^{6+}	Zn^{2+}	No significant effect	[62]
Brewer's spent grain	Sr^{2+}	Cd	Decreased by 59.7%	[91]
soybean pods@Prussian blue	Cs^{+}	K^{+}	reduced significantly,	[38]
Bamboo shoot shell@ZnO	Tc^{7+}	SO_4^{2-}	Low impact	[71]
KOH-activated Mesquite wood waste + food waste	Sr^{2+}	Ca^{2+}	Decreased by 23.7%	[28]
Citrullus lanatus L. seeds@$MnFe_2O_4$	U^{6+}	NO_3^{-}	No significant effect	[52]
Bamboo shoot shell@ZnO	Tc^{7+}	PO_4^{3-}	Low impact	[71]
horse manure@Bi_2O_3	U^{6+}	K^{+}	No significant effect	[62]
Brewer's spent grain	Sr^{2+}	Na	Decreased by 30.2%	[91]
rice straw	Sr^{2+}	Al^{3+}	Show little effect	[83]
palm tree fibers	Th^{4+}	$NaClO_4$	No effect	[73]

Table 7 (continued)

Biomass waste biochar	Radionuclide pollutant adsorbed	Competing species	Maximum change with competing species	References
soybean pods@Prussian blue	Cs^{+}	Mg^{2+}	reduced significantly,	[38]
pine needles	U^{6+}	KNO_3	Significant effect	[74]
Bamboo shoot shell@ZnO	Tc^{7+}	Cu^{2+}	Low impact	[71]
Citrullus lanatus L. seeds@$MnFe_2O_4$	U^{6+}	K^{+}	No significant effect	[52]
Brewer's spent grain	Sr^{2+}	Ni	Decreased by 29.4%	[91]
KOH-activated fish scales	U^{6+}	$NaNO_3$	Almost no effect	[46]
Bamboo shoot shell@ZnO	Tc^{7+}	Fe^{3+}	Low impact	[71]
Brewer's spent grain	Sr^{2+}	Mn	Decreased by 25.2%	[91]
Wheat straw	Th^{4+}	Na^{+}	no strong effect	[72]
Citrullus lanatus L. seeds@$MnFe_2O_4$	U^{6+}	Na^{+}	No significant effect	[52]
Bamboo shoot shell@ZnO	Tc^{7+}	Al^{3+}	Low impact	[71]
cotton straw	U^{6+}	K^{+}	45.3% reduction	[65]
Citrullus lanatus L. seeds@$MnFe_2O_4$	U^{6+}	Mg^{2+}	No significant effect	[52]
Brewer's spent grain	Co^{2+}	Mn	Zero effect	[91]
cotton straw	U^{6+}	Cu^{2+}	55.7% reduction	[65]
watermelon rind	U^{6+}	PO_4^{3-}	No significant effect	[49]
magnetic crayfish shells	Sr^{2+}	Na	Variable	[61]
Microcystis@Fe_3O_4	U^{6+}	$NaNO_3$	No significant effect	[27]
Brewer's spent grain	Co^{2+}	Na	Zero effect	[91]
cotton straw	U^{6+}	Mn^{2+}	12.1% reduction	[65]
horse manure@Bi_2O_3	U^{6+}	Al^{3+}	73.3% reduction	[62]
spent coffee grounds	Sr^{2+}	bovine serum albumin	4.3% reduction	[21]
Bamboo shoot shell@ZnO	Tc^{7+}	UO_2^{2+}	Low impact	[71]
watermelon rind	U^{6+}	NO_3^{-}	No significant effect	[49]
horse manure@Bi_2O_3	U^{6+}	Ca^{2+}	17.2% reduction	[62]
Citrullus lanatus L. seeds@$MnFe_2O_4$	U^{6+}	Cl^{-}	No significant effect	[52]
NaOH-modified peanut husk	Sr^{2+}	Co^{2+}, Cu^{2+}, Ni^{2+}, Cd^{2+}, Zn^{2+}, Mn^{2+}, Pb^{2+}, I^{-}, and Cl^{-1}	Strong effect	[80]
cotton straw	U^{6+}	Cs^{+}	33.3% reduction	[65]
spent coffee grounds	Sr^{2+}	Alginate	14.6% reduction	[21]
orange peel@MnO_2	U^{6+}	$NaClO_4$	Little effect	[42]
Brewer's spent grain	Co^{2+}	Cd	Decreased by 24.1%	[91]
watermelon rind	U^{6+}	Cl^{-}	No significant effect	[49]
horse manure@Bi_2O_3	U^{6+}	Na^{+}	No significant effect	[62]
Brewer's spent grain	Co^{2+}	Ni	Decreased by 32.3%	[91]
cotton straw	U^{6+}	Sr^{+}	46.8% reduction	[65]
spent coffee grounds	Sr^{2+}	humic acid	14.3% reduction	[21]

Where Tc^{7+} is surrogated by Re^{7+} or Cr^{7+}

For example, Jang's research group [83] studied the adsorption of Sr^{2+} onto rice straw BC beads in a fixed-bed column. The study examined the impact of operational factors on the adsorption capacity, including flow rate and starting concentrations of Sr^{2+}. It was discovered that because Sr^{2+} did not have sufficient time to come into touch with the BC beads, the breakthrough curves were steeper at elevated flow rates. With a surge in flow rate, there was a fall in both the breakthrough and saturation times. Furthermore, when the flow rate increased, the column's saturation adsorption capacity diminished. Moreover, due to an enhanced diffusion coefficient, a spike in the initial concentration of strontium resulted in a quicker mass-transfer flow from the bulk solution to the particle surface. Therefore, improved column performance was seen with a surge in driving force and a reduction in the duration of the adsorption zone during the adsorption process. In addition, the analysis found that the experimental data fit both the Yoon-Nelson and Thomas models well. This supported the Langmuir isotherm, as well as the idea that the rate of Sr^{2+} sorption decline is proportionate to the breakthrough [83]. In another study [84], NaOH-modified duckweed BC was investigated for the adsorption of Th^{4+}. At optimal conditions, a remarkable experimental qmax of 73.8 mg/g was accomplished and this is somewhat

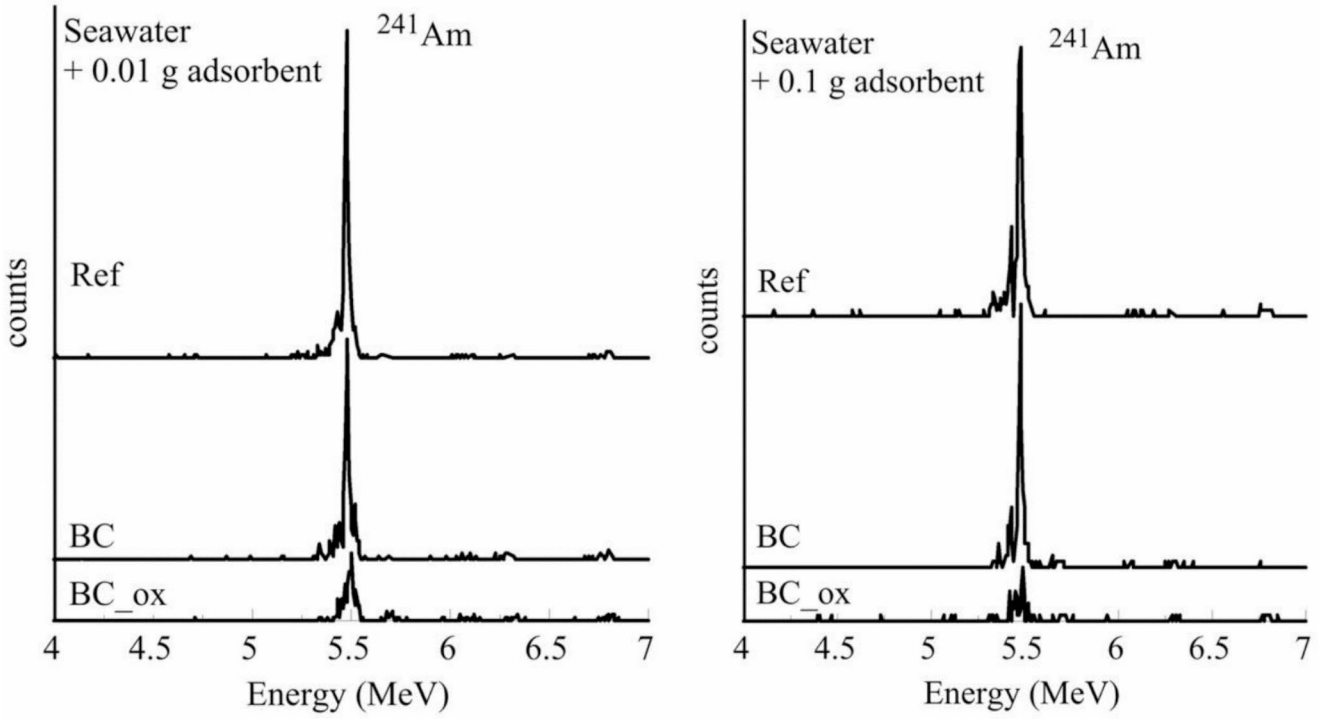

Fig. 13 Alpha spectra of ^{241}Am polluted seawater samples before and following reaction with the 10 mg and 100 mg *Luffa cylindrica* BC and oxidized *Luffa cylindrica* BC [101]

higher than that of theoretical qmax of 71.7 mg/g. In addition, the Thomas model was found to be suitable for the experimental data description with 0.975 R^2 [84].

In another study [63], the authors here employed a fix-bed column packing with phosphorus-doped pomelo peel BC to adsorptively remove U^{6+} from U^{6+}-containing solutions and actual nuclear effluent in order to illustrate the great effectiveness of phosphorus-doped pomelo peel BC in dynamic U^{6+} adsorption (Fig. 16a). The adsorption column is capable of effectively removing uranium from a 5 mg/L U^{6+} solution, as seen in Fig. 16b. The fix-bed column can also effectively remove U^{6+} from the solution when the concentration of U^{6+} is increased to 50 mg/L (Fig. 16c). Following 2000 min of adsorption, phosphorus-doped pomelo peel BC column adsorption capacity surpasses 422 mg/g, significantly surpassing that of nearly all other biochar adsorbents. In addition, the fix-bed column may be readily recycled by eluting it with 0.5 M diluted HNO_3, and its adsorption effectiveness won't reduce when it's employed straight again in the subsequent cycle (Fig. 16c). Remarkably, U^{6+} with a concentration of 14 µg/L can be removed from a genuine nuclear effluent using the fix-bed column. After going down the column, the U^{6+} content may be reduced to around 3 µg/L (Fig. 16d). These findings show that phosphorus-doped pomelo peel BC has a strong chance of being used in real-world nuclear wastewater disposal scenarios where U^{6+} is present [63]. Summarily, the majority of research found that the Thomas model best described radio-contaminant sorption by biomass waste-derived biochar, and according to this model, during radio-contaminant adsorption, plug flow dispersion predominates in the adsorption bed.

Perspective and Future Research Directions

Notably, this review revealed that significant research advancement and achievements have been made in the use of biomass waste-derived biochar for the sequestration of radio-contaminants. However, we were able to figure out problematic issues and knowledge gaps that could provide a basis for future research endeavors, and give direction for future research hotspots.

To begin with, the techno-economic evaluation of adsorbent use and the entire adsorption operation is part of crucial issues for investors, industrial engineers, the wastewater treatment sectors, legislators, and other stakeholders. However, this study area is usually neglected and thus in the future, it is obligatory to empirically evaluate the techno-economic practicability and cost-effectiveness of biomass choice, and production and application cost if it is to be accepted in the actual world. More so, in our opinion, the claim that $\Delta H° < 21.0$ or 40 kJ/mol is physisorption automatically includes all exothermic radio-contaminant adsorption operations, whereas, there are a few studies [36,

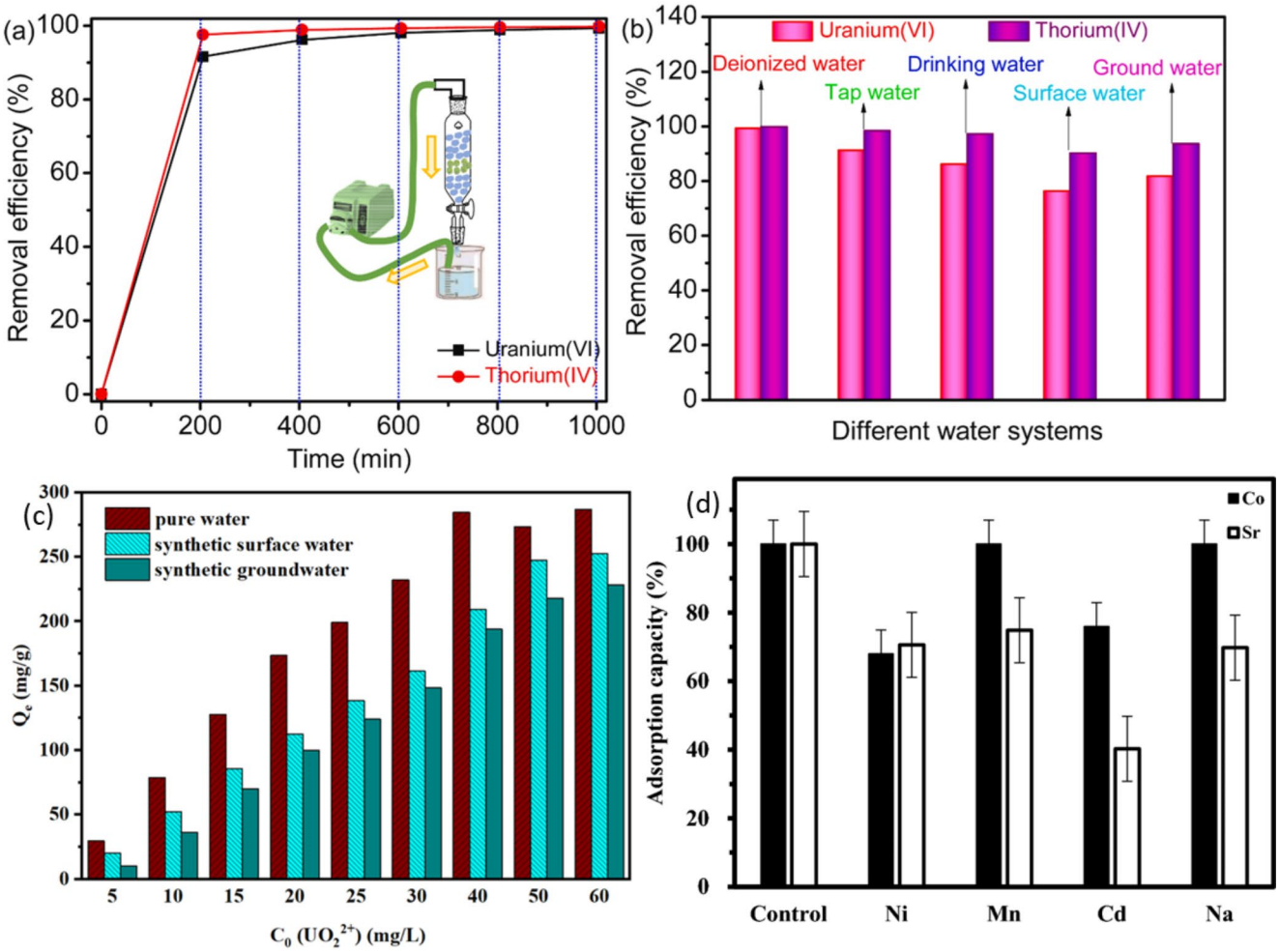

Fig. 14 impact of (**a**) residence time and (**b**) water system on the dynamic adsorption efficacy of cow manure@ TiO_2@SiO_2 BC for U^{6+} and Th^{4+} [78]. (**c**) U^{6+} clean-up by KOH-activated fish scales from different water systems [46]. (**d**) Effect of competing ions on the adsorption of Sr^{2+} and Co^{2+} by brewer-spent grain BC [91]

39, 44, 58] where the radio-contaminant adsorption is exothermic but the mechanism involve chemisorption. Thus, future researchers should pay attention to this ambiguity. Also, there has been notable progress on the reusability of expended BWDBC. However, their management and end life after multiple reuses have not been considered and there is no doubt that disposal of reused expended BWDBC can still harm the environment and defeat the original aim of win-win pollution management. Thus, we propose that the reused expended BWDBC be repurposed as a photocatalyst since many of the adsorbed radio-contaminants can respond to light. Also, they can be employed as part of the ingredients for making supercapacitors. Furthermore, there are very few works on column adsorption studies. Hence, future studies should focus more on this area and also explore various column flow configurations for radio-contaminant remediation, as this will boost the process's real-life practicability potential and acceptance. Further research might also focus on the use of innovative hybrid technologies by combining the adsorption method with other techniques like co-precipitation, photocatalytic degradation [103, 104], tribocatalytic degradation [105], in situ oxidation, electrocoagulation, and so on. In addition, while adsorption kinetics has received much attention, it is recommended that future studies expand to include desorption kinetics in order to get a deeper knowledge of the potential for regenerability and recycling of different types of BWDBC. The modeling of fuzzy inference systems, density functional theory simulation, and neural networks for radio-contaminant uptake by BWDBC is not reported. As environmental and industrial engineers move toward using AI-based tools to solve issues [82], this is a crucial topic that has to be explored. All of the above can take adsorption techniques to the next level if fully explored.

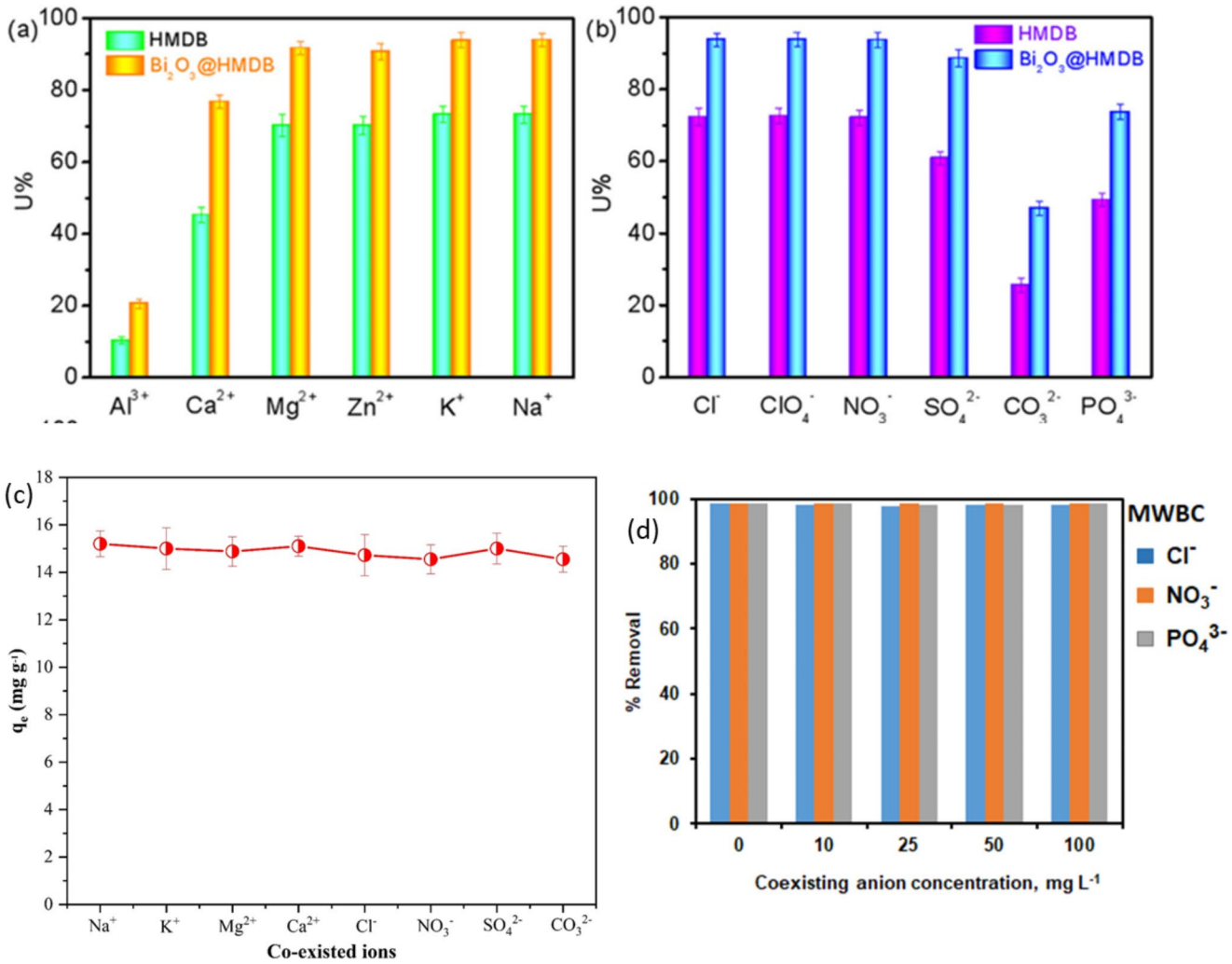

Fig. 15 (**a**) Effect of co-existing ions on the adsorption of U^{6+} by (**a-b**) horse manure BC and horse manure@Bi_2O_3 BC [62]. (**c**) *Citrullus lanatus* L. seeds@$MnFe_2O_4$ BC [52]. (d) magnetized watermelon rind [49]

Table 8 Summary of column adsorption for the removal of radio-contaminants by biomass-waste-derived biochar

Biomass waste biochar	Radio-pollutant	Best-fit model	Bed height (cm)	Vol. flowrate (mL/min)	Inlet Conc. (mg/L)	Adsorption capacity (mg/g)	Rate constant (L/min.mg)	References
rice straw	Sr^{2+}	Thomas	6	0.5	300	173.67	26.67×10^{-5}	[83]
Duckweed	Th^{4+}	Thomas	-	1	500	73.8	14.0×10^{-5}	[84]
phosphorus-doped pomelo peel	U^{6+}	-	-	1	50	422	-	[63]
NaOH modified duckweed	Th^{4+}	Thomas	-	1	500	47.1	22.2×10^{-5}	[84]
camphor wood sawdust@GO	Sr^{2+}	Thomas	3	2.5	50	581.86	16.67×10^{-5}	[45]
Duckweed	Th^{4+}	Thomas	-	1	500	55.9	18.6×10^{-5}	[84]

Conclusion

Over the years, a broad range of biomass waste-derived biochar has been used for radio-contaminant uptake; however, considering the threshold of $q_{max} > 1000$ mg/g, wheat straw BWDBC stands out with 1527.02 mg/g q_{max} for U^{6+} and 1158.16 mg/g q_{max} for Th^{4+} at pH 5 and 20 °C temperature [72] while $KMnO_4$-modified pig manure BC, camphor leaves@Bi_2O_3 BC and cow manure@ TiO_2@SiO_2 BC came close from behind with q_{max} of 979.3 mg/g for U^{6+} [66], 885.8 mg/g for I^- [68], and 710.4 mg/g for Th^{4+} [78]. Findings from the review also show that most exhausted BWDBC can be eluted/regenerated mostly with acid/base like HCl, HNO_3, KOH, and Na_2CO_3 and reused up to 3–6 times with an adsorption performance of >75% in most cases while upholding their innate structural integrity. Furthermore, it

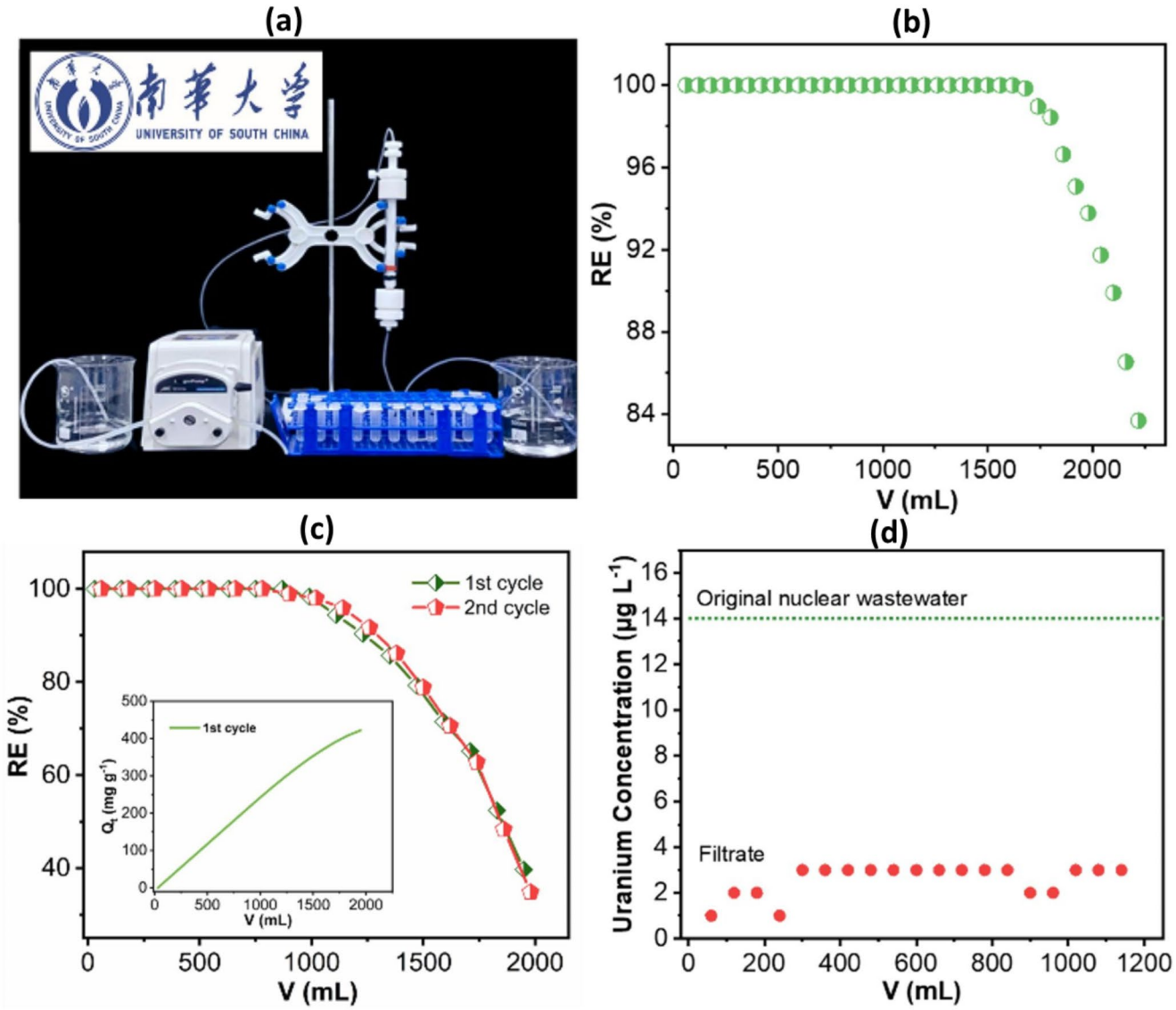

Fig. 16 (**a-c**) Dynamic adsorption of U^{6+} from U^{6+}-containing solution in a fix-bed column. (**d**) Dynamic adsorption of U^{6+} from real nuclear wastewater in a fix-bed column [63]

was discovered that chelation/complexation (especially inner-sphere complexation), pore diffusion, ion exchange, π electrons coordination, precipitation, van der Waals forces, covalent bonding, π-π interactions, and electrostatic interactions/attractions through oxygenated, and oxime functional groups are the main mechanisms of radio-contaminant adsorption. Moreover, the majority of radio-contaminant adsorption was best described by the pseudo-second-order kinetic and Langmuir isotherm. More so, the review revealed that the Thomas model best described radio-contaminant sorption in adsorption columns. Additionally, in authentic radio-wastewater and competitive adsorption scenarios, the existence of other ions typically reduced the sorption of radio-contaminants. Glancing forward, research on innovative hybrid techniques, neural network and AI modeling, density functional theory simulations, and techno-economic analysis should be considered. This review has fruitfully expounded the research advancement and achievement made in the field of study and it can be concluded that adsorption is an effective method for the sequestration of radio-contaminants in aqueous environment.

Author Contribution Stephen Sunday Emmanuel.: Conceptualization, Methodology, Writing- Original draft preparation, Validation, Writing- Reviewing and Editing, Supervision, Project administration, **Ademidun Adeola Adesibikan.**: Writing- Original draft preparation, Validation, Writing- Reviewing and Editing, **Odunayo T. Ore.**: Writing- Original draft preparation, Supervision, Validation, Project administration, Writing- Reviewing and Editing, **Ajibola A. Bayode.**: Writing- Original draft preparation, Supervision, Validation, Project administration, Writing- Reviewing and Editing, **Hamza Badamasi.**: Writing- Original draft preparation, Validation, **Saheed O Sanni.**:

Writing- Original draft preparation, Validation, **Obianuju Patience Ilo.**: Writing- Original draft preparation, Validation.

Funding No funds, grants, or other support was received.

Data Availability Data sharing is not applicable to this article as no datasets were generated or analyzed during the current study.

Declarations

Ethical Approval Not applicable.

Conflict of Interest The authors don't have any financial or non-financial conflict of interest to declare.

Ethical Approval Not applicable.

References

1. Wang, J., Xu, B.: Removal of radionuclide 99Tc from aqueous solution by various adsorbents: A review. J. Environ. Radioact. **270**, 107267 (2023). https://doi.org/10.1016/j.jenvrad.2023.107267
2. Emmanuel, S.S., Adesibikan, A.A., Bayode, A.A., Olawoyin, C.O., Isukuru, E.J., Raji, O.Y.: A review on covalent organic frameworks with mult-site functional groups as superior adsorbents for adsorptive sequestration of radio-contaminants. J. Organomet. Chem. **1015**, 123226 (2024). https://doi.org/10.1016/j.jorganchem.2024.123226
3. Emmanuel, S.S., Olawoyin, C.O., Adesibikan, A.A., Nafiu, S.A., Bayode, A.A.: Solvothermally and non-solvthermally fabricated covalent organic frameworks (COFs) for eco-friendly remediation of radiocontaminants in aquatic environments: A review. J. Organomet. Chem. **1005**, 122984 (2024). https://doi.org/10.1016/j.jorganchem.2023.122984
4. Tiwari, S.K., Bystrzejewski, M., De Adhikari, A., Huczko, A., Wang, N.: Methods for the conversion of biomass waste into value-added carbon nanomaterials: Recent progress and applications. Prog Energy Combust. Sci. **92**, 101023 (2022). https://doi.org/10.1016/j.pecs.2022.101023
5. Emmanuel, S.S., Olawoyin, C.O., Adesibikan, A.A., Opatola, E.A.: A pragmatic review on Bio-polymerized Metallic Nano-Architecture for Photocatalytic Degradation of recalcitrant dye pollutants. J. Polym. Environ. **32**, 1–30 (2023). https://doi.org/10.1007/s10924-023-02986-9
6. Ayub, Y., Zhou, J., Shen, W., Ren, J.: Innovative valorization of biomass waste through integration of pyrolysis and gasification: Process design, optimization, and multi-scenario sustainability analysis. Energy. **282**, 128417 (2023)
7. Emmanuel, S.S., Adesibikan, A.A., Saliu, O.D., Opatola, E.A.: Greenly biosynthesized bimetallic nanoparticles for ecofriendly degradation of notorious dye pollutants: A review. Plant. Nano Biol. **3**, 100024 (2023)
8. Rodriguez, R., Mazza, G., Fabani, M.P., Baldán, Y., Román, C., Riveros-Gomez, M., Mut, I., Fernandez, A.: Valorization of grape By-Products: Toward the Circular Economy Concept. Nutraceutics from Agri-Food By-Products. 117–135 (2025)
9. Chia, M.R., Phang, S.-W., Mohd Razali, N.S., Ahmad, I.: Approach towards sustainable circular economy: Waste biorefinery for the production of cellulose nanocrystals. Cellulose. **31**, 3377–3420 (2024)
10. Emenike, E.C., Iwuozor, K.O., Ighalo, J.O., Bamigbola, J.O., Omonayin, E.O., Ojo, H.T., Adeleke, J., Adeniyi, A.G.: Advancing the circular economy through the thermochemical conversion of waste to biochar: A review on sawdust waste-derived fuel. Biofuels. **15**, 433–447 (2024)
11. Jia, W., Li, S., Wang, J., Lee, J.T.E., Lin, C.S.K., Mašek, O., Zhang, H., Yuan, X.: Sustainable valorisation of food waste into engineered biochars for CO 2 capture towards a circular economy. Green. Chem. **26**, 1790–1805 (2024)
12. Iwuozor, K.O., Umeh, C.T., Emmanuel, S.S., Emenike, E.C., Egbemhenghe, A.U., Ore, O.T., Micheal, T.T., Omoarukhe, F.O., Sagboye, P.A., Ojukwu, V.E.: A comprehensive review on the sequestration of dyes from aqueous media using maize-/corn-based adsorbents. Water Pract. Technol. **18**, 3065–3108 (2023)
13. Ighalo, J.O., Conradie, J., Ohoro, C.R., Amaku, J.F., Oyedotun, K.O., Maxakato, N.W., Akpomie, K.G., Okeke, E.S., Olisah, C., Malloum, A.: Biochar from coconut residues: An overview of production, properties, and applications. Ind. Crops Prod. **204**, 117300 (2023)
14. Ighalo, J.O., Ogunniyi, S., Adeniyi, A.G., Igwegbe, C.A., Sanusi, S.K., Adeyanju, C.A.: Competitive adsorption of heavy metals in a quaternary solution by sugarcane bagasse–LDPE hybrid biochar: Equilibrium isotherm and kinetics modelling. Chem. Prod. Process. Model. **18**, 231–246 (2023)
15. Bayode, A.A., Olisah, C., Emmanuel, S.S., Adesina, M.O., Koko, D.T.: Sequestration of steroidal estrogen in aqueous samples using an adsorption mechanism: A systemic scientometric review. RSC Adv. **13**, 22675–22697 (2023)
16. Bayode, A.A., Emmanuel, S.S., Osti, A., Olorunnisola, C.G., Egbedina, A.O., Koko, D.T., Adedipe, D.T., Helmreich, B., Omorogie, M.O.: Applications of perovskite oxides for the cleanup and mechanism of action of emerging contaminants/steroid hormones in water. J. Water Process. Eng. **58**, 104753 (2024). https://doi.org/10.1016/j.jwpe.2023.104753
17. Ighalo, J.O., Rangabhashiyam, S., Dulta, K., Umeh, C.T., Iwuozor, K.O., Aniagor, C.O., Eshiemogie, S.O., Iwuchukwu, F.U., Igwegbe, C.A.: Recent advances in hydrochar application for the adsorptive removal of wastewater pollutants. Chem. Eng. Res. Des. **184,** 419–456 (2022)
18. Umeh, C.T., Akinyele, A.B., Okoye, N.H., Emmanuel, S.S., Iwuozor, K.O., Oyekunle, I.P., Ocheje, J.O., Ighalo, J.O.: Recent approach in the application of nanoadsorbents for malachite green (MG) dye uptake from contaminated water: A critical review. Environ. Nanatechnol. Monit. Manag. **20**, 100891 (2023). https://doi.org/10.1016/j.enmm.2023.100891
19. Zhang, S., Zhu, X., Zhou, S., Shang, H., Luo, J., Tsang, D.C.W.: Hydrothermal carbonization for hydrochar production and its application. In: Biochar from Biomass and Waste, pp. 275–294. Elsevier (2019)
20. Shin, J., Kwak, J., Lee, Y.-G., Kim, S., Son, C., Cho, K.H., Lee, S.-H., Park, Y., Ren, X., Chon, K.: Changes in adsorption mechanisms of radioactive barium, cobalt, and strontium ions using spent coffee waste biochars via alkaline chemical activation: Enrichment effects of O-containing functional groups. Environ. Res. **199**, 111346 (2021)
21. Shin, J., Lee, S.-H., Kim, S., Ochir, D., Park, Y., Kim, J., Lee, Y.-G., Chon, K.: Effects of physicochemical properties of biochar derived from spent coffee grounds and commercial activated carbon on adsorption behavior and mechanisms of strontium ions (Sr 2+). Environ. Sci. Pollut Res. **28**, 40623–40632 (2021)
22. Li, M., Liu, H., Chen, T., Dong, C., Sun, Y.: Synthesis of magnetic biochar composites for enhanced uranium(VI) adsorption. Sci. Total Environ. **651**, 1020–1028 (2019). https://doi.org/10.1016/j.scitotenv.2018.09.259

23. Hu, H., Jiang, B., Zhang, J., Chen, X.: Adsorption of perrhenate ion by bio-char produced from Acidosasa edulis shoot shell in aqueous solution. RSC Adv. **5**, 104769–104778 (2015)
24. Mészáros, L., Šuránek, M., Melichová, Z., Frišták, V., Ďuriška, L., Kaňuchová, M., Soja, G., Pipíška, M.: Green biochar-based adsorbent for radiocesium and Cu, Ni, and pb removal. J. Radioanal Nucl. Chem. **332**, 4141–4155 (2023)
25. Li, X., Pan, H., Yu, M., Wakeel, M., Luo, J., Alharbi, N.S., Liao, Q., Liu, J.: Macroscopic and molecular investigations of immobilization mechanism of uranium on biochar: EXAFS spectroscopy and static batch. J. Mol. Liq. **269**, 64–71 (2018)
26. Hu, H., Jiang, B., Wu, H., Zhang, J., Chen, X.: Bamboo (Acidosasa edulis) shoot shell biochar: Its potential isolation and mechanism to perrhenate as a chemical surrogate for pertechnetate. J. Environ. Radioact. **165**, 39–46 (2016)
27. Wang, B., Li, Y., Zheng, J., Hu, Y., Wang, X., Hu, B.: Efficient removal of U (VI) from aqueous solutions using the magnetic biochar derived from the biomass of a bloom-forming cyanobacterium (Microcystis aeruginosa). Chemosphere. **254**, 126898 (2020)
28. Palansooriya, K.N., Yoon, I.-H., Kim, S.-M., Wang, C.-H., Kwon, H., Lee, S.-H., Igalavithana, A.D., Mukhopadhyay, R., Sarkar, B., Ok, Y.S.: Designer biochar with enhanced functionality for efficient removal of radioactive cesium and strontium from water. Environ. Res. **214**, 114072 (2022). https://doi.org/10.1016/j.envres.2022.114072
29. Hu, H., Lv, C., Hu, A., Wang, T., Lu, H.: Influence of torrefaction intensities on bamboo (Acidosasa longiligula) shoot shell-derived biochar and its application for tc(VII) reductive immobilization. J. Taiwan. Inst. Chem. Eng. **116**, 266–271 (2020). https://doi.org/10.1016/j.jtice.2020.11.011
30. Liu, Y., Wang, Y., Xia, H., Wang, Q., Chen, X., Lv, J., Li, Y., Zhao, J., Liu, Y., Yuan, D.: Low-cost reed straw-derived biochar prepared by hydrothermal carbonization for the removal of uranium (VI) from aqueous solution. J. Radioanal Nucl. Chem. **331**, 3915–3925 (2022)
31. Da, T.-X., Chen, T., He, W.-K., Liu, P., Ma, Y., Tong, Z.-F.: Comprehensive comparisons of iodate adsorption onto corn stalk hydrothermal and pyrolytic biochar. J. Radioanal Nucl. Chem. **329**, 1277–1290 (2021)
32. Yakout, S.M., Elsherif, E.: Investigation of strontium (II) sorption kinetic and thermodynamic onto straw-derived biochar. Part. Sci. Technol. **33**, 579–586 (2015)
33. Ahmed, W., Mehmood, S., Qaswar, M., Ali, S., Khan, Z.H., Ying, H., Chen, D.-Y., Núñez-Delgado, A.: Oxidized biochar obtained from rice straw as adsorbent to remove uranium (VI) from aqueous solutions. J. Environ. Chem. Eng. **9**, 105104 (2021)
34. Lv, J., Xia, H., Ren, Q., Wang, Y., Liu, Y., Feng, Z., Li, Y., Du, Y., Wang, Y.: Hydrothermal fabrication of amino functionalized lotus seedpods-derived biochar for efficient removal of uranium (VI). J. Radioanal Nucl. Chem. **332**, 4075–4087 (2023)
35. Wang, X., Feng, J., Cai, Y., Fang, M., Kong, M., Alsaedi, A., Hayat, T., Tan, X.: Porous biochar modified with polyethyleneimine (PEI) for effective enrichment of U(VI) in aqueous solution. Sci. Total Environ. **708**, 134575 (2020). https://doi.org/10.1016/j.scitotenv.2019.134575
36. Albayari, M., Nazal, M.K., Khalili, F.I., Nordin, N., Adnan, R.: Biochar derived from Salvadora Persica branches biomass as low-cost adsorbent for removal of uranium (VI) and thorium (IV) from water. J. Radioanal Nucl. Chem. **328**, 669–678 (2021)
37. Bai, B., Liu, Q., Li, H., Liu, D., Wang, H., Zhang, C., Yang, Z., Yao, J.: Sorption of Iodine on Biochar Derived from the Processing of Urban Sludge and Garden Waste at different pyrolysis temperatures. Molecules. **29**, 3007 (2024)
38. Feng, S., Cao, X., Zheng, W., Yue, X., Li, X., Li, S., Wang, X., Feng, S.: In-situ formed prussian blue nanoparticles supported by porous biochar as highly efficient removal of cesium ions. J. Environ. Chem. Eng. **10**, 107972 (2022). https://doi.org/10.1016/j.jece.2022.107972
39. Sumalatha, B., Narayana, A.V., Khan, A.A., Venkateswarulu, T.C., Reddy, G.S., Reddy, P.R., Babu, D.J.: A sustainable Green Approach for efficient capture of Strontium from simulated Radioactive Wastewater using modified Biochar. Int. J. Environ. Res. **16**, 75 (2022)
40. Adeniyi, A.G., Emmanuel, S.S., Alharthi, M.N., Iwuozor, K.O., Emenike, E.C., Oyekunle, I.P., Micheal, T.T., Omuku, P.E., Micheal, K.T., Ojo, H.T., Amoloye, M.A.: Improving Biochar properties through Liquid-Phase Exfoliation of Onion Peel Biochar Doped with Chicken feathers. Surf. Interfaces. **52**, 104841 (2024). https://doi.org/10.1016/j.surfin.2024.104841
41. Iwuozor, K.O., Odimayomi, K.P., Emenike, E.C., Okoro, H.K., Emmanuel, S.S., Amusa, V.T., Adeniyi, A.G.: Valorisation of bamboo stalk waste: Eco-friendly synthesis and characterisation of activated carbon monolith. Indian Chem. Eng. 1–14 (2024). https://doi.org/10.1080/00194506.2024.2392205
42. Ying, D., Hong, P., Jiali, F., Qinqin, T., Yuhui, L., Youqun, W., Zhibin, Z., Xiaohong, C., Yunhai, L.: Removal of uranium using MnO2/orange peel biochar composite prepared by activation and in-situ deposit in a single step. Biomass Bioenerg. **142**, 105772 (2020)
43. Narasimharao, K., Angaru, G.K.R., Momin, Z.H., Al-Thabaiti, S., Mokhtar, M., Alsheshri, A., Alfaifi, S.Y., Koduru, J.R., Chang, Y.-Y.: Orange waste Biochar-Magnesium Silicate (OBMS) composite for enhanced removal of U(VI) ions from aqueous solutions. J. Water Process. Eng. **51**, 103359 (2023). https://doi.org/10.1016/j.jwpe.2022.103359
44. Hu, H., Yu, S., Wang, T., Lv, C.: Efficient and selective separation of Re (VII), an analogue of tc (VII), by a defective biochar with honeycomb-like porous structure. J. Chem. Technol. Biotechnol. **99**, 946–958 (2024)
45. Chakraborty, V., Das, P., Roy, P.K.: Synthesis and application of graphene oxide-coated biochar composite for treatment of strontium-containing solution. Int. J. Environ. Sci. Technol. **18**, 1953–1966 (2021)
46. Xia, D., Liu, Y., Cheng, X., Gu, P., Chen, Q., Zhang, Z.: Temperature-tuned fish-scale biochar with two-dimensional homogeneous porous structure: A promising uranium extractant. Appl. Surf. Sci. **591**, 153136 (2022). https://doi.org/10.1016/j.apsusc.2022.153136
47. Shin, J., Lee, Y.-G., Kwak, J., Kim, S., Lee, S.-H., Park, Y., Lee, S.-D., Chon, K.: Adsorption of radioactive strontium by pristine and magnetic biochars derived from spent coffee grounds. J. Environ. Chem. Eng. **9**, 105119 (2021)
48. Kwak, J., Lee, S.-H., Shin, J., Lee, Y.-G., Kim, S., Son, C., Ren, X., Shin, J.-K., Park, Y., Chon, K.: Synthesis and applications of bismuth-impregnated biochars originated from spent coffee grounds for efficient adsorption of radioactive iodine: A mechanism study. Environ. Pollut. **313**, 120138 (2022)
49. Lingamdinne, L.P., Choi, J.-S., Angaru, G.K.R., Karri, R.R., Yang, J.-K., Chang, Y.-Y., Koduru, J.R.: Magnetic-watermelon rinds biochar for uranium-contaminated water treatment using an electromagnetic semi-batch column with removal mechanistic investigations. Chemosphere. **286**, 131776 (2022)
50. Li, J., Wang, M., Zhao, X., Li, Z., Niu, Y., Wang, S., Sun, Q.: Efficient iodine removal by Porous Biochar-Confined Nano-Cu2O/Cu0: Rapid and Selective Adsorption of Iodide and Iodate ions. Nanomaterials. **13**, 576 (2023)
51. Sun, Y., Yuan, N., Ge, Y., Ye, T., Yang, Z., Zou, L., Ma, W., Lu, L.: Adsorption behavior and mechanism of U(VI) onto phytic acid-modified Biochar/MoS2 heterojunction materials. Sep. Purif. Technol. **294**, 121158 (2022). https://doi.org/10.1016/j.seppur.2022.121158

52. Ahmed, W., Mehmood, S., Núñez-Delgado, A., Ali, S., Qaswar, M., Khan, Z.H., Ying, H., Chen, D.-Y.: Utilization of Citrullus lanatus L. seeds to synthesize a novel MnFe2O4-biochar adsorbent for the removal of U (VI) from wastewater: Insights and comparison between modified and raw biochar. Sci. Total Environ. **771**, 144955 (2021)
53. Wang, W.D., Cui, Y.X., Zhang, L.K., Li, Y.M., Sun, P., Han, J.H.: Synthesis of a novel ZnFe 2 O 4/porous biochar magnetic composite for th (IV) adsorption in aqueous solutions. Int. J. Environ. Sci. Technol. **18**, 2733–2746 (2021)
54. Ye, T., Huang, B., Wang, Y., Zhou, L., Liu, Z.: Rapid removal of uranium (VI) using functionalized luffa rattan biochar from aqueous solution. Colloids Surf. Physicochem Eng. Asp. **606**, 125480 (2020)
55. Choi, J.-W., Cho, S., Choi, S.-J.: Ecofriendly, selective removal of radioactive strontium ions in aqueous solutions using magnetic banana peels. Sci. Total Environ. **778**, 146327 (2021). https://doi.org/10.1016/j.scitotenv.2021.146327
56. Younis, S.A., El-Salamony, R.A., Tsang, Y.F., Kim, K.-H.: Use of rice straw-based biochar for batch sorption of barium/strontium from saline water: Protection against scale formation in petroleum/desalination industries. J. Clean. Prod. **250**, 119442 (2020)
57. Gotore, O., Osamu, N., Rameshprabu, R., Arthi, M., Unpaprom, Y., Itayama, T.: Iodine adsorption isotherms on Matamba fruit shell stemmed biochar for wastewater re-use strategy in rural areas owing to climate change. Chemosphere. **303**, 135126 (2022). https://doi.org/10.1016/j.chemosphere.2022.135126
58. Liu, F., Wang, S., Zhao, C., Hu, B.: Constructing coconut shell biochar/MXenes composites through self-assembly strategy to enhance U (VI) and cs (I) immobilization capability. Biochar. **5**, 31 (2023)
59. Shin, J., Choi, M., Go, C.Y., Bae, S., Kim, K.C., Chon, K.: NaOH-assisted H2O2 post-modification as a novel approach to enhance adsorption capacity of residual coffee waste biochars toward radioactive strontium: Experimental and theoretical studies. J. Hazard. Mater. **435**, 129081 (2022). https://doi.org/10.1016/j.jhazmat.2022.129081
60. Lawal, A.A., Hassan, M.A., Zakaria, M.R., Yusoff, M.Z.M., Norrahim, M.N.F., Mokhtar, M.N., Shirai, Y.: Effect of oil palm biomass cellulosic content on nanopore structure and adsorption capacity of biochar. Bioresour Technol. **332**, 125070 (2021). https://doi.org/10.1016/j.biortech.2021.125070
61. Lu, W., Feng, J., Otero, M., Liao, T., Qiu, L.: Removal of Sr(II) in Aqueous Solutions. Using Magnetic Crayfish Shell Biochar (2023)
62. Liao, J., He, X., Zhang, Y., Zhu, W., Zhang, L., He, Z.: Bismuth impregnated biochar for efficient uranium removal from solution: Adsorption behavior and interfacial mechanism. Sci. Total Environ. **819**, 153145 (2022). https://doi.org/10.1016/j.scitotenv.2022.153145
63. Li, H., Zhang, X., Luo, C., Wang, H., Zou, Z., Liu, L., Yue, C.: Pomelo peel derived phosphorus-doped biochar for efficient disposal of uranium-containing nuclear wastewater: Experimental and theoretical perspectives. Sep. Purif. Technol. **333**, 125947 (2024). https://doi.org/10.1016/j.seppur.2023.125947
64. Obey, G., Adelaide, M., Ramaraj, R.: Biochar derived from non-customized matamba fruit shell as an adsorbent for wastewater treatment. J. Bioresour Bioprod. **7**, 109–115 (2022)
65. Wang, Y., Wu, X., Liu, X., Cai, C., Liang, C., Dai, L., He, X., He, R., Liu, H., Zhu, W.: Microbial etch: A novel construction method of functionalized biochar for enhanced uranium extraction in radioactive wastewater. Chemosphere. **361**, 142544 (2024). https://doi.org/10.1016/j.chemosphere.2024.142544
66. Liao, J., Ding, L., Zhang, Y., Zhu, W.: Efficient removal of uranium from wastewater using pig manure biochar: Understanding adsorption and binding mechanisms. J. Hazard. Mater. **423**, 127190 (2022). https://doi.org/10.1016/j.jhazmat.2021.127190
67. Guilhen, S.N., Mašek, O., Ortiz, N., Izidoro, J.C., Fungaro, D.A.: Pyrolytic temperature evaluation of macauba biochar for uranium adsorption from aqueous solutions. Biomass Bioenerg. **122**, 381–390 (2019). https://doi.org/10.1016/j.biombioe.2019.01.008
68. Xie, Y., Chen, H., Mei, B., Jia, L., Zhang, Y.: Construction of camphor leaves-derived biochar@bismuth for the capture of gaseous iodine. Chem. Eng. Sci. **281**, 119205 (2023). https://doi.org/10.1016/j.ces.2023.119205
69. Jin, J., Li, S., Peng, X., Liu, W., Zhang, C., Yang, Y., Han, L., Du, Z., Sun, K., Wang, X.: HNO3 modified biochars for uranium (VI) removal from aqueous solution. Bioresour Technol. **256**, 247–253 (2018)
70. Philippou, K., Anastopoulos, I., Dosche, C., Pashalidis, I.: Synthesis and characterization of a novel Fe3O4-loaded oxidized biochar from pine needles and its application for uranium removal. Kinetic, thermodynamic, and mechanistic analysis. J. Environ. Manage. **252**, 109677 (2019)
71. Hu, H., Sun, L., Gao, Y., Wang, T., Huang, Y., Lv, C., Zhang, Y.-F., Huang, Q., Chen, X., Wu, H.: Synthesis of ZnO nanoparticle-anchored biochar composites for the selective removal of perrhenate, a surrogate for pertechnetate, from radioactive effluents. J. Hazard. Mater. **387**, 121670 (2020). https://doi.org/10.1016/j.jhazmat.2019.121670
72. Zhao, Q., Xu, Z., Yu, Z.: Straw-derived biochar as the potential adsorbent for U (VI) and th (IV) removal in aqueous solutions. Biomass Convers. Biorefinery. **13**, 15707–15718 (2023)
73. Georgiou, E., Pashalidis, I.: Effective th (IV) adsorption by oxidized biochar prepared from palm tree fibers. J. Radioanal Nucl. Chem. **332**, 1413–1417 (2023)
74. Zhang, Z., Cao, X., Liang, P., Liu, Y.: Adsorption of uranium from aqueous solution using biochar produced by hydrothermal carbonization. J. Radioanal Nucl. Chem. **295**, 1201–1208 (2013)
75. Hadjittofi, L., Pashalidis, I.: Thorium removal from acidic aqueous solutions by activated biochar derived from cactus fibers. Desalin. Water Treat. **57**, 27864–27868 (2016)
76. Dai, L., Li, L., Zhu, W., Ma, H., Huang, H., Lu, Q., Yang, M., Ran, Y.: Post-engineering of biochar via thermal air treatment for highly efficient promotion of uranium(VI) adsorption. Bioresour Technol. **298**, 122576 (2020). https://doi.org/10.1016/j.biortech.2019.122576
77. Abu Shawer, A., Khalili, F.I.: Removal of Thorium (Iv) by Olive Pomaceand It's Biochar. Fawwaz I., Remov. Thorium by Olive Pomaceand It's Biochar (2024)
78. Liao, J., Xiong, T., Zhao, Z., Ding, L., Zhu, W., Zhang, Y.: Synthesis of a novel environmental-friendly biocarbon composite and its highly efficient removal of uranium(VI) and thorium(IV) from aqueous solution. J. Clean. Prod. **374**, 134059 (2022). https://doi.org/10.1016/j.jclepro.2022.134059
79. Guo, Y., Hong Nhung, N.T., Dai, X., He, C., Wang, Y., Wei, Y., Fujita, T.: Strontium ion removal from artificial seawater using a combination of adsorption with biochar and precipitation by blowing CO2 nanobubble with neutralization. Front. Bioeng. Biotechnol. **10**, 819407 (2022)
80. Kausar, A., MacKinnon, G., Alharthi, A., Hargreaves, J., Bhatti, H.N., Iqbal, M.: A green approach for the removal of Sr(II) from aqueous media: Kinetics, isotherms and thermodynamic studies. J. Mol. Liq. **257**, 164–172 (2018). https://doi.org/10.1016/j.molliq.2018.02.101
81. Liatsou, I., Christodoulou, E., Pashalidis, I.: Thorium adsorption by oxidized biochar fibres derived from Luffa cylindrica sponges. J. Radioanal Nucl. Chem. **317**, 1065–1070 (2018)
82. Igwegbe, C.A., Oba, S.N., Aniagor, C.O., Adeniyi, A.G., Ighalo, J.O.: Adsorption of ciprofloxacin from water: A comprehensive review. J. Ind. Eng. Chem. **93**, 57–77 (2021)

83. Jang, J., Miran, W., Divine, S.D., Nawaz, M., Shahzad, A., Woo, S.H., Lee, D.S.: Rice straw-based biochar beads for the removal of radioactive strontium from aqueous solution. Sci. Total Environ. **615**, 698–707 (2018). https://doi.org/10.1016/j.scitotenv.2017.10.023
84. Chen, T., Zhang, N., Xu, Z., Hu, X., Ding, Z.: Integrated comparisons of thorium (IV) adsorption onto alkali-treated duckweed biomass and duckweed-derived hydrothermal and pyrolytic biochar. Environ. Sci. Pollut Res. **26**, 2523–2530 (2019)
85. Zhao, C., Ge, L., Wang, R., Chu, H., Mai, L., Zha, W., Wang, Y., Xu, C.: Effects of cellulose addition on the physicochemical properties, pore structure and iodine adsorption of lignin-based biochar. Fuel. **352**, 129061 (2023)
86. Neusatz Guilhen, S., Rovani, S., Pitol Filho, L., Alves Fungaro, D.: Kinetic study of uranium removal from aqueous solutions by macaúba biochar. Chem. Eng. Commun. **206**, 1354–1366 (2019)
87. Mahrous, S.S., Mansy, M.S., Youssef, M.A.: The performance of iron-silicate-based biochar as a sorbent material towards 133Ba retention from radioactive liquid waste. Radiochim Acta **0,** (2024)
88. Chackoshian Khorasani, A., Zamiri Akbarzadeh, S.: Production of Biosorbent based on Walnut Shell and Polystyrene Waste for Iodine Adsorption from Aqueous Solution. Iran. Chem. Eng. J. (2024)
89. Mongkollertlop, S., Sookkheo, B.: Specific investigation for adsorption nature of iodine, reactive dye or wastewater model over low-priced bio-char derived from biomass waste. Res. Chem. Intermed. **50**, 1013–1032 (2024)
90. Zhao, E., Wang, A., Huang, L., Chen, C., Qiu, M.: Mechanism and Chemical Stability of U (VI) removal by magnetic Fe3O4@ Biochar composites. Nat. Environ. Pollut Technol. **21**, 263–268 (2022)
91. Lee, H.W., Jeon, H.G., Kim, K.-W.: Removal of cobalt and strontium by adsorption using Brewer's spent grain formed by pyrolysis. Environ. Geochem. Health. **45**, 7131–7144 (2023). https://doi.org/10.1007/s10653-023-01655-z
92. de Souza, P.H.C., Rocha, S.D.F., de Rezende, D.B.: Luffa cylindrica slow pyrolysis and solar pyrolysis: Impact of temperature and heating rate on biochar properties and iodine adsorption performance. Waste Biomass Valoriz. **14**, 1753–1768 (2023)
93. Philippou, K., Konstantinou, A., Pashalidis, I.: Thorium adsorption by oxidized biochar pine needles-the effect of particle size. Desalin. Water Treat. **194**, 411–416 (2020)
94. Ighalo, J.O., Ajala, O.J., Umenweke, G., Ogunniyi, S., Adeyanju, C.A., Igwegbe, C.A., Adeniyi, A.G.: Mitigation of clofibric acid pollution by adsorption: A review of recent developments. J. Environ. Chem. Eng. **8** (2020). https://doi.org/10.1016/j.jece.2020.104264
95. Igwegbe, C.A., Aniagor, C.O., Oba, S.N., Yap, P.-S., Iwuchukwu, F.U., Liu, T., de Souza, E.C., Ighalo, J.O.: Environmental protection by the adsorptive elimination of acetaminophen from water: A comprehensive review. J. Ind. Eng. Chem. **104**, 117–135 (2021). https://doi.org/10.1016/j.jiec.2021.08.015
96. Emmanuel, S.S., Adesibikan, A.A., Olawoyin, C.O., Idris, M.O.: Photocatalytic degradation of Maxilon Dye pollutants using Nano-Architecture Functional materials. Rev. ChemistrySelect. **9** (2024). https://doi.org/10.1002/slct.202400316 e202400316
97. Badamasi, H., Sanni, S.O., Ore, O.T., Bayode, A.A., Koko, D.T., Akeremale, O.K., Emmanuel, S.S.: Eggshell waste materials-supported metal oxide nanocomposites for the efficient photocatalytic degradation of organic dyes in water and wastewater: A review. Bioresour Technol. Rep. **26**, 101865 (2024). https://doi.org/10.1016/j.biteb.2024.101865
98. Adesibikan, A.A., Emmanuel, S.S., Nafiu, S.A., Tachia, M.J., Iwuozor, K.O., Emenike, E.C., Adeniyi, A.G.: A review on sustainable photocatalytic degradation of agro-organochlorine and Organophosphorus Water pollutants using Biogenic Iron and Iron Oxide-based nanoarchitecture materials. Desalin. Water Treat. **320**, 100591 (2024). https://doi.org/10.1016/j.dwt.2024.100591
99. Aniagor, C.O., Igwegbe, C.A., Ighalo, J.O., Oba, S.N.: Adsorption of doxycycline from aqueous media: A review. J. Mol. Liq. **334**, 116124 (2021). https://doi.org/10.1016/j.molliq.2021.116124
100. Wang, B., Zhai, Y., Wang, T., Li, S., Peng, C., Wang, Z., Li, C., Xu, B.: Fabrication of bean dreg-derived carbon with high adsorption for methylene blue: Effect of hydrothermal pretreatment and pyrolysis process. Bioresour Technol. **274**, 525–532 (2019)
101. Philippou, M., Pashalidis, I., Kalderis, D.: Removal of 241Am from Aqueous Solutions by Adsorption on Sponge Gourd Biochar, (2023)
102. Philippou, M., Pashalidis, I.: Polonium removal from waters by silver-coated Luffa Cylindrica biochar fibers. J. Radioanal Nucl. Chem. **332**, 1395–1398 (2023)
103. Adesibikan, A.A., Emmanuel, S.S., Olawoyin, C.O., Ndungu, P.: Cellulosic metallic nanocomposites for photocatalytic degradation of persistent dye pollutants in aquatic bodies: A pragmatic review. J. Organomet. Chem. **123087** (2024). https://doi.org/10.1016/j.jorganchem.2024.123087
104. Emmanuel, S.S., Idris, M.O., Olawoyin, C.O., Adesibikan, A.A., Aliyu, A.A., Suleiman, A.I.: Biosynthesized Metallic nanoarchitecture for Photocatalytic Degradation of Emerging Organochlorine and Organophosphate pollutants. Rev. ChemistrySelect. **9**, e202304956 (2024). https://doi.org/10.1002/slct.202304956
105. Emmanuel, S.S., Adesibikan, A.A.: Harvesting surface (interfacial) energy for tribocatalytic degradation of hazardous dye pollutants using nanostructured materials: A review. J. Chin. Chem. Soc. **71**, 944–977 (2024). https://doi.org/10.1002/jccs.202400157